8. SITE 749[1]

Shipboard Scientific Party[2]

HOLE 749A

Date occupied: 24 March 1988

Date departed: 24 March 1988

Time on hole: 8 hr, 15 min

Position: 58°43.03'S, 76°24.45'E

Bottom felt (rig floor; m, drill pipe measurement): 1082.0

Distance between rig floor and sea level (m): 10.50

Water depth (drill pipe measurement from sea level, m): 1071.5

Total depth (rig floor; m): 1091.50

Penetration (m): 9.50

Number of cores (including cores with no recovery): 1

Total length of cored section (m): 9.50

Total core recovered (m): 10.04

Core recovery (%): 105

Oldest sediment cored:
Depth (mbsf): 9.50
Nature: diatom ooze with ice-rafted debris
Age: Pleistocene

HOLE 749B

Date occupied: 24 March 1988

Date departed: 25 March 1988

Time on hole: 17 hr

Position: 58°43.03'S, 76°24.45'E

Bottom felt (rig floor; m, drill pipe measurement): 1080.0

Distance between rig floor and sea level (m): 10.50

Water depth (drill pipe measurement from sea level, m): 1069.5

Total depth (rig floor; m): 1203.80

Penetration (m): 123.80

Number of cores (including cores with no recovery): 14

Total length of cored section (m): 123.80

Total core recovered (m): 64.66

Core recovery (%): 52

Oldest sediment cored:
Depth (mbsf): 119.00
Nature: nannofossil ooze
Age: middle Eocene
Measured velocity (km/s): 1.58

HOLE 749C

Date occupied: 25 March 1988

Date departed: 28 March 1988

Time on hole: 2 days, 15 hr, 15 min

Position: 58°43.03'S, 76°24.45'E

Bottom felt (rig floor; m, drill pipe measurement): 1080.0

Distance between rig floor and sea level (m): 10.50

Water depth (drill pipe measurement from sea level, m): 1069.5

Total depth (rig floor; m): 1329.50

Penetration (m): 249.50

Number of cores (including cores with no recovery): 16

Total length of cored section (m): 147.50

Total core recovered (m): 29.92

Core recovery (%): 20

Oldest sediment cored:
Depth (mbsf): 197.00
Nature: nannofossil ooze and chert
Age: Eocene
Measured velocity (km/s): 1.58

Basement:
Depth (mbsf): 249.50
Nature: basalt
Measured velocity (km/s): 5.59

Principal results: Site 749 (proposed site SKP-4A) is a reentry site located on the western flank of the Banzare Bank, on the Southern Kerguelen Plateau (58°43.03'S, 76°24.45'E) in a water depth of 1069.5 m. The Banzare Bank corresponds to a smooth basement rise that crests east of the site at a water depth of about 700 m. The sediments gradually thin toward the top of the bank where several faults cut the basement structure. The site is intended to recover extensive basement rocks from the Southern Kerguelen Plateau with penetration of at least 200 m.

Basement at this site corresponds to a very strong reflector. An approach site survey located the site on *Marion Dufresne* MCS line MD47-13 (shot point 5670) where the basement reflector lies at about 0.24 s two-way traveltime (TWT) below seafloor. Downslope the sediments thicken in all directions, especially by toplap. Thus, the oldest sediment cored at this site will not correspond to the age of basement.

The upper 43.8 m of section was cored with 100% recovery using the advanced hydraulic piston corer (APC), at which point middle Eocene cherts were encountered that reduced recovery via the APC and the extended core barrel (XCB) to only 26% over the next 80 m. A change to the rotary core barrel (RCB) yielded only 7% recovery through cherts, chalks, and oozes to the basement contact at 202 m. After obtaining 5 m of basalt in the next core, the succeeding two cores were essentially empty, and a model Lamar Hayes (LH) minicone was deployed to allow the hole to be reentered after a bit change. This was the first use of a free-fall minicone for a dedicated basement site.

Inspection of the bottom hole assembly (BHA) on deck showed that severe pounding of the bit against hard bottom in high seas at this shallow site had resulted in a badly worn bit and a broken flapper valve. The latter had precluded any recovery in the last two

[1] Schlich, R., Wise, S. W., Jr., et al., 1989. *Proc. ODP, Init. Repts.*, 120: College Station, TX (Ocean Drilling Program).

[2] Shipboard Scientific Party is as given in the list of Participants preceding the contents.

cores. A novel decision was made by the Ocean Drilling Program (ODP) Cruise Operations Superintendent, Mr. Lamar Hayes, to core without a flapper valve and to institute instead a weighted mud program to prevent backflow of cuttings into the BHA. After a successful (16 min) reentry, this procedure worked beyond expectations because the next two cores produced 17.83 m of basalt at a recovery rate of 94%. As the last core was being cut, a medical emergency involving Mr. Hayes ended operations at this site, and the *JOIDES Resolution* was put on course for Fremantle, Australia. Mr. Hayes died on 28 March 1988, and the ship arrived at Fremantle on 5 April 1988.

The following lithologic units were recognized at Site 749:

Unit I (0–0.24 mbsf): Pleistocene to mid-Pliocene diatom ooze with foraminifers and ice-rafted debris; disconformity at base.

Unit II (0.24–202.0 mbsf): upper Oligocene to lower Eocene nannofossil ooze with chert, chalk, and porcellanite that is divisible into two subunits.

Subunit IIA (0.24–43.6 mbsf): upper Oligocene to middle Eocene nannofossil ooze with foraminifers plus some siliceous microfossils and minor volcanic ash in the upper 25 m.

Subunit IIB (43.6–202 mbsf): middle Eocene to lower Eocene nannofossil ooze, with chalk, chert, and porcellanite; 3% sponge spicules and radiolarians between 53 and 82 mbsf only.

Unit III (202–249.5 mbsf): clinopyroxene-plagioclase phyric basalts.

The 23.1 m of basalt recovered consists of five flows and one dike. Most flows have altered and vesicular tops that grade to fresh and more massive basalt toward the interior of the flow. The basalts are either quartz or olivine normative tholeiites and range in Mg# from 46.5 to 57.5. The high Mg# basalt contains olivine and plagioclase (An_{60-80}) phenocrysts. All other basalts have plagioclase (An_{50-60}) as the main phenocryst phase, together with occasional clinopyroxene. The groundmass phases consist of plagioclase (An_{40-50}), clinopyroxene, and Fe-Ti oxides.

These basalts are more depleted in incompatible trace elements than those from the previous Leg 120 sites, although basalts from Holes 747C and 749C have similar Zr/Nb and P/Y ratios. Both Site 747 and 749 basalts are slightly more enriched in incompatible elements than normal mid-ocean ridge basalt (MORB), and they are compositionally similar to transitional basalt (T-MORB). Based on major and trace element chemistry, Site 749 basalts are similar to the Nauru Basin plateau basalts (Deep Sea Drilling Project [DSDP] Leg 89). In contrast to basalts from Site 747, the basalts from Site 749 do not form a coherent group or trend on key variation diagrams. This indicates that the basalts from Site 749 cannot be related to each other by simple fractional crystallization or partial melting alone.

Alteration minerals occur in the basalts in the groundmass, amygdules, and veins and as a replacements for plagioclase phenocrysts. The alteration assemblage consists of laumontite (and stilbite), interlayered smectite, calcite, and occasional quartz, which is diagnostic of the high-temperature zeolite facies (100°–200°C). This alteration assemblage at Site 749 is not observed at normal mid-ocean ridge segments, but it does occur in places with high heat flow such as Iceland. The shallow depth of this alteration zone combined with its relatively high temperature indicates a high paleoheat flow.

The oldest sediments above basement are dated from 54 to 55 Ma. Benthic foraminifers indicate that the paleodepth at this site has been virtually constant (between 1000 and 1500 m) since the early Eocene. Sedimentation rates, however, vary considerably, being inferred as high as 70 m/m.y. for the lower and lower middle Eocene, then dropping to a minimum of 7 m/m.y. for the middle middle to upper middle Eocene and 3.6 m/m.y. for the upper Eocene and Oligocene. The abnormally high sedimentation rate during the early and early middle Eocene may be attributable to constant synsedimentary scouring and redeposition of pelagic oozes, particularly from exposed basement surfaces, thereby contributing to a type of sediment "drift" deposit at this site.

BACKGROUND AND OBJECTIVES

The Kerguelen Plateau is divided into two distinct domains (Schlich, 1975; Houtz et al., 1977). To the north, the Kerguelen-Heard Plateau extends from the Crozet Basin to about 54°S and includes the plateau's only subaerial manifestations: Kerguelen, Heard, and McDonald islands. To the south, the Southern Kerguelen Plateau lies between 57° and 64°S, where it merges into the Princess Elizabeth Trough (see "Introduction" chapter, this volume). Site 749 (58°43.03′S, 76°24.45′E) is located on the Southern Kerguelen Plateau on the western flank of the Banzare Bank at a water depth of about 1100 m.

Two northeast-trending multichannel seismic reflection lines (RS02-27 and RS02-29), separated by approximately 50 km, one northwest-trending multichannel seismic reflection line (MD47-13), and several *Eltanin 47* single channel seismic lines on the Banzare Bank provide good regional control of the area close to Site 749 (Fig. 1). The Banzare Bank is characterized by a smooth basement rise that culminates at a water depth of about 700 m and is overlain by a thick sedimentary cover. The sediments gradually thin toward the top of the bank where normal faults, north-trending to the north and northwest-trending to the south and southeast, affect the basement structure.

Site 749 (target site SKP-4A) is on French multichannel seismic reflection line MD47-13 (shot point 5670) trending northwest across the Banzare Bank. At this location, the sedimentary section is much reduced and basement lies within 200–250 m below seafloor (mbsf). The location of the site is given along with the seismic section MD47-13 on Figure 2.

Objectives

Site 749 is the most important basement site of the Kerguelen Plateau drilling program. The site provides the best opportunity to obtain extensive basement rocks from the Southern Kerguelen Plateau. Deep penetration of at least 200 m was planned at this site.

The prime objective of drilling Site 749 was to determine the nature and age of the Kerguelen Plateau basement. Petrographic studies and geochemical analyses of the rocks were planned to investigate several different possibilities regarding the nature of the plateau: continental fragment, oceanic island basalt, or mid-oceanic ridge basalt (see "Introduction" chapter, this volume). Assuming a basaltic basement, deep penetration would allow a significant number of basaltic flows to be sampled. We planned to compare the results obtained at this site to the other Kerguelen Plateau basement sites (Leg 119, Site 738; Leg 120, Sites 747 and 750 [not planned as a basement site, but recovered basement nevertheless]).

Drilling Strategy

The drilling strategy at Site 749 called for hydraulic piston coring (APC) followed by the extended core barrel (XCB) until refusal. Then the rotary core barrel (RCB) with reentry was to be used to core the lower part of the sedimentary section and at least 200 m of basement rock.

SITE GEOPHYSICS

JOIDES Resolution departed Site 748 on 23 March 1988 shortly before midnight (2245 hr local [L] time). The magnetometer was towed immediately after departure, and continuous bathymetric and magnetic recording started at 1415 hr (UTC) along a line almost due west (265°), heading toward Site 749 (proposed site SKP-4A).

Site 749, the deep-penetration basement site on the Banzare Bank, Southern Kerguelen Plateau, lies about 80 nmi west of Site 748 on *Marion Dufresne* line MD47-13, shot point 5670 (Fig. 1). At 2215 hr (UTC) on 23 March 1988, *JOIDES Resolution* reduced speed to about 6 kt, and the seismic profiling gear was deployed. The ship intersected the French survey profile (MD47-13) at about 2250 hr (UTC), changed course at this time, and started the presite survey at a distance of 12 nmi northwest of target site SKP-4A. The final site approach was

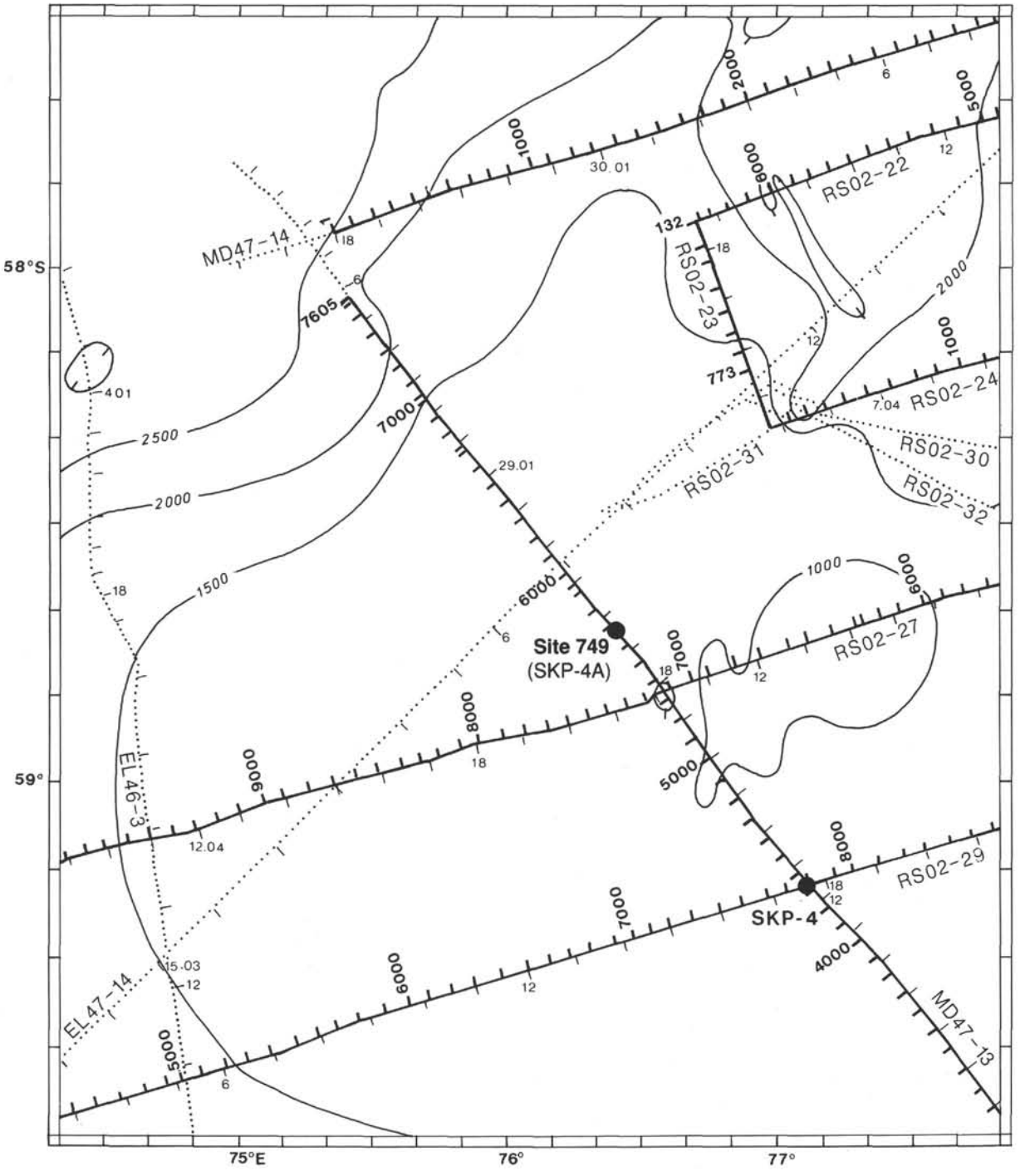

Figure 1. Track lines in the vicinity of Site 749. Bold lines denote *Rig Seismic* (RS02) and *Marion Dufresne* (MD47) multichannel seismic reflection profiles. The bathymetry is from Schlich et al., 1987.

made with global positioning satellite (GPS) navigation along a course of 142°, following the original *Marion Dufresne* survey line.

A beacon was dropped on the initial crossing of the proposed site (SKP-4A). The *JOIDES Resolution* seismic data recorded over the site showed excellent correlation with the *Marion Dufresne* multichannel seismic reflection profile shot in 1986, and location of the site was unambiguous. The gear was retrieved at 0040 hr (UTC) on 24 March 1988, 1 nmi beyond the selected site, and the ship proceeded back to the beacon to commence drilling (Fig. 3). The final coordinates of Site 749 are 58°43.03′S and 76°24.45′E; the water depth (from sea level), as measured from the drill pipe (DPM) and corrected for the height of the rig floor above sea level, at the three holes (749A, 749B, and 749C) ranges between 1069.5 and 1071.8 m.

The Banzare Bank, to the west of the southern end of the Raggatt Basin, is centered at 58°40′S and 77°20′E and corresponds to a clear topographic high that crests at about 700 m below sea level (Fig. 1). The center part of this domal feature is about 40 km across and has been eroded to expose basement

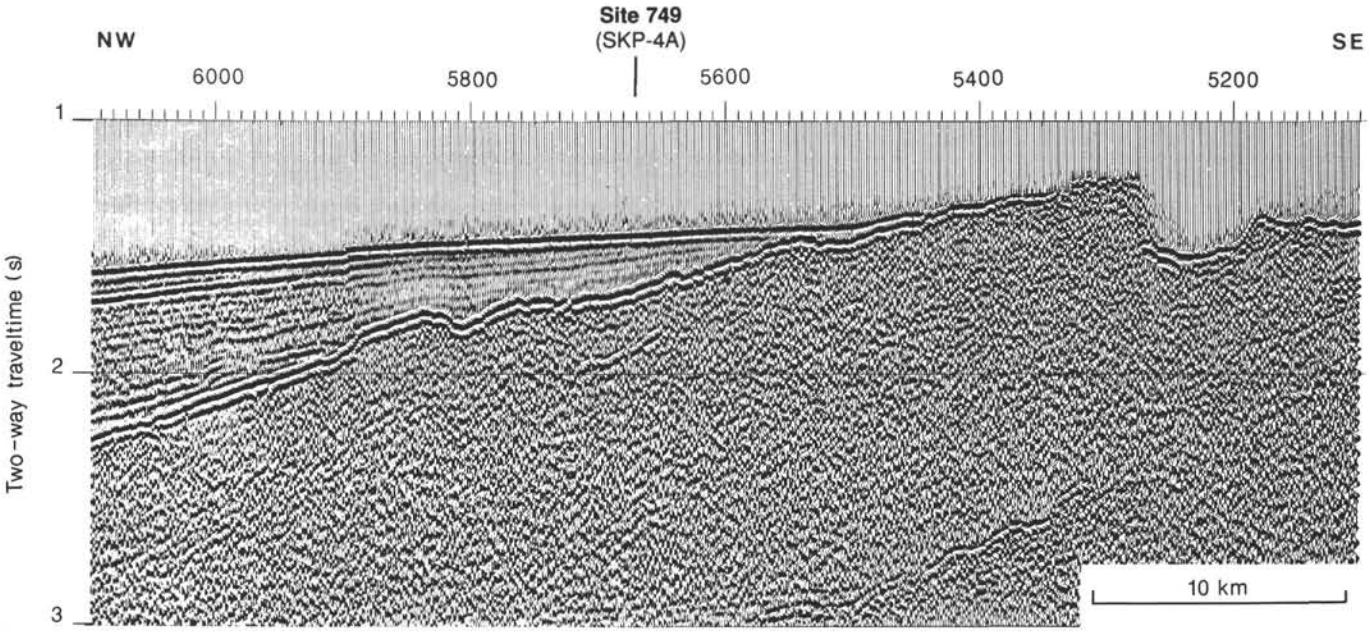

Figure 2. Seismic section MD47-13 (shot points 5100–6100) and SKP-4A site location (Site 749).

outcrops. To the north, the Banzare Bank extends to the southern end of the 77°E Graben, which corresponds at this location to a major normal fault facing to the east.

A series of normal faults trending 100°–110° abuts the eastern flank of the Banzare Bank. To the south and to the west, several normal faults with ill-defined directions affect the basement structure. These tectonic features are outlined on the isochron map of the top of the acoustic basement drawn for the area close to the drill site (Fig. 4). Downslope, the sediment cover thickens in all directions, essentially by toplap, without obvious unconformity. The sediment distribution at Site 749 is shown on the total sediment isopach map (Fig. 5).

The *JOIDES Resolution* survey line, shot with two 80-in^3 water guns and recorded with a 100-m hydrophone streamer, is shown on Figure 6. The correlation of this single-channel seismic record with the French multichannel seismic reflection profile (Fig. 2), which was used to locate Site 749, is straightforward.

At Site 749 the basement corresponds to a very strong reflector. On the *Marion Dufresne* seismic line MD47-13 (shot point 5670), the basement is at about 0.22 s TWT below seafloor; on the *JOIDES Resolution* seismic record (Line 3), the basement reflector lies at about 0.24 s TWT. The difference may be explained by a slight discrepancy in navigation, but it can also be related to the characteristics of the seismic acquisition system used on both ships. The correlation of the *Marion Dufresne* and *JOIDES Resolution* seismic section at Site 749 is shown on Figure 7. The vertical velocity distribution has been estimated by taking into account previous sonobuoy experiment results obtained on the Kerguelen Plateau and calculated seismic reflection stack velocities. Assuming a mean velocity of 1.8 km/s, the basement was expected at about 200 m below seafloor.

OPERATIONS

Site 748 to Site 749

Site 749 lays about 80 nmi to the west of Site 748. The vessel's track took her to a way point to the northwest, allowing the site approach profile to be made on a southeasterly heading. The seismic gear was streamed about 12 nmi from the intended drill site, and the positioning beacon was launched on the first pass over the site at 0830 hr (L, 0036 hr UTC), 24 March 1988.

Site 749 (SKP-4A)

Hole 749A

The bit and BHA that had been used for Holes 748A and 748B were again employed for the APC/XCB work at Site 749. For the initial core, the bit was positioned a full 5 m above the precision depth recorder (PDR) depth of 1087.3 m. Again the core barrel was recovered full of sediment, and it was necessary to respud to ascertain that the seafloor was cored.

Hole 749B

The subsequent attempt established seafloor depth at 1080.0 m. Five APC cores were taken with full recovery in carbonate ooze before chert was encountered at 43.8 mbsf. We then recovered three full-interval XCB cores for a total of 1 m of core in interbedded soft ooze and chert. In an effort to recover a representative core of ooze, one additional APC core was attempted. The barrel contained 5.9 m of core, but the cutter shoe was damaged and the plastic liner had failed as a result of its contact with a chert bed.

We then managed to obtain fairly good recovery with the XCB for three cores until the chert concentration increased, resulting in a lower core recovery and rate of penetration (ROP) and more XCB equipment damage with depth. Penetration was halted at 124 m for a round trip for the RCB system.

Hole 749C

The vessel was offset 40 m to the east before we began drilling in Hole 749C. The hole was advanced to the coring point 102 mbsf with a center bit in place at the core bit. The intercalated ooze and chert were again poorly recovered. Basalt was penetrated at 202 mbsf, and Core 120-749C-12R produced 5.1 m of basalt core. Only a trace of rock was recovered from the following two cores, and a round trip was made to change bits and check the coring system.

The pipe trip began in deteriorating weather and a building swell. With the entire BHA still protected in the hole, the trip

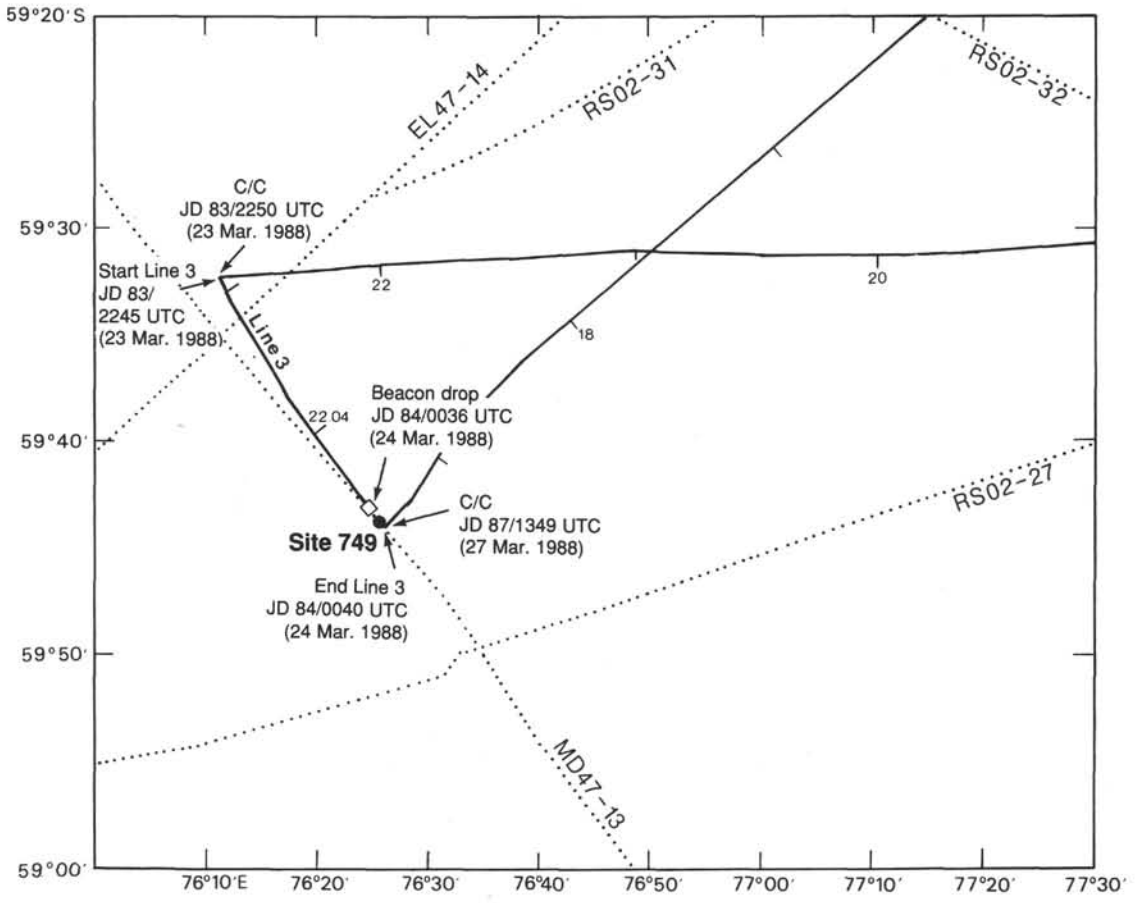

Figure 3. *JOIDES Resolution* site approach and Site 749 location.

was stopped to deploy the free-fall funnel (FFF) or minicone, which was the reentry device of choice for this dedicated basement site. The minicone operation was hampered by rolls of up to 10° and vessel heave to 14 ft but was accomplished in 2 hr. When the bit had cleared the seafloor, the trip was interrupted for 3 1/2 hr due to excessive vessel motion and the resulting hazard to rig personnel and equipment. Following the weather delay, the drill string was recovered. We found that the core bit was worn out, and the float valve flapper was broken again. Parts of the flapper had probably prevented the latter core barrels from seating fully and/or obstructed the entry of core into the inner barrel.

The extreme vessel motion conditions in combination with a relatively short drill string were considered to be a factor in the two float flapper failures. The new float valve was, therefore, made up without a flapper.

The downtrip and reentry proceeded smoothly and were executed in just over 4 hr. The bottom sediment (Oligocene nannofossil ooze) was quite firm, and the television camera showed the rim of the reentry cone standing about 1 m above the firm mud line. The actual reentry took only 16 min. A bridge or ledge was hit at 105 mbsf, and the trip was completed using the top drive for circulation and rotation. Only 2 m of solid fill was "felt" at total depth (TD).

In lieu of the missing flapper, a weighted mud program was instituted to prevent backflow of cuttings into the BHA. This worked better than expected and could probably have been continued to the projected 400 m TD for the hole. Two consecutive RCB cores were taken, with 94% basalt core recovery over a 19-m interval. The material obtained was crucial to the scientific objectives of the voyage and assured the success of operations at Site 749.

At 2030 hr (L), 27 March 1988, operations were suspended because of a medical emergency when Mr. Lamar Hayes, ODP Operations Superintendent, suffered a massive heart attack. The drill string was pulled, the drill collars were laid down, and the ship departed for Fremantle, Australia at 0100 hr (L) on 28 March 1988. All ships and stations in the area were contacted, including Kerguelen Island, Antarctic stations, and the AMVER emergency network, but there were no opportunities for evacuation or repatriation of the patient. At 0415 hr, 28 March 1988, Mr. Hayes passed away. Responsible parties on board and at ODP Headquarters chose to interrupt the expedition for compassionate reasons, and the ship proceeded on course for Fremantle, arriving on 5 April 1988 in the early morning.

The coring summary for Site 749 appears in Table 1.

LITHOSTRATIGRAPHY AND SEDIMENTOLOGY

Introduction

Site 749 is located in 1069.5 m of water on the Banzare Bank, Southern Kerguelen Plateau. The site objective was to drill through a thin Paleogene pelagic sequence and core 200 m of underlying basement. At this site, we cored 202 m of upper Oligocene to lower Eocene pelagic nannofossil ooze, chalk, and chert and 47.5 m of basalt.

Three holes were drilled at Site 749. Hole 749A reached 9.5

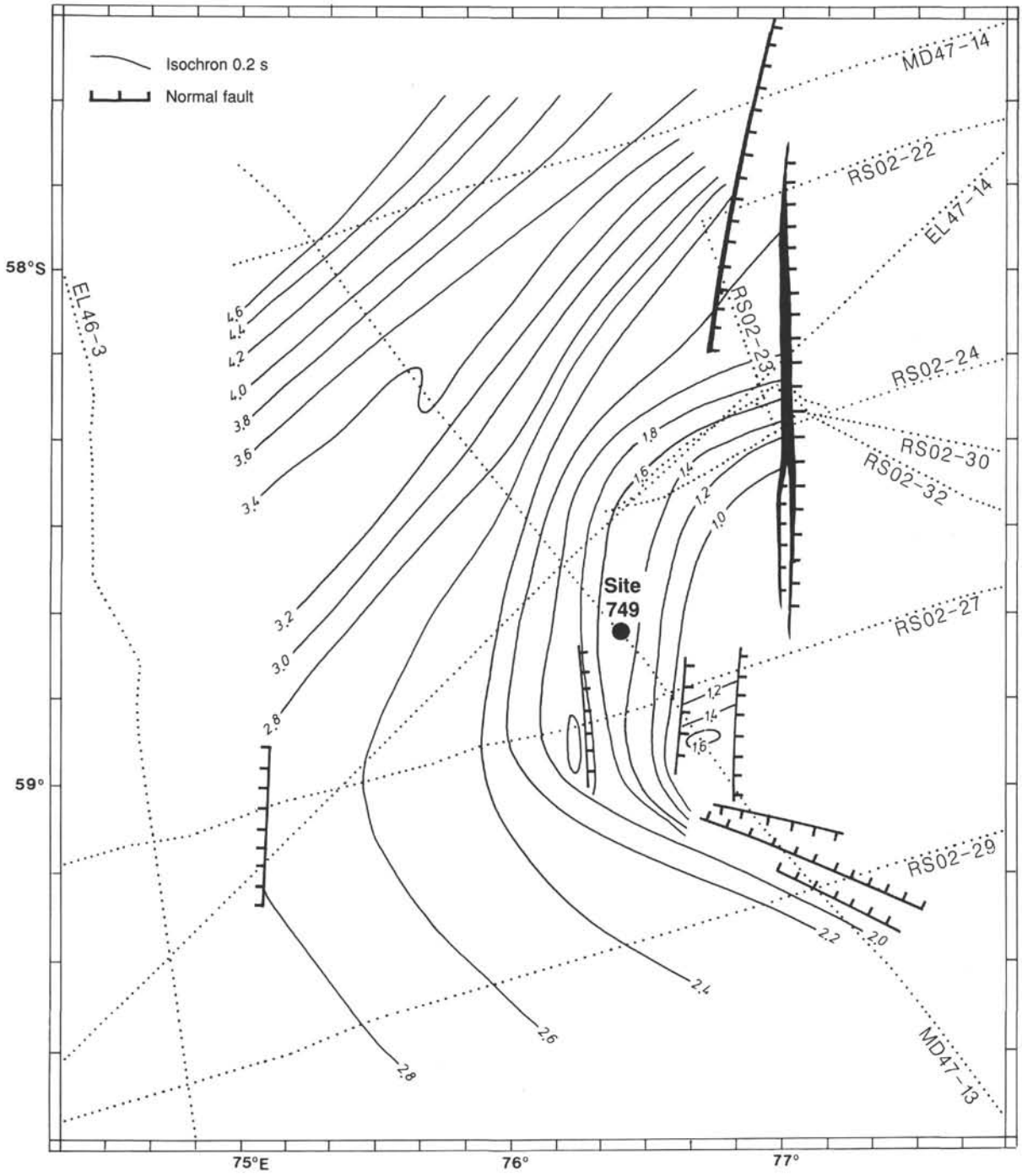

Figure 4. Isochron map of the acoustic basement contoured in seconds (TWT).

mbsf with 100% recovery using the APC. It was suspected that this core did not contain a complete mud line due to an overshot or excessive ship heave (see "Operations" section, this chapter). Hole 749B was APC and XCB cored to 123.8 mbsf before we ended drilling because of poor recovery (25.6% between 43.8 and 123.8 mbsf). Hole 749C was washed to 102.0 mbsf and rotary cored through 100.0 m of pelagic sediment to 202 mbsf with an average recovery of 6.7%. The contact between the pelagic sequence and basement was not recovered. Basement was interpreted to lie at 202 mbsf (based on weight on bit; see "Operations" section, this chapter).

Two lithologic units were recognized at this site as summarized in Table 2. Unit I consists of 0.24 m of Pleistocene diatom ooze with foraminifers and a mid-Pliocene lag deposit of sand- to pebble-sized grains of volcanic and ice-rafted debris. Unit II consists of 201.76 m of upper Oligocene to lower Eocene pelagic sediments, primarily nannofossil ooze, foraminifer nannofossil ooze, nannofossil chalk, chert, and porcellanite. Unit II is divided into two subunits based on chert occurrence: Subunit IIA is composed of nannofossil ooze with foraminifers, and Subunit IIB, of nannofossil ooze and chert. Figure 8 provides a summary of lithologic results and core recovery.

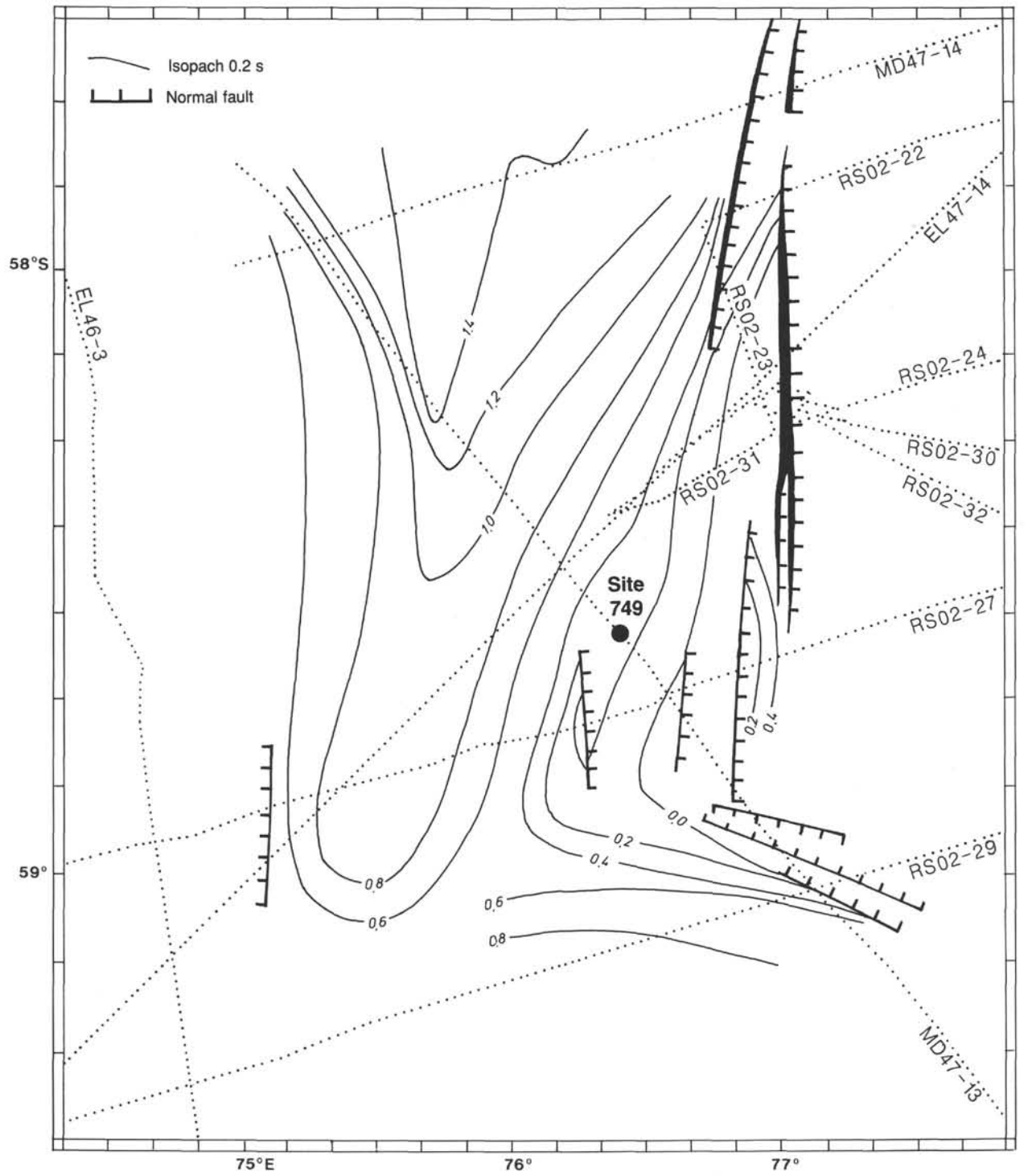

Figure 5. Total sediment isopach map contoured in seconds of reflection time.

Unit I: Diatom Ooze with Foraminifers

Interval: Cores 120-749A-1H-1, 0–40 cm, and 120-749B-1H-1, 0–24 cm.
Depth: 0–0.4 mbsf (Hole 749A) and 0–0.24 mbsf (Hole 749B).
Thickness: 0.40 m (Hole 749A) and 0.24 m (Hole 749B).
Age: Pleistocene to mid-Pliocene.

Unit I is sufficiently distinct to be classified as a separate unit in spite of its reduced thickness. It is composed of very pale brown (10YR 8/1) diatom ooze with foraminifers, gray calcareous siliceous ooze, and sand- to pebble-size ice-rafted and volcanic debris. A lag deposit of ice-rafted and volcanic debris forms the base of Unit I (Cores 120-749A-1H-1, 33–40 cm, and 120-749B-1H-1, 17–24 cm; Fig. 9). The composition of this lag deposit is similar in Holes 749A and 749B and includes clasts of quartz, biotite gneiss, quartzite, garnetiferous schist, potassium feldspar, granite, basalt, and pumice. Bioturbation has disseminated portions of Unit I throughout the upper 126 cm of Subunit IIA. The base of Unit I was chosen at the first occurrence of abundant nannofossils.

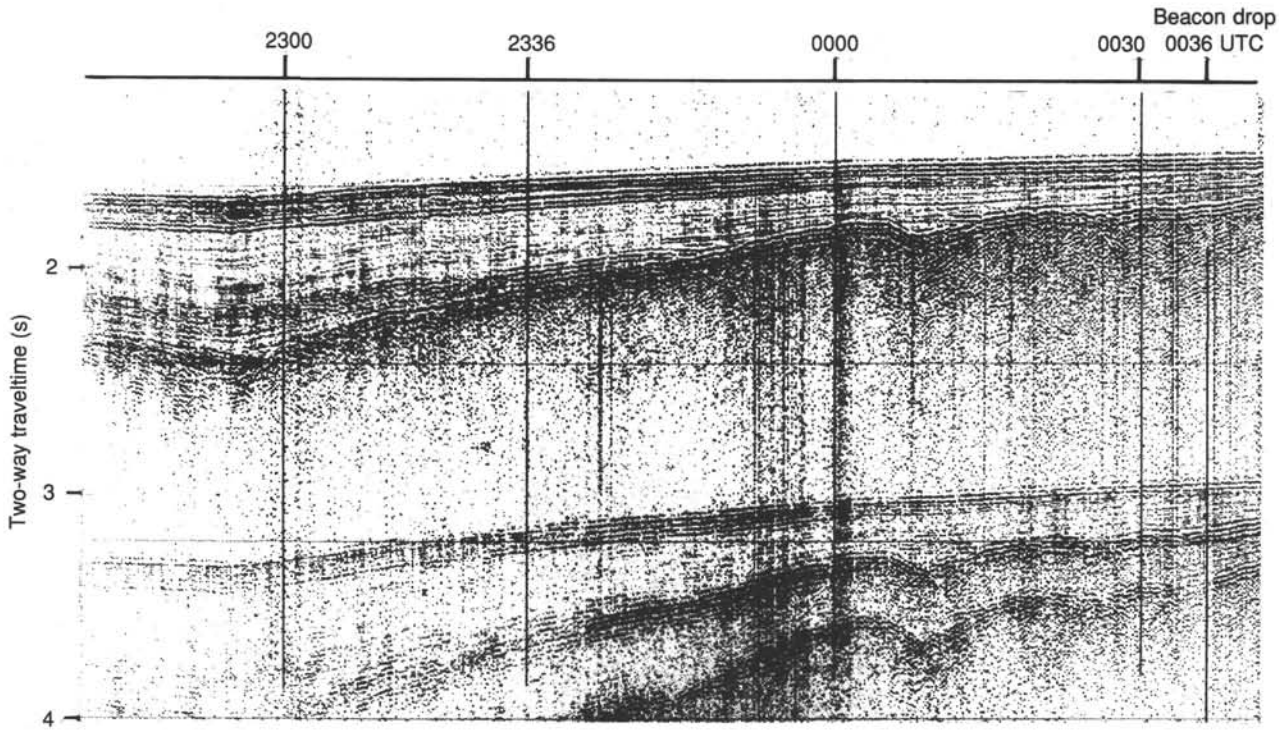

Figure 6. *JOIDES Resolution* single-channel reflection profile on approach to Site 749 (analog record).

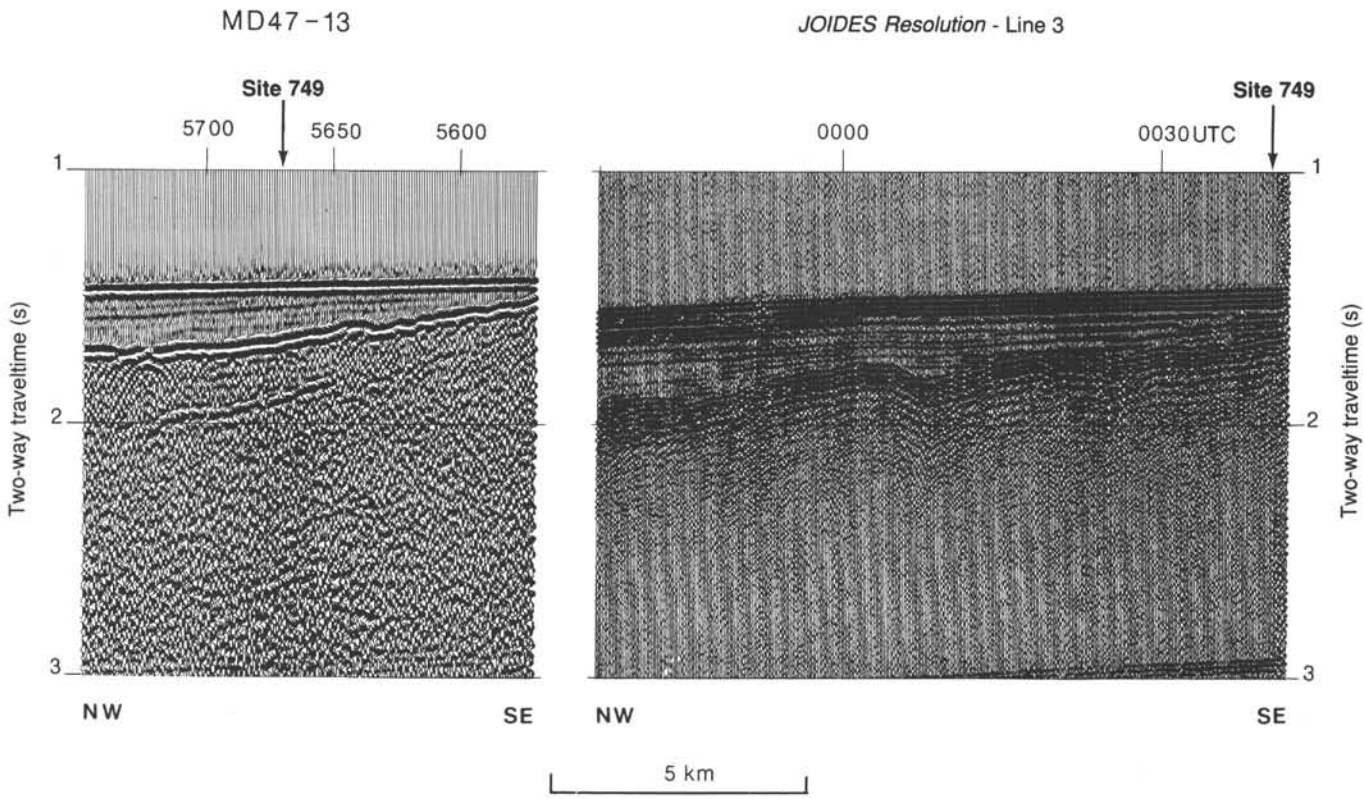

Figure 7. Correlation of the *Marion Dufresne* multichannel seismic reflection profile and the *JOIDES Resolution* single channel survey line in the vicinity of Site 749.

Table 1. Coring summary, Site 749.

Core no.	Date (March 1988)	Time (local)	Depth (mbsf)	Cored (m)	Recovered (m)	Recovery (m)
120-749A-						
1H	24	1645	0–9.5	9.5	10.04	105.7
Coring totals				9.5	10.04	105.7
120-749B-						
1H	24	1730	0–5.8	5.8	5.87	101.0
2H	24	1806	5.8–15.3	9.5	9.43	99.2
3H	24	1825	15.3–24.8	9.5	9.71	102.0
4H	24	1845	24.8–34.3	9.5	9.63	101.0
5H	24	1915	34.3–43.8	9.5	9.57	101.0
6X	24	2040	43.8–53.3	9.5	0.33	3.5
7X	24	2115	53.3–62.8	9.5	0.64	6.7
8X	24	2150	62.8–72.3	9.5	0	0
9H	24	2230	72.3–81.8	9.5	5.86	61.7
10X	24	2355	81.8–91.3	9.5	7.10	74.7
11X	25	0050	91.3–100.8	9.5	2.46	25.9
12X	25	0210	100.8–110.3	9.5	2.27	23.9
13X	25	0335	110.3–119.8	9.5	1.78	18.7
14X	25	0545	119.8–123.8	4.0	0.01	0.3
Coring totals				123.8	54.66	52.2
120-749C-						
1R	25	1850	102.0–111.5	9.5	0.01	0.1
2R	25	1930	111.5–121.0	9.5	0.01	0.1
3R	25	2005	121.0–130.5	9.5	0.05	0.5
4R	25	2035	130.5–140.0	9.5	0.02	0.2
5R	25	2100	140.0–149.5	9.5	0	0
6R	25	2130	149.5–159.0	9.5	0.78	8.2
7R	25	2200	159.0–168.5	9.5	3.87	40.7
8R	25	2235	168.5–178.0	9.5	0.71	7.5
9R	25	2310	178.0–187.5	9.5	0	0
10R	25	2350	187.5–197.0	9.5	1.39	14.6
11R	26	0200	197.0–206.5	9.5	0.11	1.2
12R	26	0645	206.5–216.0	9.5	5.09	53.6
13R	26	1215	216.0–225.5	9.5	0.05	0.5
14R	26	1700	225.5–230.5	5.0	0	0
15R	27	1640	230.5–240.0	9.5	8.33	87.7
16R	27	2030	240.0–249.5	9.5	9.50	100.0
Coring totals				147.5	29.92	20.3

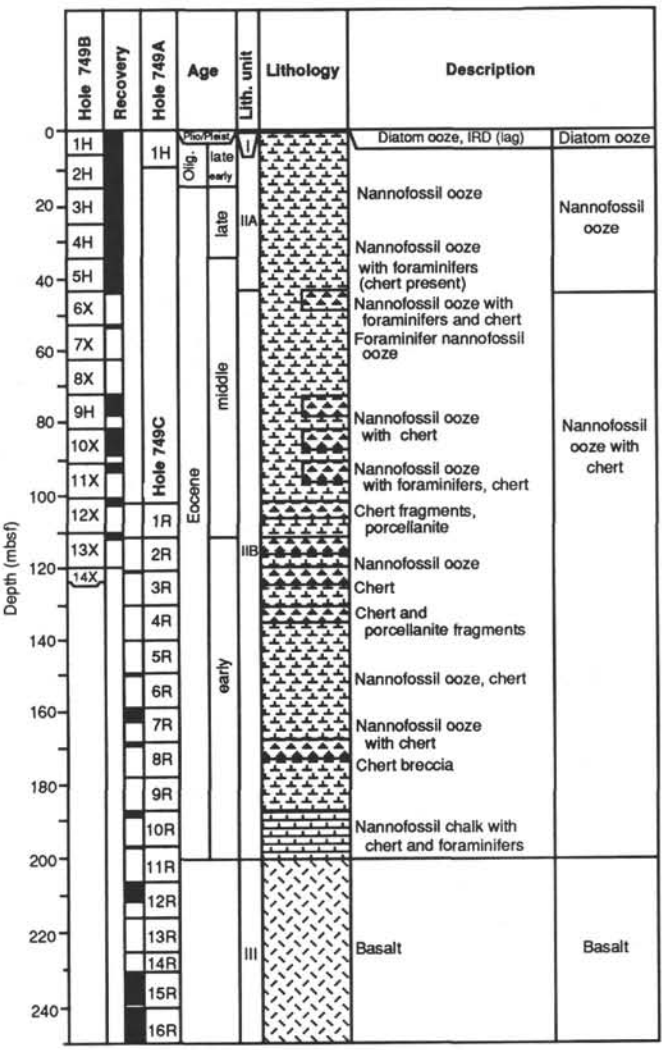

Figure 8. Lithostratigraphy of Site 749, Banzare Bank on the Southern Kerguelen Plateau. Recovered intervals indicated by shading in recovery column. For key to patterns in lithology column, see "Explanatory Notes" chapter (this volume). Note that the position of the sediment/basement contact at 202 mbsf (Unit II/III contact) is based on a decrease in the penetration rate.

Table 2. Summary of dominant lithologic units at Site 749, Banzare Bank on the Southern Kerguelen Plateau.

Unit or subunit	Lithology	Features	Depth (mbsf)	Core intervals	Thickness (m)	Age
I	Diatom ooze with foraminifers and ice-rafted debris	Lag deposit	0–0.50 (A) 0–0.24 (B)	120-749A-1H-1, 0–40 cm, and 120-749B-1H-1, 0–24 cm	0.40 (A) 0.24 (B)	Pleistocene to mid-Pliocene
II	Nannofossil ooze, nannofossil ooze with foraminifers		0.24–202.0	120-749B-1H, 24 cm, to TD and 120-749C-1R to 120-749C-10R-CC	201.76	late Oligocene to early Eocene
IIA	Nannofossil ooze with foraminifers	Foraminifer content variable	0.4–9.5 (A) 0.24–43.56 (B)	120-749A-1H-1, 40 cm, to TD and 120-749B-1H, 24 cm, to 120-749B-6H-1, 0 cm	(Total 43.56) 9.1 (A) 43.56 (B)	late Oligocene to middle Eocene
IIB	Nannofossil ooze and chert	Siliceous microfossils rare to absent	43.6–123.8 (B) 102.0–202 (C)	120-749B-6H-1, 0 cm, to TD and 120-749C-1R to 120-749C-10R-CC	(Total 158.2) 80.0 (B) 100.0 (C)	middle Eocene to early Eocene
III	Basalt		202–249.5 (C)	120-747C-11R-CC to TD	47.5 (C)	

Note: The position of the sediment/basement contact (Unit II/III contact) at 202 mbsf is based on a decrease in the sedimentation rate; TD = total depth.

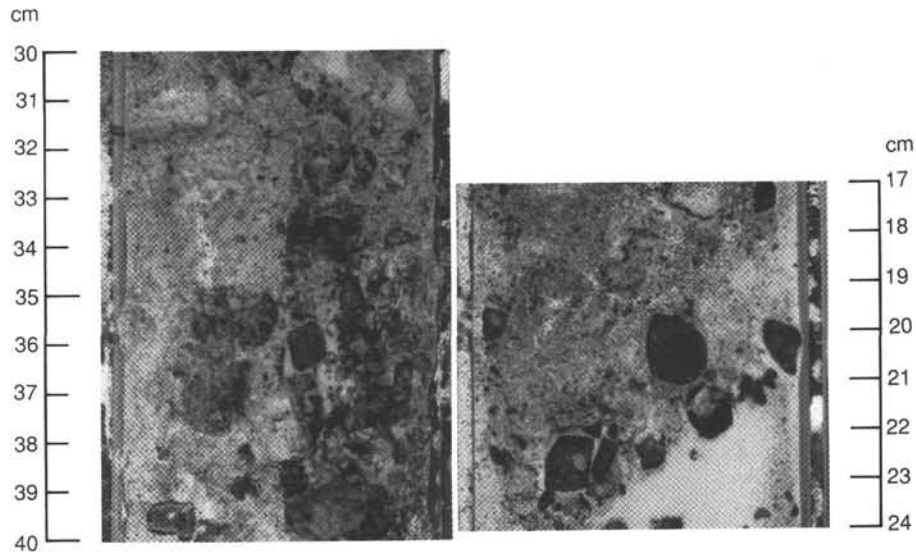

Figure 9. Lag deposit of ice-rafted and volcanic debris in Cores 120-749A-1H, 30–40 cm, and 120-749B-1H, 17–24 cm.

Unit II: Nannofossil Ooze and Chalk with Chert and Porcellanite

Interval: Core 120-749B-1H-1, 24 cm to TD, and Cores 120-749C-1R to 120-749C-10R-CC.
Depth: 0.24–202.0 mbsf (note that the position of the sediment/basement contact at 202.0 mbsf is based on a decrease of penetration rate).
Total thickness: 201.76 m.
Age: late Oligocene to early Eocene.

Unit II is composed of very white (10YR 8/1) nannofossil ooze and chalk with chert and porcellanite. It has been divided into two subunits (IIA and IIB) based on the first occurrence of chert.

Subunit IIA: Nannofossil Ooze with Foraminifers

Interval: Core 120-749A-1H-1, 40 cm, to TD and Cores 120-749B-1H-1, 24 cm, to 120-749B-6H-1, 0 cm.
Depth: 0.4–9.5 mbsf (TD) (Hole 749A) and 0.24–43.56 mbsf (Hole 749B).
Thickness: 9.1 m (Hole 749A) and 43.56 m (Hole 749B).
Total thickness: 43.56 m.
Age: late Oligocene to middle Eocene

Subunit IIA is primarily composed of white nannofossil ooze with foraminifers and foraminifer nannofossil ooze. Foraminifer content increases downhole from less than 10% in Cores 120-749A-1H and 120-749B-1H to 20% in Core 120-749B-5H (Fig. 10). The mean grain size increases from 14.8 μm to an average of 29.3 μm, reflecting the change in foraminifer abundance (Fig. 10 and Table 3). Wet-bulk density measurements reflect the homogeneous nature of this subunit (Fig. 10).

Intervals slightly enriched in diatoms are distinguishable by their creamy white color and occur in the upper portion of this subunit in Cores 120-749B-2H-2, 88–95 cm; 120-749B-2H-4, 0–30 cm and 95-135 cm; and 120-749B-2H-6, 45–95 cm. These influxes are reflected in the upper 30 m of the hole by the percentage of carbonate depletions (Fig. 10). Siliceous microfossils are rare in Core 120-749B-4H (24.8–34.3 mbsf) and completely absent in Core 120-749B-5H (34.3–43.8 mbsf) (Fig. 10).

Volcanic ash appears in Cores 120-749B-2H-1, 114–118 cm, and 120-749B-3H-2, 50–70 cm, but it represents less than 1% of the sediment. Authigenic pyrite occurs as rare, black flaky specks scattered throughout Cores 120-749B-2H to 120-749B-3H-2, 0–27 cm. Bivalve fragments of a small oyster species (see "Biostratigraphy" section, this chapter) are present in Cores 120-749B-3H-1, 112 cm, and 120-749B-4H-2, 43 cm.

A noncalcareous opaque mineral occurs as rare yellow specks scattered throughout Sections 120-749B-4H-6, 120-749B-5H-1, and 120-749B-5H-2. Two horizontal burrows, one in Core 120-749B-4H-6, 99 cm, and the other in Core 120-749B-5H-2, 128 cm, have been replaced by this material. Examination of the mineral by scanning electron microscope (SEM) showed that the burrows are filled with crenulated, authigenic smectite (as illustrated by Welton, 1984, p. 72), but mineral determination of the outer crust has not been made. Bioturbation is slight throughout Subunit IIA and the burrows appear as faint tan mottles. A few burrows are outlined in purple (e.g., Cores 120-749B-5H-4, 102–104 cm, and 120-749B-5H-7), which is caused by authigenic pyrite.

Subunit IIB: Nannofossil Ooze and Chert

Intervals: Core 120-749B-6H-1 to TD and Cores 120-749C-1R to 120-749C-10R-CC.
Depth: 43.6–123.8 mbsf (TD) (Hole 749B) and 102.0–202 mbsf (Hole 749C).
Thickness: 80.0 m (Hole 749B) and 100.0 m (Hole 749C).
Total thickness: 158.2 m.
Age: middle to early Eocene.

Subunit IIB is composed of nannofossil ooze, nannofossil ooze with foraminifers, nannofossil chalk with foraminifers, chert, and porcellanite. The pelagic sediments making up this subunit are generally white (10YR 8/1). Intervals appear cream/white where foraminifer abundance increases. Foraminifer abundance decreases from 25% to an average of 8% between Cores 120-749B-7X (53.3 mbsf) and -9H (72.3 mbsf) (Fig. 10) and is generally less than 10% except for isolated intervals.

Siliceous microfossils are absent from this subunit except in Cores 120-749B-7X and -9H, where sponge spicules and radiolarians form 3% of the ooze. A few corroded sponge spicules occur in Cores 120-749C-7R and -10R. Chert of black, dark grayish brown or olive color is common throughout this subunit. Chalk patinas are commonly found on chert and porcellanite fragments and foraminifer ghosts are observed in some cherts. Some chert is banded or laminated.

Bluish gray to purple splotches composed of flaky authigenic pyrite (generally $<2\%$) are found scattered throughout Cores 120-749B-7X and -9H and Cores 120-749C-7R and -10R. In

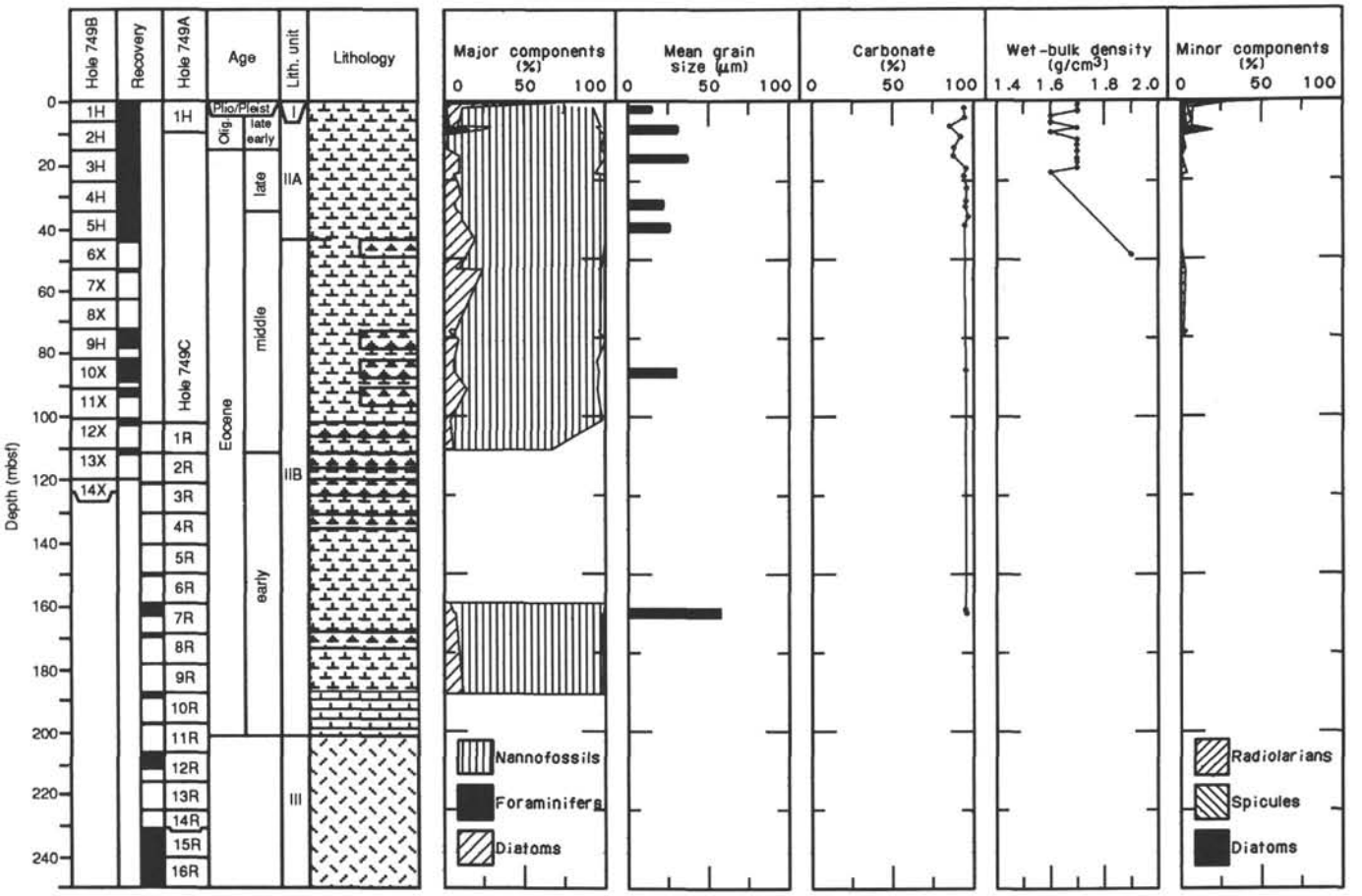

Figure 10. Lithologic summary, Site 749. Downhole mean grain size plotted vs. sub-bottom depth, measured with a Labtec 100, laserscan automatic particle-size analyzer; summary plots of downhole smear slide data and ash levels; downhole variation of carbonate and wet-bulk density measurements plotted vs. sub-bottom depth; and gamma-ray and sensitivity logs showing basal units.

Table 3. Mean grain size and percentages of sand, silt, and clay fractions of Site 749 shipboard samples.

Core, section, interval (cm)	Depth (mbsf)	Mean grain size (μm)	Sand (%)	Silt (%)	Clay (%)
120-749B-					
1H-2, 50–52	2.00	14.8	3	79	18
2H-2, 48–50	7.78	30.3	19	52	9
3H-2, 27–29	17.07	36.6	25	68	7
4H-5, 62–64	31.42	21.0	10	71	19
5H-4, 49–51	39.29	25.2	14	71	15
10X-3, 50–52	85.30	29.9	17	76	7
120-749C-					
7R-2, 68–70	161.18	58.1	52	45	3

some intervals, this coloration highlights and outlines burrows and mottling features. Other observed structures found in the ooze were centimeter-scale laminae in Core 120-749C-7R-2, 18–19 cm, and lenticular laminae on a millimeter scale in Core 120-749C-7R-2, 34–35 cm, 51–52 cm, and 74–75 cm. These laminations are bluish gray to purple in color and contain traces of authigenic pyrite.

Unit III: Basalt

Interval: Core 120-749C-11R-CC to TD.
Depth: 202–249.5 mbsf (TD).
Thickness: 47.5 m.
Age: Undetermined.

There were no obvious downhole gradients within Unit II that signaled the sediment/basement contact apart from the decrease in penetration rate at 202 mbsf (see "Igneous Petrology" section, this chapter). Poor recovery, however, may have masked any definable changes. The contact is consistent with the seismically apparent onlapping pelagic sequence, possibly developed on a long-exposed basement high.

Correlation of Units among Leg 120 Sites

The lithology of Unit II at Site 749 is similar in age and character to those of corresponding units recognized at Sites 747 and 748 (Fig. 11). However, these units are not stratigraphically contiguous. Seismic reflection profiles show that they are separated by distinctive structural features such as faults and basins as follows (see "Site Geophysics" sections for Sites 747, 748, and 749 chapters):

1. Site 747 lies in the transition zone between the Northern and Southern Kerguelen Plateaus;
2. Site 748 lies east of a major tectonic feature, the 77°E Graben in the Raggatt Basin; and
3. Site 749 lies west of the 77°E Graben on the Banzare Bank.

Subunit IIA is similar at all the sites. The facies is primarily composed of nannofossil ooze and nannofossil ooze with foraminifers in shades of white from snow white to creamy white. Subunit IIA ranges from middle Eocene to late Miocene in age and is overlain by 1–34 m of diatom ooze. The facies averages

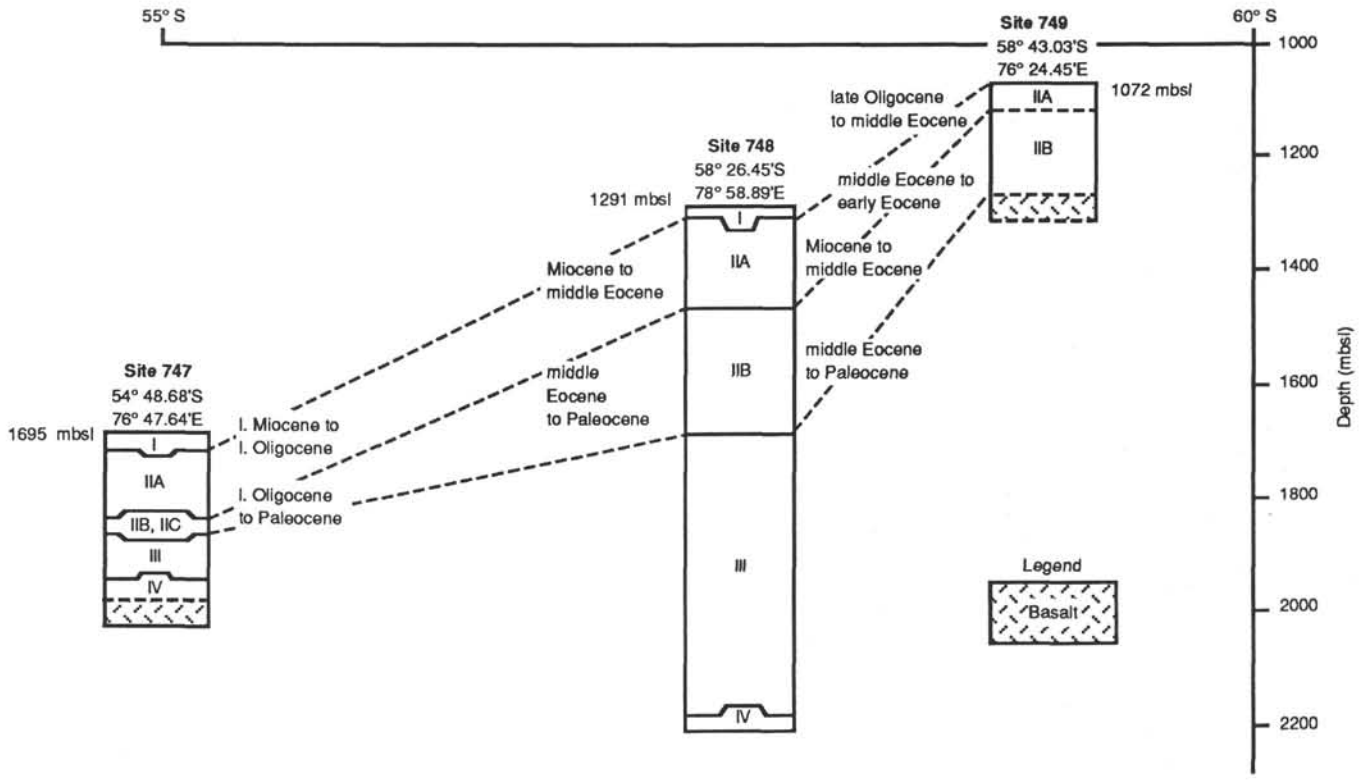

Figure 11. Correlation diagram of lithostratigraphic columns of Unit II in Sites 747, 748, and 749. This diagram is based on lithologic and age similarities and not on stratigraphic continuity.

about 125 m thick between Sites 747 and 748; it appears to thin toward Site 749, decreasing in thickness to 44 m. The thinning of Subunit IIA at Site 749 is probably caused by erosion of the upper layers of pelagic sediments since an unconformity occurs at the top of the subunit (see "Sedimentation Rates" section, this chapter).

Subunit IIB is primarily composed of nannofossil ooze and chalk in colors of pale brown and shades of white from snow white to creamy white with variable chert abundance. The lithology of this subunit is very similar at Sites 748 and 749 in spite of the poor recovery. Cherty horizons at Site 748 and 749 do not extend to Site 747. The cherty facies is Paleocene to middle Eocene in age and contains a middle Eocene unconformity.

Subunits IIB and IIC at Site 747 are buried by less than 160 m of pelagic ooze. At Sites 748 and 749, Subunit IIB is overlain by less than 180 and 44 m of pelagic ooze, respectively. The equivalent of the cherty Subunit IIB (Subunits IIB and IIC) at Site 747 is 32 m thick and appears to thicken southward to an average of 140 m at Site 748 and 749. The degree of chalk lithification appears similar at Sites 747 and 748 but less at Site 749. The lithification is related to depth of burial of the sediment.

The basal part of the sequence at Site 749 is much younger than at the other two sites. This indicates a significant pre-middle Eocene period of nondeposition/erosion of the basement high at Site 749.

BIOSTRATIGRAPHY

Introduction

Site 749 is located on the western flank of the Banzare Bank on the Southern Kerguelen Plateau. It lies at 58°43.03'S, 76°24.45'E in 1069.5 m water depth. This site was drilled with the main objective of penetrating 200 m of basement, yet it provided valuable stratigraphic and sedimentologic information as well.

Three holes were cored. Cores 120-749A-1H and 120-749B-1H were taken in an (unsuccessful) attempt to obtain the mud line. Five APC cores with full recovery were obtained from Hole 749B; subsequently, one APC and eight XCB cores with poor recovery were taken. As penetration and retrieval problems increased with depth, rotary coring operations were used below 123.8 mbsf. Hole 749C was washed down to 102 mbsf, then cored through 100 m of calcareous nannofossil oozes and cherts before basement was reached at 202 mbsf.

Except for a thin cover (about 30 cm) of lower Pleistocene and condensed mid-Pliocene foraminifer and diatomaceous sands and oozes with coarse ice-rafted material, the entire stratigraphic record recovered at Site 749 is Paleogene, extending from the upper Oligocene (in Core 120-749A-1H, 38 cm, and Core 120-749B-1H, 24 cm) through the lower Eocene (in Core 120-749C-10R-CC). Contact between basement and sediment was not retrieved. The oldest sediment recovered (Core 120-749C-10R-CC) represents the early Eocene calcareous nannofossil Biozone NP12 and is estimated to be 54–55 Ma (Berggren et al., 1985a, 1985b).

Planktonic foraminifers and calcareous nannoplankton provided the main biostratigraphic control, complemented by diatoms for the Oligocene and silicoflagellates for the middle Eocene. Radiolarians occur throughout, but poor recovery of middle and lower Eocene sediments because of drilling problems in chert formations precludes establishment of precise correlations between calcareous and siliceous groups. Biostratigraphic results are summarized in Figure 12.

Planktonic Foraminifers

There were three holes at Site 749: first, a surface HPC core (120-749A-1H); next, Hole 749B, from which a mud line core,

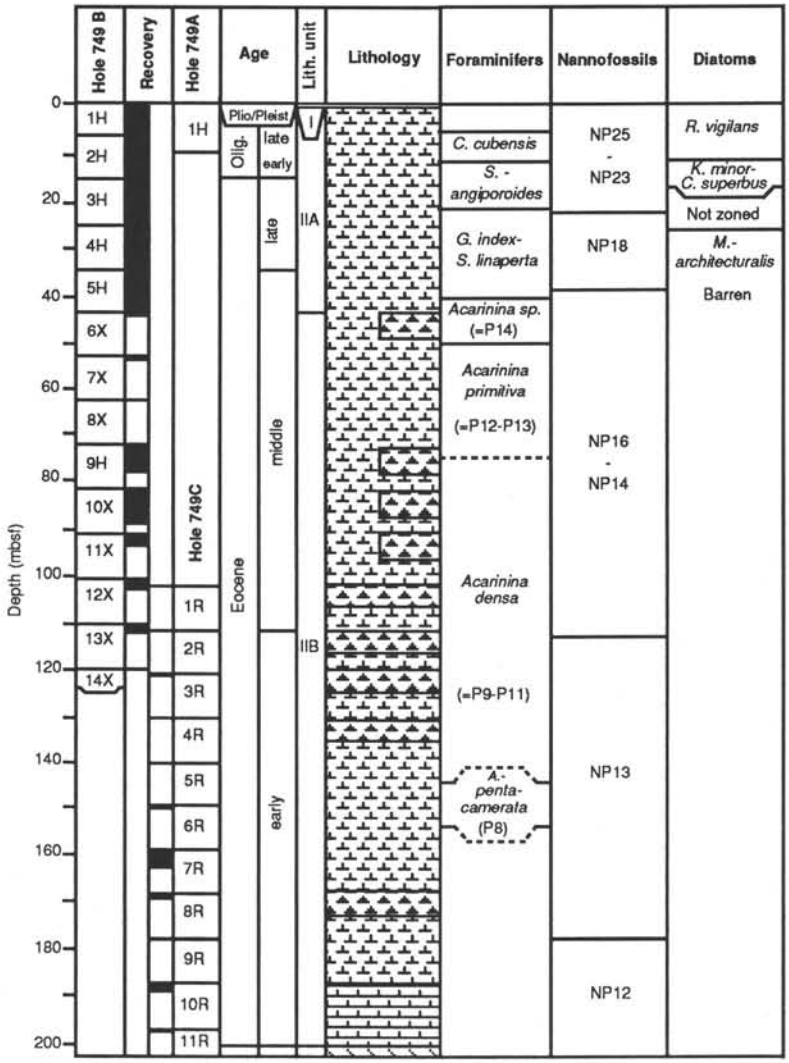

Figure 12. Biostratigraphic summary of Site 749.

5 full HPC cores, and 9 additional cores were taken. Finally, penetration (and retrieval) problems in the middle Eocene cherts, comparable to those experienced at Site 748, required a change to rotary coring at 102 mbsf and a series of 16 cores were obtained in Hole 749C.

The Paleogene stratigraphic sequence at Site 749 starts in the upper Oligocene (except for a superficial interval >0.5 m thick of Pliocene-Pleistocene foraminifer and diatomaceous sands and oozes with ice-rafted detrital material ranging in size from gravel to sand-silt size). The fauna in Sample 120-749A-1H-CC is of middle Oligocene age and is characterized by *Globigerina brazieri, G. woodi, Catapsydrax dissimilis,* and *Chiloguembelina cubensis.* The fauna in Sample 120-749B-1H-CC is similar but chiloguembelinids are absent in the fine fraction. Thus, the last appearance datum (LAD) of *Chiloguembelina* occurs in the stratigraphic interval between Cores 120-749A-1H-CC (10.04 mbsf) and 120-749B-1H-CC (5.8 mbsf). This event (around 30 Ma) has been used in interpreting the magnetic stratigraphy at this site, specifically in identifying Anomaly Correlative 10, centered at about 8 mbsf (Berggren et al., 1985a, 1985b; see "Paleomagnetics" and "Sedimentation Rates" sections, this chapter).

Core 120-749B-2H-CC contains an early Oligocene fauna characterized by, among others, *Subbotina angiporoides, Globigerina brazieri, G. brevis, Chiloguembelina cubensis, Tenuitella gemma,* and *T. munda;* it belongs to the *S. angiporoides* Zone. The overlap of *Chiloguembelina cubensis* and *Subbotina angiporoides* indicates an early Oligocene age older than Anomaly Correlative 10; the LAD of *S. angiporoides* (around 32 Ma) at this level has been used in the identification of Anomaly Correlative 11, which extends from about 11 to 14 mbsf (see "Magnetostratigraphy" and "Sedimentation Rates" sections, this chapter).

The Eocene/Oligocene boundary lies within Core 120-749B-3H based on the LADs of *Subbotina linaperta* and *Globigerapsis index* in addition to *Paragloborotalia nana, Subbotina hagni,* and abundant chiloguembelinids in Core 120-749B-3H-CC. Similar faunas occur in Cores 120-749B-4H-CC and 120-749B-5H-CC.

The LAD of *Acarinina* spp. in Core 120-749B-5H-CC indicates the proximity of the middle/late Eocene boundary. Subbotinids (*S. linaperta*), globigerapsids (*Globigerapsis index*), and acarininids (*Acarinina primitiva* and *A. collactea* spec. div.) characterize middle Eocene Samples 120-749B-6X-CC and 120-749B-7X-CC, and the interval is placed in the *Acarinina primitiva* Zone. The youngest occurrence of *Acarinina densa, A. pentacamerata,* and *Pseudohastigerina wilcoxensis* in Core 120-749B-9X-CC suggests a level within the early to middle part of the Lutetian because of the absence of *Globigerapsis index,* which has its first appearance datum (FAD) at a level approxi-

mately equivalent to Zone P11 (Toumarkine and Luterbacher, 1985).

Similar faunas extend down from Cores 120-749B-10X-CC through 120-749B-14X-CC. *Globigerapsis senni* has been observed in Core 120-749B-10X-CC. Inasmuch as many of the taxa observed in this sequence (Cores 120-749B-10X to -14X) range from the late early Eocene into the middle Eocene, it is not possible at the present stage of investigation to determine whether the early/middle Eocene boundary is located within this sequence.

Hole 749C was rotary cored from 102 mbsf and in part overlaps Core 120-749B-12X. There was essentially no recovery, apart from chert fragments, until Core 120-749C-6R-CC, which contains an early Eocene (P8) fauna characterized by *Acarinina pentacamerata,* the *A. wilcoxensis-A. pseudotopilensis* group, *Subbotina linaperta, S. patagonica, Planorotalites chapmani, P. australiformis* and neither *A. densa* (indicative of Zone P9) or pseudohastigerinids (the FAD of which we observed elsewhere on the Kerguelen Plateau at a level correlative with [?lower] Zone P8). This fauna is joined by *Acarinina coalingensis* and *A. soldadoensis* in Cores 120-749C-7R-CC and 120-749C-8R-CC.

There was no recovery in Core 120-749C-9R-CC, and the lowest fossiliferous core (120-749C-10R-CC) contains a similar early Eocene fauna of acarininids (*A. coalingensis, A. angulosa, A. pentacamerata, A. soldadoensis, A. pseudotopilensis,* and *A. wilcoxensis*), subbotinids (*S. patagonica*), planorotaliids (*P. australiformis*), and chiloguembelinids. We have placed this lower intra-chert interval (Cores 120-749C-7R to -10R) below the level of no recovery (120-749C-3R to -8R) in an "*Acarinina wilcoxensis* Zone." This is not a formally designated zone, but it is meant simply to denote an interval characterized by a taxon restricted to the early Eocene and whose range does not overlap *A. densa,* which is characteristic of Zone P9.

In summary, the main planktonic foraminifer biostratigraphic results obtained at Site 749 include:

1. Recovery of a relatively complete, if strongly condensed, upper Eocene–upper Oligocene interval, and an extended middle Eocene and a highly expanded lower Eocene section, suggestive of high rates of sedimentation/accumulation;
2. A typically temperate to high-latitude Eocene-Oligocene fauna with no evidence of tropical, low-latitude faunal elements at any level; and
3. Magnetostratigraphic correlation that indicates the presence of Anomaly Correlatives 10 and 11 in the Oligocene at Site 749. This will enable us to make rather precise correlation within the Oligocene between Sites 749 and 748 as well as with Site 747.

Benthic Foraminifers

All core-catcher samples of Holes 749B and 749C were analyzed for their benthic foraminifer content. In addition, the mud-line sample (120-749B-1H, 0–2 cm) was studied after being stained with Rose Bengal. Benthic foraminifers are generally well preserved and abundant in all samples; however, they are rare in comparison with planktonic foraminifers. About 100 specimens in each sample were picked from the >125-μm fraction.

The following benthic foraminifer assemblages were recognized in the sedimentary sequence of Holes 749B and 749C. These assemblages are defined and numbered according to the criteria and stratigraphic boundaries established for Sites 747 and 748 (see Fig. 13).

Assemblage 1a: Pleistocene

This assemblage is represented by Sample 120-749B-1H, 0–2 cm. The fauna is dominated by *Trifarina earlandi* and *Bulimina aculeata. Melonis pompilioides, Cibicidoides wuellerstorfi, Pullenia bulloides,* and *Oridorsalis* sp. cf. *O. umbonatus* are additional frequent constituents. Rare components are *Pyrgo murrhina* and *Pyrgo* sp., *Trochammina globulosa, Eggerella bradyi, Gyroidina soldanii, G. lamarckiana, Cassidulina teretis, Eponides tumidulus, Parafissurina* sp., *Lenticulina* sp., and *Fissurina orbignyana.* A large piece of a tubiform *Marsipiella*-like agglutinated specimen was identified.

It is noteworthy that no stained (live) specimens were observed, although a representative number of benthic foraminifers was investigated. This suggests that this so-called mud-line sample originates from at least 2 to 5 cm below the sediment/water interface. Recent investigations of similar faunas on the continental slope of the eastern Weddell Sea have shown that stained (live) specimens of some specific taxa are found down to 5–7 cm within the sediment (Mackensen and Douglas, in press). However, the benthic foraminifer assemblage of this sample closely corresponds to the assemblage of Sample 120-748B-1H-CC (0.20 mbsf), which is at least 0.62 m.y. old (see "Biostratigraphy" section, "Site 748" chapter, this volume). This agrees well with dating by means of diatoms, which indicates an early Pleistocene age below the uppermost few centimeters.

Assemblage 3: Late Oligocene–Late Eocene

The upper boundary of this assemblage was taken at the last occurrence (LO) of *Nuttallides umbonifera,* as it was at Sites 747 and 748. At Site 749, the boundary probably coincides with a major unconformity at about 0.30 mbsf, between the Pleistocene mud-line sample and upper Oligocene Sample 120-749A-1H-CC. Samples 120-749A-1H-CC, 120-749B-2H-CC, and 120-749B-3H-CC are grouped in this assemblage. In Sample 120-749A-1H-CC, *N. umbonifera* is rare; we did not find it in Sample 120-749B-2H-CC, but it was a common constituent of the fauna in Sample 120-749B-3H-CC.

Other common constituents of this assemblage are *Pullenia bulloides, P. subcarinata, Globocassidulina subglobosa, Oridorsalis umbonatus, Cibicidoides mundulus, Stilostomella* spp., and *Trifarina* sp. cf. *T. fluens. Laticarinina pauperata* is frequent in Cores 120-749A-1H-CC and 120-749B-2H-CC but not in the upper Eocene sample (120-749B-3H-CC). *Pleurostomella* sp., *Fissurina* spp., *Gyroidina* sp., *Karreriella bradyi, Trifarina* sp. cf. *T. earlandi, Vulvulina spinosa,* and *Spiroplectammina cubensis* are rare accessory components throughout the sequence.

In Sample 120-749A-1H-CC, a few specimens of *Bulimina mexicana* are present. The known stratigraphic range of this species is reported from lower Miocene to Pleistocene, which is in contrast with the early late Oligocene age of this sample.

Turrilina alsatica is one of the characteristic and most abundant species in Sample 120-749B-2H-CC, which is dated by means of planktonic foraminifers as early Oligocene. Denser sampling of the Oligocene sequence should be undertaken to define the LO of this species more precisely. This is interesting because this taxon is widely used in the northern Atlantic (northern Europe and Labrador continental margin) for identifying the Paleogene/Neogene boundary. However, a hiatus encompassing much of the late Oligocene is present there. This is similar to the situation at Site 749. This species was also found at Site 647 in the Labrador Sea, where it characterizes a benthic foraminifer assemblage zone at the top of the Paleogene (Kaminski et al., in press).

In Sample 120-749B-3H-CC, a form that is a common component of the microfossil assemblage could not be identified on board the ship. Most likely this form belongs to *Bolboforma,* regarded as a cyst stage of an unknown fossil group (possibly calcitic Chrysomonodales [Algae]), which is thought to be of planktonic origin (see Mackensen and Speigler, this volume).

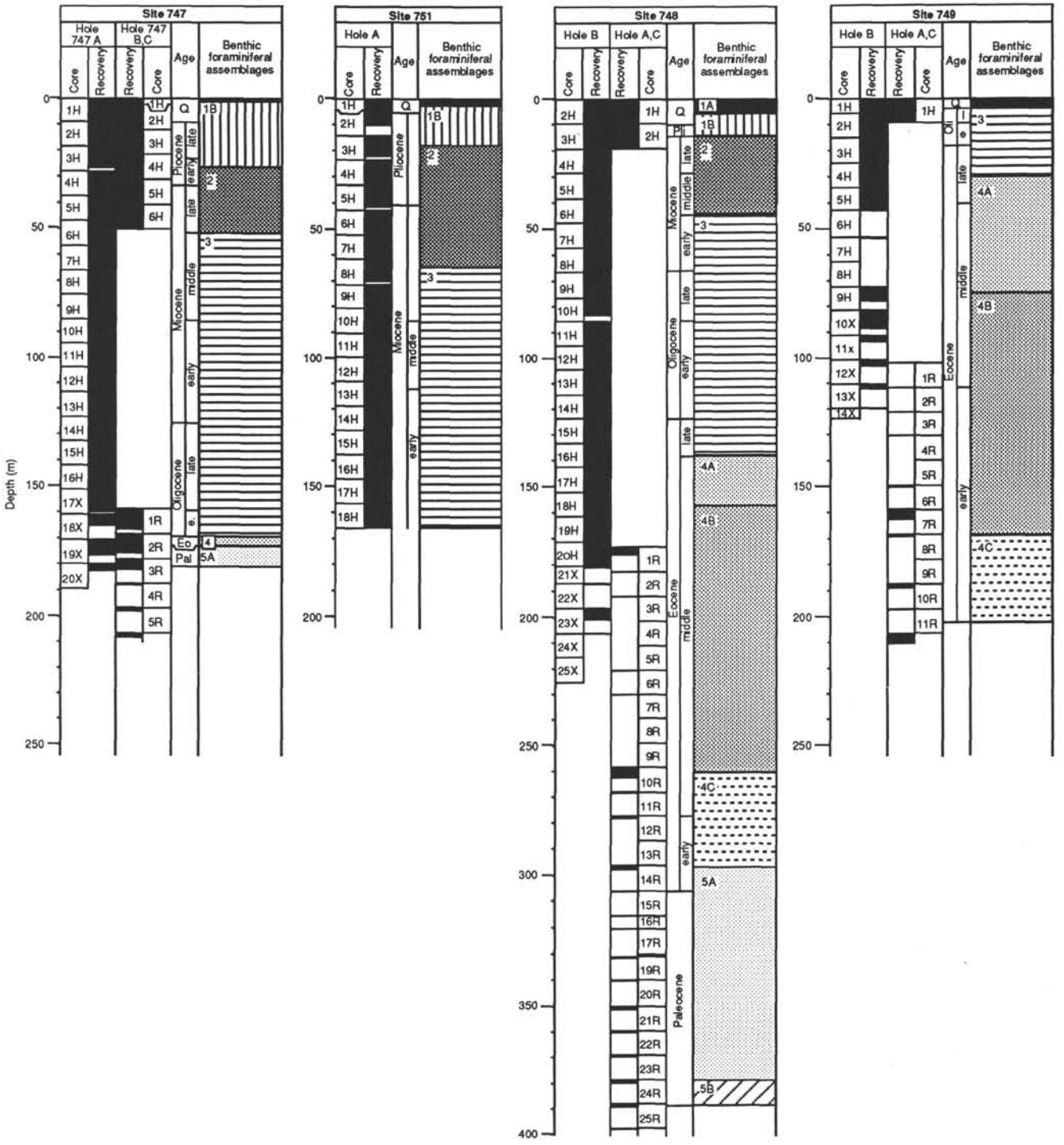

Figure 13. Correlation of benthic foraminifer faunal assemblages of Sites 747, 748, and 751. See text for discussion of Assemblages 1 to 5.

Assemblage 4a: Late to Middle Eocene

Samples 120-749B-4H-CC through 120-749B-7H-CC are grouped in this assemblage. At the previous Leg 120 sites, the upper boundary was defined by the LOs of *Nuttallides truempyi* and *Bulimina elongata*. As pointed out in the Site 748 chapter, *N. truempyi* is a typical lower bathyal to abyssal species that was rare at shallower (middle to upper bathyal) depths, especially during the late Eocene. At Site 749 with a present water depth of 1072 m (218 m shallower than Site 748), *N. truempyi* was not found in the uppermost samples of this assemblage. Consequently, the upper boundary is taken at the LO of *Bulimina elongata*.

Nuttallides truempyi was not found in the middle Eocene below Sample 120-749B-7H-CC. *Bulimina elongata* is frequent in the upper part of this section whereas it is rare in the lower part. In contrast with what was observed at Site 748, *Bulimina alazanensis* becomes here the most abundant buliminid in the middle part of this assemblage zone. *Nuttallides umbonifera* is found in very low numbers down to Sample 120-749B-4H-CC.

In other respects, the fauna is comparable to the benthic foraminifer assemblages at the previous Leg 120 sites. *Stilosto-*

mella spp. are abundant throughout the section. *Cibicidoides praemundulus, Alabamina dissonata, Gaudryina* sp., *Gyroidina* spp., *Anomalinoides semicribratus, Lenticulina* sp., and *Osangularia mexicana* are common. *Karreriella* sp., *Uvigerina* sp. cf. *U. hispidocostata, Turrilina brevispira, Trifarina* spp., *Pleurostomella* spp., *Fissurina* spp., *Lagena* spp., *Vulvulina mexicana, V. spinosa, Oridorsalis umbonatus, Stensioina micra, Plectina elongata, Chilostomella*? sp., *Globocassidulina subglobosa, Pullenia eocaenica,* and *Anomalina spissiformis* are accessory components in most samples. In some samples, fragments of *Saccorhiza ramosa* were identified.

Assemblage 4b: Middle Eocene

The upper boundary of this assemblage is defined by the LO of *Bulimina bradburyi.* Because there was no recovery in Core 120-749B-8H, this assemblage boundary is situated somewhere between Samples 120-749B-7H-CC and 120-749B-9H-CC (between 62.8 and 81.8 mbsf). This assemblage is present in Samples 120-749B-9H-CC through 120-749B-14H-CC, as well as in Samples 120-749C-6R-CC and 120-749B-7R-CC. Cores 120-749B-1R to -5R were without recovery; Sample 120-749B-14X-CC only yielded a piece of chalk and chert, which was insufficient for a quantitative benthic foraminifer analysis.

Bulimina bradburyi, Oridorsalis umbonatus, Osangularia mexicana, Lenticulina spp., *Alabamina dissonata, Cibicidoides subspiratus, Stilostomella* spp., *Plectina elongata, Anomalinoides capitatus,* and *Turrilina brevispira* are common constituents. Frequent accessory components are *Anomalina spissiformis, Spiroplectammina spectabilis, Vulvulina spinosa, Vaginulina* spp., *Tritaxia* sp., *Pullenia eocaenica,* and, in Sample 120-749C-7R-CC, *Nuttallides truempyi.* Some of the rare components are *Hanzawaia cushmani, Cibicidoides eocaena, Lagena* spp., *Pleurostomella* spp., *Nonionella*? sp., *Trifarina* sp., *Gyroidina* sp., *Bulimina alazanensis, B. macilenta, Nodosaria* sp., *Vulvulina mexicana, Spiroplectammina subhaeringensis, Karreriella chapapotensis,* and *Aragonia velascoensis.*

Assemblage 4c: Early Eocene

The main constituents of the middle Eocene fauna remain the same in the early Eocene, but *Bulimina alazanensis* and *B. macilenta* do not occur. Their early Eocene predecessor is *Bulimina trinitatensis.* Samples 120-749C-8R-CC and 120-749C-10R-CC are grouped together in this assemblage, Core 120-749C-9R was empty, and Core 120-749C-11R hit basement with 0.11-m recovery.

The upper boundary of this assemblage is defined by the LO of *B. trinitatensis. Tappanina selmensis* occurs in addition to the common species of Assemblage 4b. *Anomalinoides semicribratus* still occurs commonly in this early Eocene assemblage. It is reported from Zone P12 to N14 (Van Morkhoven et al., 1986). Samples 120-749C-8R-CC and 120-749C-10R-CC are dated by means of planktonic foraminifers and nannofossils as P8–P7 and NP13 and NP12, respectively. Consequently, it may be necessary to adjust the FAD of this stratigraphically important marker for this latitude.

In summary, all benthic foraminifer assemblages tentatively distinguished at the two previous Leg 120 sites were recognized at Site 749 within their correct stratigraphic ranges (Fig. 13). Different proportions between species and slightly different compositions of the assemblages reflect differences in environmental conditions between sites, which are, to a first approximation, mainly related to water depth. Throughout the Cenozoic, Sites 748 and 749 seem to have remained in a water depth range similar to their present lower bathyal water depth. Closer sampling will help to establish more detailed paleoecologic reconstructions, based on relatively well-known environmental factors limiting the distribution of similar living subpolar assemblages (Mackensen et al., 1985; Mackensen, 1987).

In addition, the preliminary data from these three sites contribute new and basic information to the worldwide efforts toward a Paleogene and Neogene benthic foraminifer stratigraphy (Van Morkhoven et al., 1986; Berggren and Miller, in press).

Calcareous Nannofossils

The foraminifer and diatomaceous sands and oozes that constitute the upper 30 cm of Cores 120-749A-1H and 120-749B-1H were not analyzed for their calcareous nannofossil content.

Biostratigraphic subdivision of the lower Oligocene through lower Eocene calcareous nannofossil oozes recovered at Site 749 is based primarily on the analysis of core-catcher samples. Poor recovery from Core 120-749B-6H to the bottom of Hole 749C hampers precise biostratigraphic control for most of the middle and lower Eocene interval. However, biostratigraphic intervals (e.g., lower middle Eocene) that were not obtained at Sites 747 and 748 apparently were recovered at Site 749.

Calcareous nannofossils were abundant and generally well preserved in Oligocene and middle Eocene oozes. In lower Eocene oozes (Cores 120-749B-14X to 120-749C-10R), preservation was variable and calcareous nannofossils seem to have been sorted out according to size (the large discoasters such as *Discoaster lodoensis* and the large placoliths of taxa such as *Chiasmolithus expansus* or *Toweius magnicrassus* are exceedingly rare).

A late early or late Oligocene age is assigned to Core 120-749A-1H-CC and Cores 120-749B-1H-CC to 120-749B-2H-CC. Assemblages are dominated by *Reticulofenestra bisecta, R. floridana, Reticulofenestra* sp. cf. *R. hampdenensis, Chiasmolithus altus,* and *C. oamaruensis* and are indicative of Zones NP23–NP25 undifferentiated. Cores 120-749B-3H-CC and 120-749B-4H-CC yield typical late Eocene assemblages indicative of Zone NP18, with *Chiasmolithus oamaruensis, Neococcolithes dubius, Reticulofenestra umbilica, R. hillae,* and *R. bisecta.*

In Core 120-749B-5H-CC, calcareous nannofossil assemblages are more diversified and characterize the middle Eocene Zone NP16. Rapid biozonal succession between Cores 120-749B-1H and 120-749B-5H suggests either a very slow sedimentation rate or the development of an unconformity or unconformities. Shore-based studies of very closely spaced samples will provide further information concerning biostratigraphic continuity/discontinuity over this Oligocene–middle Eocene interval.

Typical middle Eocene assemblages occur from Cores 120-749B-5H-CC to 120-749B-13X-CC. Delineation of the NP15/NP16 zonal boundary is difficult because of the absence of the primary zonal marker (*Rhabdosphaera gladius*), as in most oceanic sections, and also because of the absence of secondary markers that are useful at low and temperate latitudes and the scarcity of *Nannotetrina fulgens.* The occurrence of this latter taxon in Core 120-749B-10X-CC probably indicates Zone NP15.

Discoaster sublodoensis (common) occurs in Cores 120-749B-12X-CC and 120-749B-13X-CC. Core 120-749B-12X-CC is assigned to the upper part of Zone NP14; Core 120-749B-13X-CC to its lower part (based respectively on the absence or presence of *Discoaster lodoensis* and *D. kuepperi*). Thus, the lower/middle Eocene boundary (Ypresian/Lutetian boundary) occurs within Core 120-749B-13X (at about 119 mbsf) (Aubry, 1983).

Calcareous nannofossil assemblages in Core 120-749B-14X-CC are nondiagnostic. In this sample, calcareous nannofossils are rather poorly preserved and a size sorting (as described above) is observed.

There was no recovery from Cores 120-749C-1R and -5R. A few pieces of chert were recovered in Cores 120-749C-2R, -3R, and -4R. Smear slides were prepared from the calcareous nannofossil oozes that encrust the chert. However, as a result of intense silicification, few calcareous nannofossils are preserved in these oozes, and no diagnostic species were found, except the late

early Eocene *Toweius magnicrassus*. Cores 120-749C-6R to -8R yield abundant calcareous nannofossils, moderately to poorly preserved and exhibiting size sorting (as described above). This interval is assigned to Zone NP13 despite the exceedingly rare occurrence of *Discoaster lodoensis* in Samples 120-749C-6R-CC and 120-749C-8R-CC.

There was no recovery from Core 120-749C-9R. Core 120-749C-10R-CC yields a calcareous nannofossil assemblage typical of Zone NP12 with common *Tribrachiatus orthostylus* and *Discoaster lodoensis*. This is the deepest sediment recovered above basalt in this hole. There was very poor recovery from Cores 120-749C-11R, -12R, and -13R. No calcareous nannofossil oozes were recovered from these cores, but 10 cm of mixed cuttings were recovered at the top of Core 120-749C-12R. Smear slides were prepared from material sampled at 2 and 9 cm in this core in order to check for the presence of calcareous nannofossils and, if affirmative, the possible occurrence of species indicative of levels older than those recovered. Both samples yielded a mixture of Oligocene and late to early Eocene calcareous nannofossil taxa. No forms older than those observed in Sample 120-749C-10R-CC were observed. Thus, it can be established confidently that the oldest sediment overlying basement at Site 749 is of early Eocene age and belongs to Zone NP12. Based on the age of the LAD of *Tribrachiatus orthostylus* (Berggren et al., 1985a, 1985b), its age is estimated at 54–55 Ma.

In summary, the main calcareous nannofossil biostratigraphic results obtained at Site 749 include:

1. recovery of a relatively complete, thick, upper Oligocene to lower Eocene section with an expanded lower Eocene sequence and a probable middle/upper Eocene unconformity;
2. characterization of rich, typically temperate to high-latitude, early middle Eocene calcareous nannofossils; and
3. assignment of the oldest sediments resting on basement to the lower Eocene calcareous nannofossil Zone NP12, with an estimated age of 54–55 Ma (which does not imply, in this geological context, that the underlying basalt is of the same age).

Radiolarians

At Site 749, core-catcher Samples 120-749A-1H-CC, 120-749B-1H-CC through 120-749B-4H-CC, 120-749B-7X-CC, and 120-749B-9H-CC contain few to abundant, moderately to well-preserved Paleogene radiolarians. Neogene age indicators are not observed in these samples.

Hole 749A

Only one core was recovered. Abundant radiolarians are seen in Sample 749A-1H-CC, which includes *Calocyclas semipolita, Cyclampterium milowi, Eucyrtidium* sp. of Chen (1975), and *Cyrtocapsella* sp. cf. *C. longithorax*. This assemblage is similar to those of Samples 120-748B-11H-CC through 120-748B-13H-CC and of the lower Oligocene of Site 274 (Chen, 1975).

Hole 749B

Sample 120-749B-1H-CC contains specimens of *C. semipolita* with short abdomens, *Lychnocanium* sp. (*Lynchnocanella conica* of Petrushevskaya, 1975), *Sethoconus* sp. of Hays (1965), and abundant *Stylosphaera*(?) sp. This assemblage resembles that of Sample 120-748B-9H-CC. The age of Core 120-748B-9H is late Oligocene. Sample 120-749B-2H-CC includes *C. semipolita, C. milowi*(?), *Sethoconus* sp. of Hays (1965), *C.* aff. *longithorax*, and *Eucyrtidium* sp. of Chen (1975). This assemblage is similar to those of Core 120-749A-1H-CC and of the lower Oligocene of Chen (1975).

Samples 120-749B-3H-CC and 120-749B-4H-CC contain *C. milowi*(?), *Lychnocanoma amphitrite, Periphaena* sp., and *Stylacontarium* sp. with robust spines. Similar assemblages were observed in Cores 120-748B-15H-CC through 120-748B-18H-CC, which are of middle to late Eocene age. *Eucyrtidium*(?) sp. with long and radiate apical horns are also observed in Sample 120-749B-3H-CC. At the previous site, this form was seen in Samples 120-748B-14H-CC and 120-748B-15H-CC (upper Eocene).

Sample 120-749B-7X-CC contains *C. milowi*(?), *L. amphitrite, Periphaena* sp., *Lophoconus titanothericeraos, Eusyringium fistuligerum, Lophocyrtis biaurita,* and *Sethochytris babylonis,* which indicate an Eocene age. This assemblage is similar to that of Site 264 (Chen, 1975), which is late middle Eocene to late Eocene in age. Sample 120-749B-9H-CC contains few radiolarians, including *C. milowi*(?), *L. amphitrite, Periphaena* sp., *L. titanothericeraos,* and *S. babylonis,* which indicate an Eocene age.

In summary, rich, typically high-latitude radiolarian assemblages were recovered at Site 749. Shore-based studies will attempt to correlate them with calcareous plankton biostratigraphy.

Diatoms

Diatoms were recovered only from Core 120-749A-1H and Cores 120-749B-1H through -3H. A major hiatus within the upper 40 cm of Holes 749A and 749B separates mid-Pliocene from lower upper Oligocene. This hiatus represents a minimum of 25 m.y., from approximately 4 to 29 Ma. The underlying diatom-bearing interval within the first four cores of Hole 749B is of late Eocene to early late Oligocene age. At the present time, sample spacing is considered to be too widely spaced, given the low sedimentation rate of this interval (see "Sedimentation Rates" section, this chapter), for accurate identification of zonal boundaries.

Pliocene-Pleistocene

Lower Pleistocene diatom assemblages of the *Coscinodiscus elliptopora/Actinocyclus ingens* Zone (0.62–1.58 Ma) occur in the upper 15–20 cm of Core 120-749B-1H-1. No reworking of Pliocene or Oligocene diatoms was noted in these lower Pleistocene sediments.

A thin, diatom-bearing, sandy-gravel horizon, interpreted as a lag deposit (see "Lithostratigraphy and Sedimentology" section, this chapter) is present immediately above the unconformity. Smear slides from Samples 120-749B-1H-1, 23 cm, and 120-749B-1H-1, 27 cm, contain rich assemblages of mid-Pliocene diatoms, including *Actinocyclus actinochilus, Coscinodiscus kolbei, C. vulnificus, Cosmiodiscus insignis, Eucampia antarctica, Nitzschia interfrigidaria, N. weaveri, Rouxia naviculoides, Thalassiosira torokina,* and a mixture of rare reworked diatoms from the upper Miocene and underlying Oligocene. The above assemblage is absent from the overlying lower Pleistocene interval.

The sandy interval appears to be a condensed sequence of mid-Pliocene age that was deposited in a regime of strong current activity, or it may represent the remnant of a formerly thicker interval that has been deflated. In both of the above cases, only those diatoms that were protected beneath coarser detritus remain. The dominance of mid-Pliocene diatoms in these assemblages and the low abundance of *Nitzschia kerguelensis,* a diatom that dominates Pleistocene and upper Pliocene Southern Ocean sediments, in Sample 120-749B-1H-1, 23 cm, and the absence of this diatom in Sample 120-749B-1H-1, 27 cm, argues against a Pleistocene and upper Pliocene age for this sample. In other words, the age of diatoms in the sandy interval is most likely primary and not due to subsequent redeposition or reworking.

Burrows

Large burrows occur throughout Section 120-749B-1H-1 and contain a mixture of mid-Pliocene, late Miocene, and Oligocene diatoms. The absence of *Nitzschia kerguelensis,* a late Pliocene

to Holocene diatom, in these burrows indicates that they were formed and filled during the mid-Pliocene, prior to the evolution of *N. kerguelensis* and prior to the deposition of the upper 15–20 cm of lower Pleistocene at Site 749. The study of diatom assemblages within the burrows may provide clues regarding sediments that were once present above the unconformity and subsequently stripped or deflated.

Oligocene-Eocene

Sediments immediately beneath the unconformity in Sample 120-749B-1H-1, 38 cm, are assigned to the lower to upper Oligocene *Rocella vigilans* Zone based on the abundant occurrence of *R. vigilans* and the absence of *R. gelida*. Also present in this sample are *Coscinodiscus rhombicus, Hemiaulus taurus, Lisitzinia ornata,* and *Synedra jouseana*. The presence of *Coscinodiscus rhombicus* suggests an age less than 30 Ma for this sample.

The base of the *R. vigilans* Zone, as determined by the lowest occurrence of the nominative taxon, occurs within the interval between Samples 120-749A-1H-CC and 120-749B-2H-CC (between 9.5 and 15.3 mbsf). The lowest occurrence of *L. ornata* occurs within the *R. vigilans* Zone in Sample 120-749B-1H-1-CC and suggests an age of 31 Ma for this sample. Other diatom datums within the *R. vigilans* Zone include the highest occurrence of *Actinocyclus ehrenbergii* var. *tenella* and of *Cestodiscus reticulatus* and the lowest occurrence of *Rocella semigelida*.

The top of the lower Oligocene *Coscinodiscus superbus* Zone (and the base of the overlying *Pyxilla reticulata* Zone) is identified by the highest occurrence of *C. superbus*. The top of the *P. reticulata* Zone, defined by the highest occurrence of *P. reticulata,* is not identified here because wide sample spacing of core catchers resulted in the coincident highest occurrences of *P. reticulata* and *C. superbus*.

The top of the upper Eocene *Melosira architecturalis* Zone is identified in Sample 120-749B-3H-CC by the highest occurrence of the nominative taxon.

Silicoflagellates and Ebridians

Silicoflagellates are present in the Pliocene-Pleistocene intervals of Holes 749A and 749B, but they are not discussed here due to the limited recovery of sediments of this age. Oligocene and middle Eocene silicoflagellate and ebridian assemblages are well represented in samples where they are well preserved.

Silicoflagellates

Lower Oligocene silicoflagellate assemblages observed between Samples 120-749B-1H-CC and 120-749B-3H-CC include *Dictyocha deflandrei, D. fibula, Distephanus boliviensis, D. crux, Mesocena apiculata, Naviculopsis biapiculata, N. constricta,* and *N. trispinosa*. No zonations are applied to this interval.

Middle Eocene silicoflagellate assemblages present in Sample 120-749B-9H-CC, include *Cannopilus hemisphaericus, Corbisema apiculata, C. bimucronata rotatoria, C. triacantha, Dictyocha grandis, Mesocena apiculata inflata, M. apiculata curvata, M. oamaruensis, M. occidentalis, Naviculopsis biapiculata, N. constricta,* and *N. foliacea*. This assemblage is part of the *Dictyocha grandis* Range Zone of middle Eocene age.

Ebridians and Endoskeletal Dinoflagellates

Ebridians and endoskeletal dinoflagellates are long ranging and the following taxa occur in the upper Oligocene through middle Eocene interval: *Ammodochium rectangulare, Ebriopsis crenulata, Hovasserbia brevispinosa, Pseudoammodochium dictyoides, P. sphericum* (ebridians), *Actiniscus* sp., and *Carduifolia gracilis* (endoskeletal dinoflagellate).

Macrofauna

Small oysters of little stratigraphic significance occurred in Hole 749B at two levels (Cores 120-749B-3H, 112 cm, and 120-749B-6H-CC). They will be discussed in a report on the macrofauna from Leg 120 in the *Scientific Results* volume.

The fauna from Core 120-749B-3H, 112 cm, consists of fragments of up to 12 individuals, most with excellently, if incompletely, preserved dentition, wall structure, and muscle scars. Specimens are typically ostreid and may even belong to the genus *Ostrea*. Maximum specimen size is 20 mm.

The specimens do not occur as isolated individuals but as a loosely united cluster, probably attached in life to some floating substrate such as a whale or piece of wood. Molding of some specimens may give clues to substrate geometry.

The material from Core 120-749B-6H-CC consists of a few incomplete but well-preserved fragments, sufficient to indicate that they are parts of oyster-type shells. Preservation of the incomplete shells is excellent. Shell form is much less irregular than for the samples higher in the hole, and the living specimens were probably larger and roughly circular, perhaps 40 mm in diameter. Fragments represent two or three individuals.

Conclusions

The most significant results obtained at Site 749 are:

1. The identification of a part of the Paleogene sequence that was not recovered at previous Leg 120 sites. Lower middle Eocene sediments were recovered in Cores 120-749B-12X and -13X, and the lower/middle Eocene boundary (= Ypresian/Lutetian boundary; Aubry, 1983) lies within Core 120-749B-13X. Although poor core recovery will limit the scope of studies over this interval, the material obtained completes our sampling of the calcareous and siliceous microfaunas and microfloras and the calcareous nannofossils, which developed in this area from the late Paleocene through the late Oligocene. At the conclusion of Site 749 operations, the only stratigraphic intervals in the Paleogene that had not been recovered on Leg 120 were the upper lower to lower upper Paleocene and possibly the upper middle Eocene (Bartonian).
2. The provision of data that support the probable development of a regional unconformity between the middle and the upper Eocene as suspected at Site 748. The extent of the hiatus represented by this unconformity is not yet known. It should be possible to establish precisely its duration (at least 2.5 m.y.) by means of onshore studies. Alternatively, the late middle Eocene may be represented by a very condensed section at both sites.
3. The confirmation of the regional development of characteristic benthic foraminifer assemblages that can serve as stratigraphic markers and paleoenvironmental indicators. Benthic foraminifer assemblages indicate that Site 749 has been at approximately the same water depth since the early Eocene.
4. The dating of the oldest sediment overlying basalt. The basement/sediment contact was not recovered, and the intervening unrecovered interval is at least 5 m thick. However, it is unlikely that sediment older than middle early Eocene (Zone NP12) is present. The age of the oldest sediment is estimated at 54–55 Ma. However, considering the present geological/geophysical context of Site 749, this does not imply that the underlying basalt is 54–55 m.y. old (see "Site Geophysics" section, this chapter).
5. The provision of biostratigraphic data to support the recognition of early Oligocene Anomaly Correlatives 10 and 11 in the paleomagnetic record.

In addition, the results obtained from a study of the diatom assemblages in the mid-Pliocene lag deposit and in burrows through the upper Oligocene oozes in Core 120-749B-1H sug-

gest either nondeposition at this site until at least the late Miocene, or deposition followed by complete erosion. No upper Pleistocene sediments were recovered, suggesting either strong current activities in the vicinity of Site 749 or nonrecovery of surface sediments.

Finally, Site 749 provides a lower Eocene sequence that can be shown to consist of thickened, redeposited sediments. Abnormally high sedimentation rates (see "Sedimentation Rates" section, this chapter) and variable preservation and sorting out of the calcareous nannofossils suggest constant synsedimentary scouring and redeposition of pelagic oozes during the early Eocene.

The main characteristics of the sedimentary history at Site 747 are illustrated in Table 4.

PALEOMAGNETICS

Introduction

Site 749, located on the Banzare Bank of the Southern Kerguelen Plateau (58°43.03'S, 76°24.45'E), provided only a limited magnetostratigraphic record but a sufficient number of basement samples from several lava flows for paleolatitude determinations. Only the top 15 m of sediment gave an interpretable magnetic signal. In this report, we compare results from thermal and alternating field (AF) demagnetization experiments on basalt samples from Sites 747, 748, and 749. A synthesis of these results will be used for a preliminary estimate of the paleoposition of the Kerguelen Plateau.

Sediments

The natural remanent magnetizations (NRMs) of archive halves of Cores 120-749A-1H and 120-749B-2H through -5H were measured with the cryogenic magnetometer. The results after AF demagnetization at 9 mT are shown for Holes 749A and 749B in Figure 14. The intensities of magnetization after AF demagnetization (approximately 1 mA/m) are well above the noise level of the magnetometer (0.1 mA/m). At 8 mbsf the inclinations from Holes 749A and 749B are negative and indicate a normal polarity interval. Since these normal intervals occur at the same depth, we assume that they represent the same polarity subchron. Thus, the inclinations of Hole 749B can be used to extend the record of Hole 749A to 15 mbsf, below which the magnetic signal becomes random and uninterpretable. An interpretation of the inclination records from both Holes 749A and 749B in terms of normal and reversed polarities is shown in Figure 14.

The magnetic reversal sequence in Figure 14 can only be interpreted with the help of biostratigraphic information. The normal interval below 7 mbsf is identified as Anomaly Correlative 10 using the planktonic foraminifers *Chiloguembelina cubensis* ("Biostratigraphy" section, this chapter). The normal polarity chron below 10 mbsf (Fig. 14) occurs at the same level as the last appearance datum of *Subbotina angiporoides* (Berggren et al., 1985a; "Biostratigraphy" section, this chapter). From the sedimentation rate curve ("Sedimentation Rates" section, this chapter), we can tentatively associate the normal interval at 2 mbsf with Anomaly Correlative 9 using the time scale of Berggren et al. (1985b).

Igneous Rocks

Seven samples from the basalt flows of Site 749 were demagnetized with alternating fields up to 60 mT. A small viscous overprint was in most cases removed after AF demagnetization at 5–10 mT. All samples, except one, possess single-component magnetizations as is evident from the straight lines on orthogonal vector projections (Zijderveld plots). One typical result (Sample 120-749C-16R-6, 107–109 cm) from AF demagnetization of basalt samples is shown in Figure 15. The direction of magnetization is very stable and tightly clustered on the stereographic projection.

One sample (120-749C-16R-6, 84–86 cm) was stepwise thermally demagnetized up to 590°C (Fig. 16). Its direction of magnetization was very stable during thermal demagnetization up to 590°C, as shown by a single straight line in the orthogonal vector projection and the close grouping on the stereoplot. At 590°C the sample has lost 95% of its initial remanence, which suggests magnetite (Curie point = 580°C) as the major carrier of magnetization.

Table 4. Main characteristics of the sedimentary history at Site 749.

Core, section, interval (cm)	Depth (mbsf)	Lithostratigraphy	Age (Ma)	Microfossil groups
120-749B-1H-1, 0 cm	0	Lower Pleistocene–mid-Pliocene diatom foraminifer oozes	<3.1	Diatoms
120-749B-1H-1, 24 cm	0.24	\/\/\/\/\/\/\/\/\/\/ Condensed section of middle upper Oligocene to upper Eocene calcareous nannofossil and planktonic foraminifer oozes	~29	Planktonic foraminifers Diatoms
120-749B-4H-CC	34.30	\/\/\/\/\/?/\/\/\/\/	<39.8	Calcareous nannofossils
120-749B-5H-CC	43.80	Lower middle to upper middle Eocene calcareous nannofossil and planktonic foraminifer oozes	>42.3	Calcareous nannofossils
120-749B-12X-CC	110.30	————————	<52	Calcareous nannofossils
120-749B-13X-CC	123.80	Expanded lower Eocene sequence resulting from synsedimentary scouring and redeposition	>52	Calcareous nannofossils
120-749C-10R-CC	197.00	\/\/\/\/\/\/\/\/\/\/	54–55	Calcareous nannofossils
120-749C-11R-3	202.00	Basement	??	

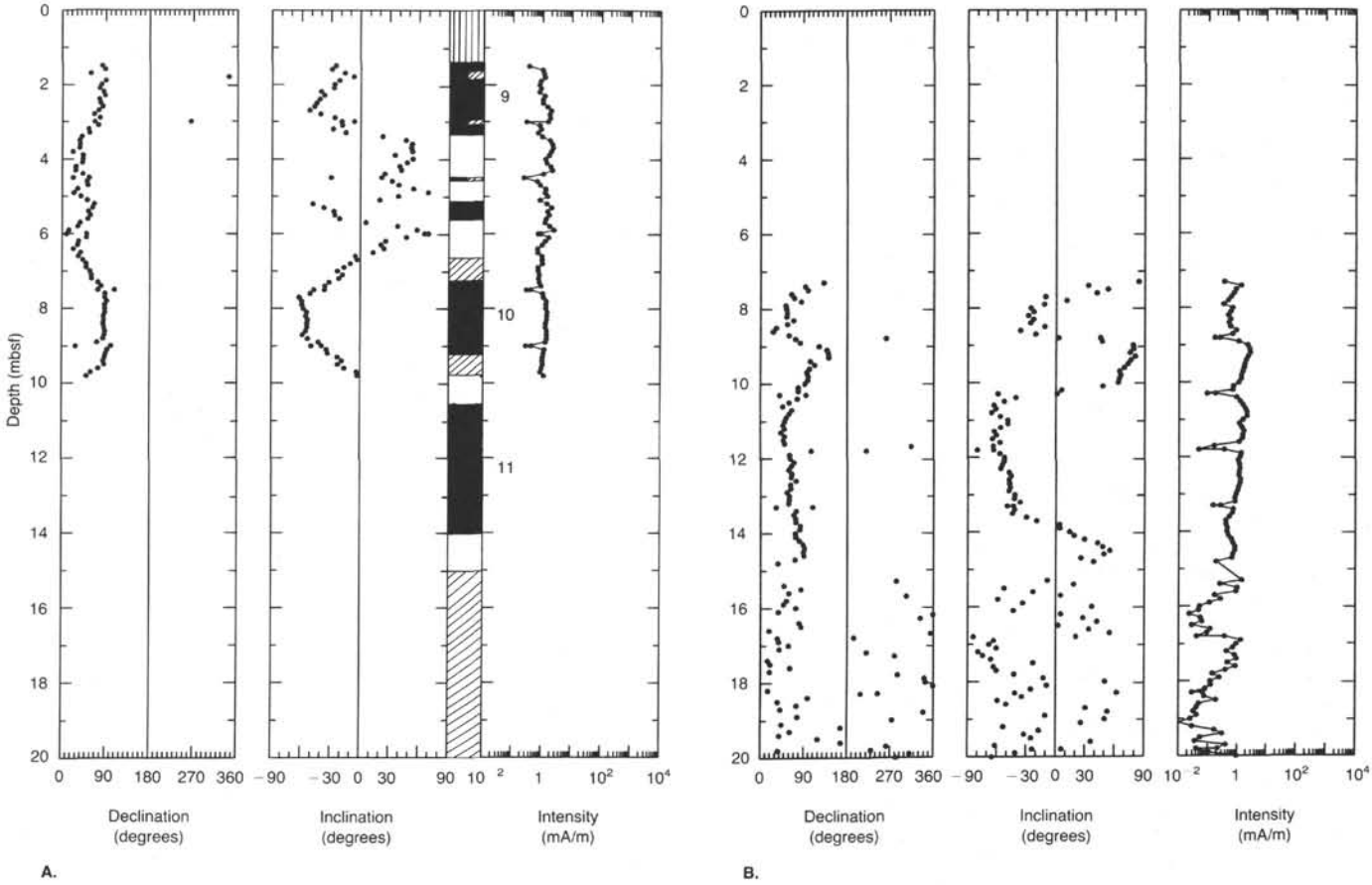

Figure 14. Declination, inclination, and intensity after AF demagnetization of archive halves at 9 mT. **A.** Magnetic remanence of Core 120-749A-1H from Hole 749A. **B.** Magnetic remanence from cores of Hole 749B. The magnetic reversal sequence from B has been added to A assuming they overlap at the normal interval at 8 mbsf.

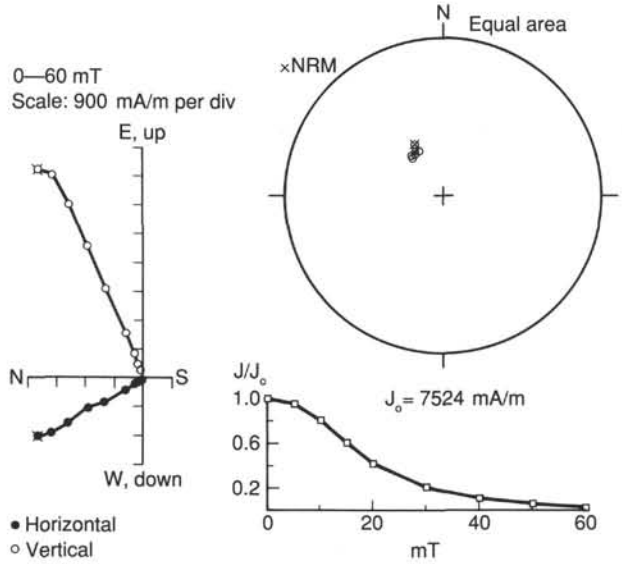

Figure 15. AF demagnetization of Sample 120-749C-16R-6, 107–109 cm. A small viscous component of magnetization is removed at 10 mT. The straight line above 10 mT in the Zijderveld diagram represents a single-component magnetization. The directions during AF demagnetization are tightly clustered in the stereographic projection. The intensity decay curve is representative for a stable magnetization.

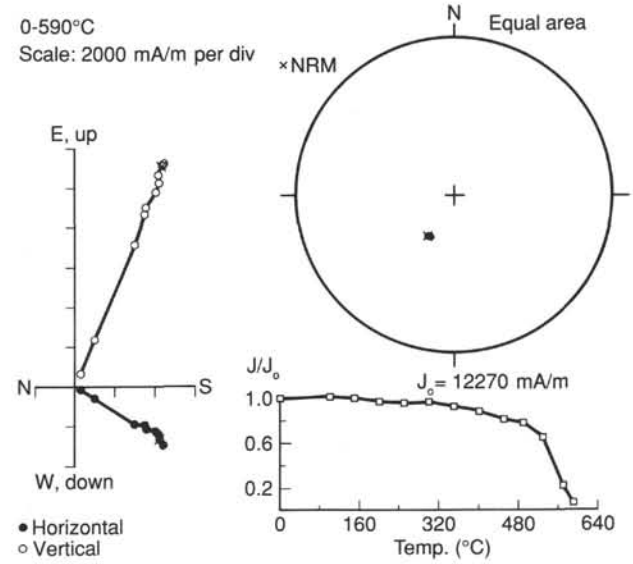

Figure 16. Thermal demagnetization of Sample 120-749C-16R-6, 84–86 cm. The NRM is a stable single-component magnetization. Most blocking temperatures are above 480°C. There is no indication of a second magnetic phase in the intensity decay curve. The magnetic mineral is most likely magnetite, which has a Curie temperature of 580°C.

The inclination of the characteristic magnetization of a sample is determined from a straight line that passes through three or more data points and the origin on a Zijderveld plot. These inclinations together with intensity of NRM, M_O, and median destructive field (MDF) are shown in Table 5. The median destructive fields range from 10 to 18 mT, suggesting rather stable magnetizations. These MDF values are typical for ocean-floor basalts (Furuta and Levi, 1983; Pechersky et al., 1983). The eight samples were collected from five different basalt units ("Igneous Petrology" section, this chapter). The horizontal lines in Table 5 delineate the boundaries between samples from the five units.

The declinations of all samples are arbitrary because the cores were unoriented. Except for Sample 120-749C-15R-5, 73–75 cm, the six remaining samples have absolute inclination values ranging from 52° to 69°. Sample 120-749C-15R-5, 73–75 cm, had an unstable direction and its inclination (I) changed considerably during AF demagnetization. Therefore, it was not included in the following calculation of an average inclination. Further measurements on samples from the flow of Sample 120-749C-15R-1, 121–123 cm, will show whether its comparatively low inclination of 52° is representative for that flow (Table 5).

Sample 120-749C-12R-5, 45–47 cm, which comes from an intruded dike, had a reversed magnetization (I = +69°). In order to include the dike inclination in the calculation of a mean inclination for all basement samples from Site 749, the polarity of its inclination was reversed.

For the calculation of mean inclination, special statistics have to be used because the rocks were unoriented with respect to declination. The algorithm developed by Kono (1980) was employed in the computation of mean inclinations and their error limits. One thermally demagnetized and six AF demagnetized samples gave a mean inclination of −63° and a 95% confidence limit of 2.3°. An inclination of −63° is equivalent to a magnetic paleolatitude of 44°S under the assumption of an axial geocentric dipole field.

The variation of inclination values between different flows reflects either secular variation of the earth's field or the presently insufficient number of samples measured from each unit. Three samples from the same flow (Core 120-749C-16R) have essentially identical inclinations, which favors secular variation as a possible cause for the differences between units. Only additional shore-based measurements will be able to resolve this question.

Table 5. Paleomagnetic results from demagnetization experiments on basalts from Hole 749C.

Core, section, interval (cm)	I (°)	M_O (mA/m)	MDF (mT)	Demag
120-749C-				
12R-2, 99–101	−69	4242	13	AF
12R-5, 45–47	+69	2767	10	AF
15R-1, 121–123	−52	3320	12	AF
15R-5, 73–75	—	1314	15	AF
15R-6, 124–126	−58	5463	16	AF
16R-5, 111–113	−65	3630	17	AF
16R-6, 84–86	−65	12270	—	Th
16R-6, 107–109	−64	7525	18	AF

Note: One sample was thermally demagnetized and the remaining samples were AF demagnetized. The characteristic inclinations (I) were determined from orthogonal vector projections. M_O = NRM intensity; MDF = median destructive field, which is required to AF demagnetize one half of the NRM. The horizontal lines represent boundaries between rock units.

Results From Basement of Site 747

From the five basaltic flows of Site 747, eight samples were stepwise AF demagnetized and one sample was progressively thermally demagnetized up to 590°C. An example of the AF demagnetization results is shown in Figure 17, and the results of thermal demagnetization are shown in Figure 18. All nine samples have single-component magnetizations. The inclinations, NRM intensities, and median destructive fields (for AF only) are summarized in Table 6. The boundaries between samples from different flows are represented by horizontal lines in Table 6.

The MDFs range from 11 to 32 mT. These MDF values are about 50% higher than the MDFs of basalts from Site 749 (see Table 5). The inclination for each of the nine samples was determined from a straight line through the demagnetization data and the origin of each orthogonal vector projection. The mean inclination from the nine demagnetized samples at Site 747 is −52° with an error of 3.8% at the 95% confidence level. The corresponding paleolatitude is 33°S. This paleolatitude value represents a preliminary estimate, the value of which will be revised after measuring the remaining 26 basement samples from Site 747 during shore-based studies.

Results from Basement of Site 748

A short summary of the paleomagnetic results of Site 748 will be given here. Two basalt samples were AF demagnetized, and one sample was thermally demagnetized. The mean inclination was 69° with a 95% confidence limit of 0.5°, which gives a corresponding paleolatitude of 52°S. Because of the highly altered nature of these basement samples, it was not certain whether the NRM was a primary or an overprinted magnetization.

Comparison of Magnetic Directions of Basalts from Sites 747 through 749

The paleomagnetic results from basalt samples of Sites 747 through 749 are summarized in Table 7. The mean inclinations

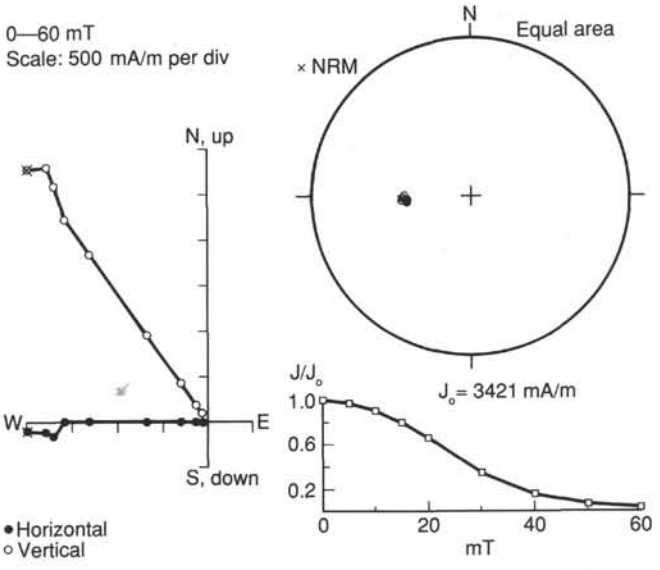

Figure 17. AF demagnetization of Sample 120-747C-11R-3, 94–96 cm. A viscous overprint is erased at 15 mT peak AF, above which the remanence is a stable single-component magnetization. The median destructive field is 27 mT.

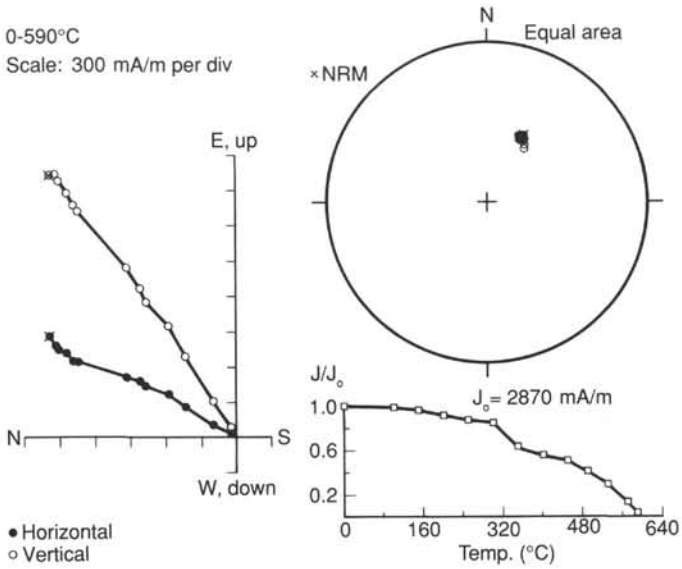

Figure 18. Thermal demagnetization of Sample 120-747C-12R-3, 84–86 cm. A chemical or viscous overprint is erased at 500°C, when the first magnetic phase (probably maghemite) became essentially nonmagnetic (converted to hematite). The characteristic magnetization, which is carried by magnetite, was demagnetized between 500° and 570°C.

Table 6. Paleomagnetic results from demagnetization experiments on basalts from Hole 747C.

Core, section, interval (cm)	I (°)	M_O (mA/m)	MDF (mT)	Demag
120-747C-				
11R-1, 42–44	−57	2912	17	AF
11R-2, 94–96	−50	5063	11	AF
11R-2, 136–138	−52	1793	12	AF
11R-3, 28–30	−43	3098	13	AF
11R-3, 94–96	−55	3421	27	AF
12R-3, 84–86	−54	2871	—	Th
12R-4, 3–5	−54	2714	18	AF
15R-1, 32–34	−40	1420	32	AF
15R-2, 86–88	−71	4792	28	AF

Note: See Note to Table 5 for an explanation of the terms and abbreviations used.

Table 7. Mean paleomagnetic results from basalts of Sites 747 through 749.

							I(Ant)	
Site	N	I(pm) (°)	α_{95} (°)	I(pr) (°)	Paleo-latitude (°S)	Present latitude (°S)	Upper Tertiary (°)	Jurassic (°)
747	9	−52	3.8	−71	33	55	−64	−42
748	3	−69	0.5	−73	52	58		
749	7	−63	2.3	−73	44	59	−67	−47

Note: The error estimates at the 95% confidence level (α95) were calculated for N samples at each site. I(pm) is the paleomagnetic mean inclination and I(pr) is the present inclination in an axial dipole field. The paleolatitude was calculated from I(pm). Assuming that Sites 747 and 749 were part of the Antarctic block, inclinations, I(Ant), were obtained for each site in the upper Tertiary and Jurassic, using the apparent polar wander path of Antarctica (McElhinny, 1973).

of the characteristic magnetizations at each site are compared with the present inclinations, which were calculated for each site under the assumption of an axial geocentric dipole field. The magnetic paleolatitudes of the three sites are shown in relation to their present geographic latitudes.

The similarity of the paleomagnetic inclination (−69°) and the present-field inclination (−73°) at Site 748 implies either a quite recent formation of the basalt or the possibility of a present-field overprint. Our conjecture of magnetic overprinting receives further support from the presence of a second strongly magnetic phase in addition to magnetite (see intensity decay in the Site 748 chapter, Fig. 42). Based on the available evidence, we interpret the magnetic mineral, the remanence of which decays below 400°C, as maghemite (gamma-Fe_2O_3), which is the low-temperature oxidation product of magnetite (Fe_3O_4).

Maghemite is a metastable form of Fe_2O_3, which often decays into the weakly magnetic hematite (alpha-Fe_2O_3) upon heating, as suggested by the intensity-decay curve illustrated in the Site 748 chapter (Fig. 42). A detailed rock magnetic investigation of Curie temperatures and magnetic mineralogy should give more information about the nature of remanence in Site 748 basalts. For the reasons outlined above, we will not include the results from Site 748 in the further discussion of paleomagnetic directions.

Considerable differences between the paleomagnetic and present inclinations of Sites 747 and 749 indicate that displacement in the direction of the geomagnetic meridian has taken place since the formation of the basalt. Shallower paleomagnetic inclinations than present inclinations at each site suggest southward movement of the sites with respect to the geomagnetic pole. If no tectonic movements have taken place between the Kerguelen Plateau (represented to a first approximation by Sites 747 and 749) and Antarctica, the virtual geomagnetic poles (VGP) of Sites 747 and 749 should fall on the apparent polar wander path (APWP) of Antarctica. The APWP for East Antarctica has been summarized by McElhinny (1973). The lack of declination data at the two Kerguelen sites permits only the calculation of two circles for the VGP positions, which intersect the APWP of Antarctica in the appropriate time interval, as shown below.

By comparing inclinations obtained from poles on the APWP of Antarctica with the two paleomagnetic inclinations for Sites 747 and 749, one can detect displacements between the two blocks in the direction of the magnetic meridian. Paleopole positions for East Antarctica are only available for the upper Tertiary, Jurassic, and Cambro-Ordovician (McElhinny, 1973). Based on this Antarctic APWP, we obtained inclinations that Antarctic rocks would be expected to have at the positions of Sites 747 and 749. These "imaginary" inclinations of the Antarctic block at Sites 747 and 749 are shown in Table 7 for the Jurassic and the upper Tertiary.

The paleomagnetic inclination (−52°) of Site 747 falls between the two inclinations expected for the Antarctic block in the Jurassic (−42°) and the upper Tertiary (−64°) (see Table 7). Similarly, the inclination (−63°) of Site 749 lies between the inclinations expected for this site in the Jurassic and upper Tertiary (−47° and −67°, respectively). Assuming that our basalts are between Jurassic and upper Tertiary in age, this comparison of inclinations from the Kerguelen Plateau and Antarctica suggests that no major tectonic movement has taken place between the two blocks since the formation of the basalts.

The assumption about the age of the basalt is consistent with the age of the sediments above the basalt layers, even though the basalts may be much older. These deepest sediments at Sites 747 and 749 are Santonian and Eocene in age respectively ("Biostratigraphy" sections, "Site 747" chapter and this chapter). The availability of radiometric ages for the basalts and possibly a

more detailed polar wander path for Antarctica will help to refine our understanding of the relation between the Kerguelen Plateau and Antarctica.

The intermediate paleolatitudes (33° and 44°) for Sites 747 and 749 suggest a southward motion of the Kerguelen Plateau since the formation of the basalts. In addition to this major tectonic motion, there is possible further information that can be extracted from the paleolatitudes (Table 7). If one subtracts the present latitudinal difference (4°) between Sites 747 and 749 from their difference in paleolatitudes, one obtains a net difference in latitude of 7° between the two sites. There are three possible explanations for this 7° difference.

The first possibility is that the paleolatitudes from Sites 747 and 749 are similar or the same, which cannot be excluded with the present error estimates (Table 7). Measurement on shore of the remaining two thirds of the basalt samples will certainly decrease the error bars on the paleolatitudes, which should help to decide for or against this first possible explanation.

A second possible explanation for the difference in paleolatitudes could be a considerable age difference between the basalts from Sites 747 and 749. Unfortunately, one cannot use the age of the sedimentary sequence overlying the basalts, which was Santonian in age at Site 747 and Eocene at Site 749 (see "Biostratigraphy" sections, "Site 747" chapter and this chapter) to obtain an estimate for the age difference between the basalts from the two sites. Seismic data for Site 749 show that the lower sedimentary sequences disappear before the site ("Site Geophysics" section, this chapter). Dating of the basalts will resolve this uncertainty.

The third possibility is that Sites 747 and 749 belong to different tectonic provinces. The two sites are approximately 450 km apart, and the Central Kerguelen Plateau (Site 747) may have moved south with respect to the Southern Kerguelen Plateau (Site 749).

Presently, we cannot decide between these three speculative models for the difference in paleolatitudes at Sites 747 and 749. Additional experiments, data from Site 750, and a comparison with Site 738 (Leg 119) should permit us to select one tectonic model for the Kerguelen Plateau.

SEDIMENTATION RATES

Except for a thin upper sequence (38 cm in Hole 749A, 24 cm in Hole 749B) of mid-Pliocene and lower Pleistocene sediments consisting of foraminifer and diatom oozes and sands with coarse ice-rafted material, Site 749 recovered a sedimentary section over 200 m thick that consists primarily of Paleogene calcareous nannofossil oozes interbedded in the middle Eocene with chert layers. This section extends from the lower Eocene (about 54–55 Ma) to the upper Oligocene (about 28–29 Ma).

Planktonic foraminifers and calcareous nannofossils are well preserved and diversified in these oozes; they provide the main biostratigraphic control. Diatoms are common and well preserved in the Oligocene interval (Cores 120-749B-1H-1, 30 cm, to -3H), and silicoflagellates are exceptionally abundant and diversified in the middle Eocene interval (Cores 120-749B-5H to -12X). Both groups of siliceous microfossils provide complementary biostratigraphic data.

The biostratigraphic datum levels used to construct the sedimentation rate curve presented in Figure 19 are listed in Table 8. Planktonic foraminifer and calcareous nannofossil datums are taken from Berggren et al. (1985a, 1985b). The age of diatom datums are based largely on calibration from Sites 747 and 748 (see "Explanatory Notes" chapter, this volume). Because they are extremely condensed, no sedimentation rate is estimated for the upper Neogene sediments recovered at Site 749.

The sedimentation rate of Paleogene oozes varied considerably at Site 749 (Fig. 19), showing a general decrease from the early Eocene through the Oligocene. A surprisingly high rate of 70 m/m.y. is estimated for the deposition of the lower Eocene oozes (Cores 120-749B-13X to 120-749C-10R). A rate of sedimentation for the middle Eocene oozes (recovered in Cores 120-749B-5H to -12X) is difficult to estimate because of poor biostratigraphic control in this interval and because of the possible development of a middle/upper Eocene unconformity (see "Biostratigraphy" section, this chapter).

Assuming continuous sedimentation through the middle Eocene (thus taking datums N3 and F4, and N6 and F6 as end controls), the rate is estimated at 6.45 m/m.y. However, taking N4 as the youngest control point, the rate increases to 8 m/m.y. This difference implies either the development of an unconformity or a marked rate change during the middle Eocene. Considering the spread of the datums available at this time, it is not possible to resolve this question. Integrated and detailed shore-based biostratigraphic studies of the middle Eocene sequence are required. There is, on the other hand, good biostratigraphic (and magnetostratigraphic) control in the upper Eocene and Oligocene, and datums from the different microfossil groups agree well. The sedimentation rate through the late Eocene and the Oligocene is estimated at 3.6 m/m.y.

The slow rate of sedimentation during the late Eocene and the Oligocene contrasts strongly with an abnormally high rate of 70 m/m.y. during the early Eocene. This exceptional rate suggests that the lower Eocene oozes correspond to a thickened, redeposited sediment. Changing calcareous nannofossil preservation and diversity through these lower Eocene oozes are evidence that part of the sediment is redeposited. There is no evidence of reworking of older sediments in these oozes, however. Thus, we envision synsedimentary scouring and redeposition of pelagic oozes at the onset of early Eocene sedimentation, following a possibly long period of nondeposition and erosion of an exposed domelike basement structure swept by strong bottom currents.

INORGANIC GEOCHEMISTRY

Introduction

At Site 749, located on the Southern Kerguelen Plateau about 50 nmi west of Site 748, three holes were drilled into 202 m of Eocene, Oligocene, and Pliocene-Pleistocene sediments and 47.5 m of underlying basaltic basement. Only within the upper 160 m of nannofossil calcareous and minor siliceous ooze were undisturbed soft sediments suitable for interstitial water (IW) squeezing recovered. Further downhole, abundant chert layers, poor core recovery, and disturbed lithology excluded sampling of IW.

Estimated sedimentation rates are around 3 cm/1000 yr for the Oligocene and late Eocene (see "Sedimentation Rates" section, this chapter). The whole sedimentary sequence is discontinuous, showing major hiatuses between the Pliocene-Pleistocene (which, in fact, only consists of the upper 30–40 cm of the drilled sequence; see "Lithostratigraphy and Sedimentology" section, this chapter) and the Oligocene and between the early and the middle Eocene (see "Lithostratigraphy and Sedimentology" section, this chapter).

Only five samples from depths between 4 and 162 mbsf were obtained, with squeezed fluids amounting to 20–41 cm^3. Shipboard analysis of pH, alkalinity, salinity, sulfate, chlorine, magnesium, calcium, and silica were conducted according to the methods described by Gieskes and Peretsman (1986; see also "Explanatory Notes" chapter, this volume). The results from routine IW analysis are reported in Table 9. Concentrations are given in millimoles per liter (mM) except for silica, which is reported in micromoles per liter (μM).

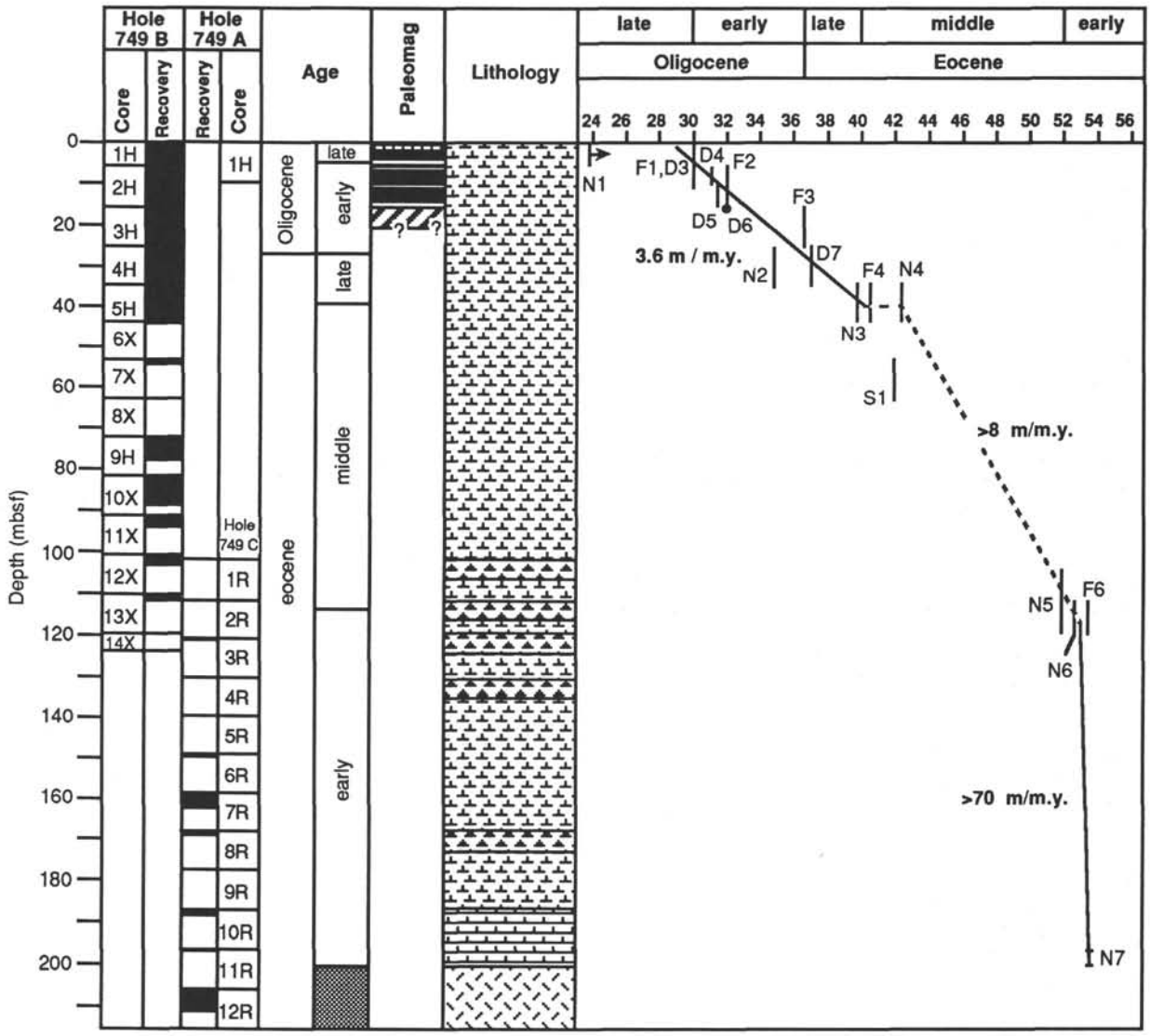

Figure 19. Sedimentation rate curve for the Paleogene section, Site 749. See "Explanatory Notes" chapter (this volume) for key to lithologic symbols; see "Paleomagnetics" section, this chapter, for key to paleomagnetics symbols. LAD = last appearance datum and FAD = first appearance datum. See Table 8 for datum codes.

Results

Salinity and Chlorinity

Salinity values range from 35.8 to 36.1 g/kg (average = 35.96 g/kg) and show little variation (Fig. 20). The chlorine concentrations are uniform at 566 and 567 mM, respectively, except for a very low initial value of 556 mM reflecting the proximity to bottom seawater. The high chlorine concentrations correlate with the high salinity and both show the overall seawater derivation of the IW.

Alkalinity and pH

Alkalinity values display a decrease from 2.842 at the top to 1.886 mM at 161.95 mbsf downhole (Fig. 20). As in most natural waters, total alkalinity equals carbonate alkalinity and is controlled by the HCO_3 concentration at pH >7 (Drever, 1982); therefore, carbonate precipitation is the most likely process of lowering the alkalinity. Another lowering effect is silicate precipitation, which is indicated by drastic drops between 111.75 and 161.95 mbsf in alkalinity (from 2.420 to 1.886 mM) and dissolved silica (from 513 to 137 mM). The observed pH values range between 7.35 and 7.55 and show no systematic variation (Fig. 20).

We conclude that depth-controlled changes in the carbonate and silica system are responsible for the decrease in alkalinity. The carbonate system buffers the pH around 7.45 ± 0.10.

Sulfate

Sulfate concentrations decrease steadily from 28.66 mM at 4.45 mbsf to 27.74 mM at 111.75 mbsf and then rise to 28.28 mM at 161.95 mbsf (Fig. 20). The overall sulfate reduction, however, is very small. Reducing conditions such as anoxic pore water or high organic carbon contents in the sediments do not exist (see "Organic Geochemistry" section, this chapter). The high sulfate concentrations reflect the highly oxidizing environment of the IW.

Magnesium and Calcium

Magnesium concentrations decrease from 53.32 mM at 4.45 mbsf to 52.31 mM at 111.75 mbsf and then rise to 52.89 mM at

Table 8. Datum levels used to establish the sedimentation rate curve (Fig. 19) for the Paleogene at Site 749.

Datum	Species	LAD/FAD	Core, section, interval (cm)	Depth (mbsf)	Age (Ma)
Planktonic foraminifers:					
1	*Chiloguembelina* spp.	LAD	120-749A-1H-CC	0 5.87	30.0
2	*S. angiporoides*	LAD	120-749B-2H-CC	5.87 5.87	32.0
3	*G. index*	LAD	120-749B-3H-CC	15.30 24.80	36.6
3	*S. linaperta*	LAD	120-749B-3H-CC	15.30 24.80	36.6
4	*Acarinina* spp.	LAD	120-749B-5H-CC	34.30 43.80	40.6
5	*A. primitiva*	LAD	120-749B-6X-CC	43.80 53.30	42.8
6	*A. densa*	FAD	120-749B-13X-CC	119.80 123.80	53.5
Calcareous nannofossils:					
1	*R. bisecta*	LAD	120-749A-1H-CC	0 5.80	23.7
2	*R. umbilica*	LAD	120-749B-4H-CC	24.80 34.30	46.0
3	*C. oamaruensis*	FAD	120-749B-4H-CC	34.30 43.80	39.8
4	*C. solitus*	LAD	120-749B-5H-CC	34.30 43.80	42.3
5	lower/middle Eocene boundary		120-749B-13X-3	119.00	52.0
6	*D. sublodoensis*	FAD	120-748B-13X-CC	119.80 123.80	52.6
7	*T. orthostylus*	LAD	120-749C-10R-CC	187.50 197.00	53.7
Diatoms:					
1	*A. ingens*	LAD	120-749B-1H-1, 2	0 0.02	>0.62 <1.58
2	*N. interfrigidaria*	LAD	120-749B-1H-1, 23	0.02 0.23	>2.8 <3.1
3	*C. rhombicus*	FAD	120-749B-1H-1, 38	0.23 0.38	30.0
4	*L. ornata*	FAD	120-749B-1H-1, CC	5.80 15.30	31.0
5	*R. vigilans*	FAD	120-749A-1H-CC	10.04 15.30	31.5
6	*S. jouseana*	FAD	120-749B-2H-CC	15.30 24.80	32.0
6	*P. reticulata*	LAD	120-749B-2H-CC	5.80 15.30	32.0
7	*M. architecturalis*	LAD	120-749B-3H-CC	15.30 24.80	37.0

Note: LAD = last appearance datum and FAD = first appearance datum.

Table 9. Interstitial water chemical data, Site 749.

Core, section, interval (cm)	Depth (mbsf)	Vol. (cm^3)	pH	Alk. (mM)	Sal. (g/kg)	Mg^{2+} (mM)	Ca^{2+} (mM)	Cl^- (mM)	SO_4^{2-} (mM)	SiO_2 (μM)	Mg^{2+}/Ca^{2+}
120-749B-											
1H-3, 145–150	4.45	30	7.43	2.842	35.8	53.32	10.99	556	28.66	758	4.85
3H-5, 145–150	22.75	30	7.35	2.614	36.0	53.19	11.20	567	28.58	532	4.75
10X-3, 145–150	86.25	41	7.46	2.461	36.1	52.32	12.15	567	27.97	443	4.31
13X-1, 145–150	111.75	30	7.55	2.420	35.9	52.31	12.88	567	27.74	513	4.06
120-749C											
7R-2, 145–150	161.95	20	7.40	1.886	36.0	52.89	12.86	566	28.28	137	4.11

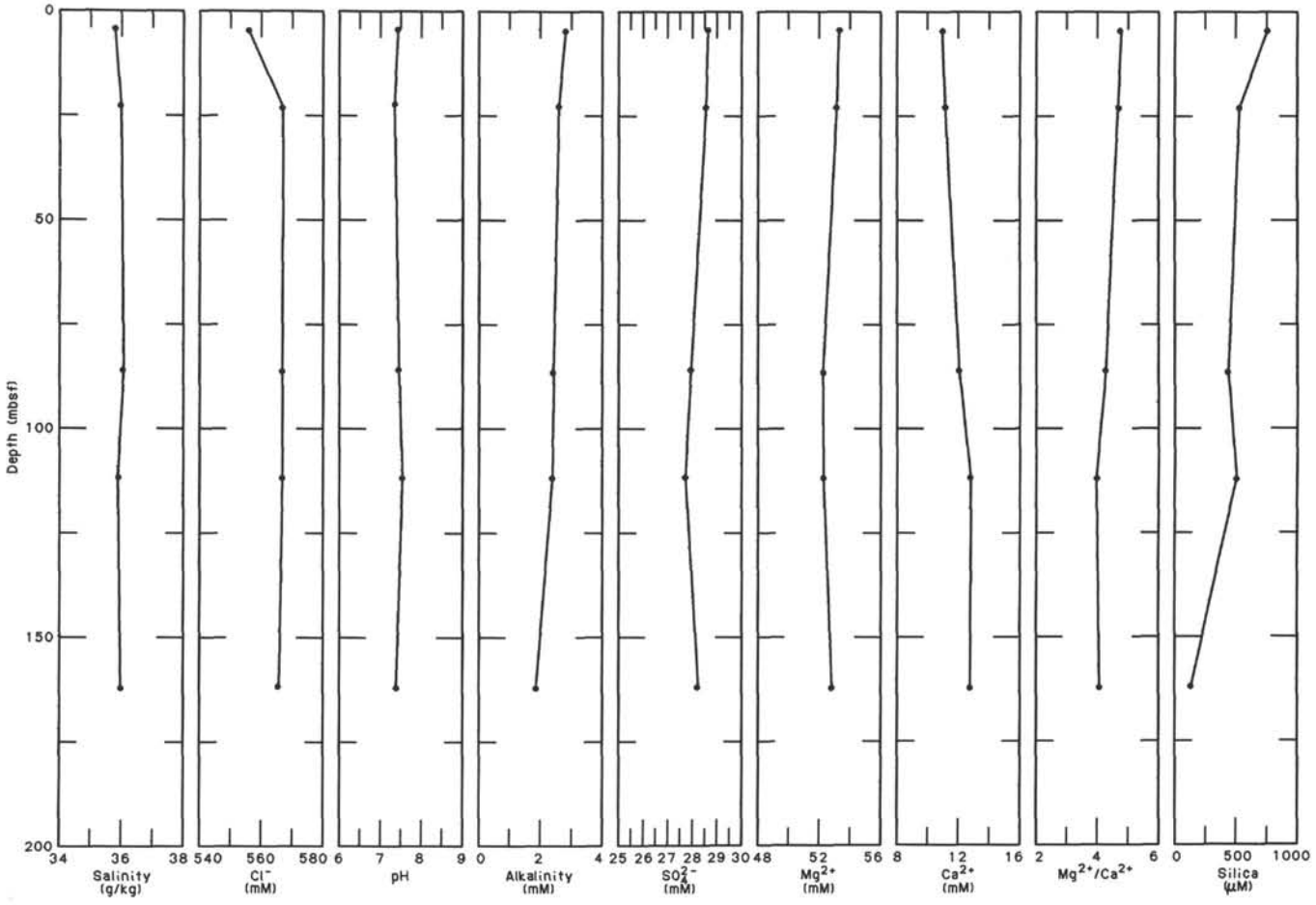

Figure 20. Summary of interstitial water analyses, Site 749, as a function of depth.

161.95 mbsf (Fig. 20). In contrast, calcium increases from 10.99 mM at 4.45 mbsf to 12.88 mM at 111.75 mbsf and then decreases very slightly to 12.86 mM at 161.45 mbsf (Fig. 20). Down to 111.75 mbsf, Mg and Ca concentrations show a conservative behavior, meaning that cation exchange is the controlling factor due to depth-related calcium undersaturation of IW and thus calcium release to IW and magnesium uptake by the carbonate sediment. This is also shown by the linear relationship between the two elements in all except the last sample (120-749C-7R-2) (Figs. 20 and 21).

Silica

Silica concentrations range between 758 and 137 μM and are a result of the dissolution of biogenic siliceous material (such as diatoms). The highest value is at the top and the lowermost value is at the bottom of the sequence. The drop at the bottom cannot be explained by the disappearance of soluble silica (diatoms are still present) but rather by chert formation and thus silica precipitation. Another explanation is seawater contamination, which would also explain the irregularities in calcium, magnesium, and sulfate.

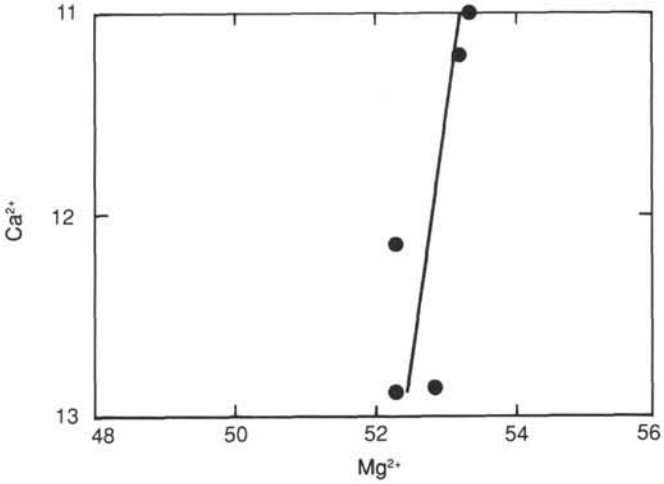

Figure 21. Mg^{2+} vs. Ca^{2+} plot of interstitial water samples from Site 749.

Summary

Salinity and chlorinity reflect the seawater nature of the IW (Fig. 20). The highly oxidizing environmental conditions favor the high sulfate and alkalinity values. Calcium and magnesium concentrations are controlled by conservative cation exchange except in the lowermost sample, the irregular behavior of which is also reflected by the low silica value. Seawater contamination resulting from RCB coring is a possible explanation for the discordant behavior of this sample.

ORGANIC GEOCHEMISTRY

Inorganic Carbon

Due to poor recovery, inorganic carbon analyses were conducted on only 16 samples from Holes 749B and 749C, the results of which are reported in Table 10 and Figure 22. The organic carbon content of samples was below the analytical resolution of the instruments on board ship.

Percent carbonate contents are relatively high at this location with most values in the range of 85%–95% (Fig. 22). A relatively minor decrease of 10% was recorded near the top of the sequence from 5.0 to 17.0 mbsf. This change reflects a slight increase in siliceous microfossil abundance (see "Sedimentology" section, this chapter). From 17.0 mbsf to basement, carbonate contents are constant and generally exceed 94%. The bulk carbonate consists mainly of calcareous nannofossils and foraminifers.

Hydrocarbon Gases

For safety purposes, sediment samples from Site 749 were routinely measured for hydrocarbon gases using the headspace extraction technique (see "Explanatory Notes" chapter, this volume). Hydrocarbon gases were not detected in any of the samples analyzed from this site. This finding is consistent with the low TOC contents reported above.

PHYSICAL PROPERTIES

Introduction

The physical properties program at Site 749 was designed to aid in the interpretation of seismic reflection profiles and the stratigraphic data recovered by coring. The goal at Site 749 was to obtain ~200 m of basement rock overlain by a relatively thin sediment section. Three holes were cored: 749A, 749B, and 749C. Hole 749A did not recover the mud line and was therefore discontinued after a single APC core. Hole 749B recovered 14 APC and XCB cores to ~122 mbsf with limited recovery below Core 120-749B-5H. The RCB was used in Hole 749C to recover sediment and basalt to ~250 mbsf; however, the majority of recovery was limited to Cores 120-749B-15R and -16R at the base of the hole.

Table 10. Total inorganic and carbonate contents of Holes 749B and 749C samples.

Core, section, interval (cm)	Depth (mbsf)	Inorganic carbon (%)	Carbonate (%)
120-749B-			
1H-2, 50–52	2.00	11.25	93.7
1H-4, 50–52	5.00	11.30	94.1
2H-2, 48–50	7.78	10.26	85.5
2H-4, 86–88	11.16	11.02	91.8
2H-6, 128–130	14.58	10.53	87.7
3H-2, 27–29	17.07	10.46	87.1
3H-4, 131–133	21.11	11.40	95.0
3H-6, 93–95	23.73	11.25	93.7
4H-2, 108–110	27.38	11.49	95.7
4H-5, 62–64	31.42	11.40	95.0
4H-6, 105–107	33.35	11.34	94.5
5H-2, 73–75	36.53	11.58	96.5
5H-4, 49–51	39.29	11.31	94.2
10X-3, 50–52	85.30	11.42	95.1
120-749C-			
7R-2, 68–70	161.18	11.44	95.3
7R-3, 29–31	162.29	11.52	96.0

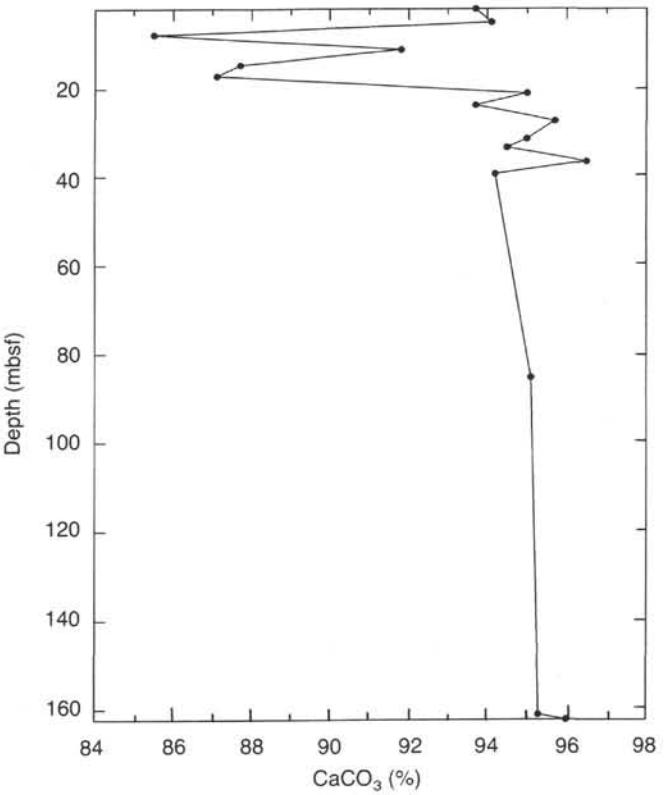

Figure 22. Percent carbonate plotted vs. depth, Site 749.

Physical properties measurements were consistently made on sediment to ~40 mbsf in Hole 749B, where chert reduced core recovery significantly. Below this depth, few samples were taken until core recovery improved in Hole 749C. Therefore, gaps in physical properties data exist from ~40 to 206.8 mbsf because limited material was available in this interval. Minicores and cubes were taken at selected intervals from the sample half of basement cores to examine variations arising from the alteration of basalt within individual flows and between adjacent flows.

The physical properties determined included index properties (wet- and dry-bulk density, grain density, water content, and porosity) (see Fig. 23 and Table 11); compressional wave velocity (see Fig. 24 and Table 12); vane shear strength (see Fig. 25 and Table 14); thermal conductivity (see Fig. 26 and Table 14); and continuous measurements of bulk density and *P*-wave velocity using the gamma ray attenuation porosity evaluator (GRAPE) and *P*-wave logger (PWL), respectively (see Fig. 27).

These data are compiled in both tabular and graphic form. The methods employed in the measurement of the physical properties obtained during Leg 120 are described in the "Explanatory Notes" chapter (this volume). A more detailed discussion of these measurements can be found in Lambe and Whitman (1969) and Boyce (1976, 1977).

Index Properties

The index properties measured at Site 749 were determined from gravimetric data using a Penta pycnometer and a Scientec balance. Samples were dried using a Labconco freeze dry apparatus. Values of wet-bulk density, dry-bulk density, grain density, water content, and porosity were determined for each sample. These results are summarized in Table 11 and Figure 23.

Index properties are relatively constant in the upper 40 m of Hole 749B, reflecting the generally homogeneous nannofossil ooze recovered from this interval. This nannofossil ooze is de-

Table 11. Index properties determinations, Site 749.

Core, section, interval (cm)	Depth (mbsf)	Water content (%)	Porosity (%)	Wet-bulk density (g/cm^3)	Dry-bulk density (g/cm^3)	Grain density (g/cm^3)
120-749B-						
1H-2, 52	2.02	36.12	61.01	1.76	1.13	2.80
1H-4, 52	5.02	34.78	58.23	1.73	1.13	2.65
2H-2, 48	7.78	42.64	64.35	1.61	0.92	2.45
2H-4, 86	11.16	37.04	60.92	1.69	1.06	2.68
2H-6, 128	14.58	38.26	62.53	1.71	1.05	2.73
3H-2, 27	17.07	38.22	62.20	1.69	1.04	2.69
3H-4, 131	21.11	34.86	59.52	1.75	1.14	2.78
3H-6, 93	23.73	34.11	57.69	1.76	1.16	2.67
4H-2, 108	27.38	36.32	60.59	1.75	1.11	2.73
4H-5, 62	31.42	34.57	57.72	1.74	1.14	2.62
4H-6, 105	33.35	33.45	57.80	1.78	1.18	2.76
5H-2, 73	36.53	36.47	60.98	1.76	1.12	2.76
5H-4, 49	39.29	38.01	61.39	1.67	1.04	2.63
10X-3, 50	85.30	32.99	57.27	1.96	1.31	2.76
120-749C-						
7R-2, 68	161.18	34.65	59.66	1.76	1.15	2.83
7R-3, 29	162.29	30.74	54.76	1.81	1.25	2.76
7R-2, 68	161.18	34.65	59.66	1.76	1.15	2.83
7R-3, 29	162.29	30.4	54.76	1.81	1.25	2.76
12R-1, 31	206.81	5.72	14.29	2.73	2.57	2.79
12R-1, 79	207.29	5.13	13.62	2.87	2.72	2.97
12R-1, 103	207.53	5.93	14.34	2.62	2.46	2.70
12R-2, 9	208.09	6.85	16.87	2.67	2.49	2.81
12R-2, 94	208.94	6.25	15.54	2.82	2.64	2.81
12R-3, 52	210.02	3.46	8.79	2.78	2.68	2.73
12R-4, 126	212.19	3.01	8.21	2.94	2.85	2.93
15R-1, 99	231.49	0.28	0.80	2.92	2.92	2.91
15R-2, 106	233.06	0.99	2.76	2.90	2.87	2.88
15R-3, 42	233.92	0.96	2.67	3.08	3.05	2.88
15R-4, 17	235.17	2.39	6.28	3.09	3.02	2.78
15R-4, 100	237.50	1.71	4.75	2.96	2.91	2.92
15R-6, 118	239.18	2.43	6.57	2.89	2.82	2.87
16R-1, 14	240.14	1.36	8.59	2.91	2.87	6.95
16R-2, 24	241.74	4.61	10.98	2.44	2.33	2.59
16R-3, 12	243.06	7.37	17.36	2.40	2.23	2.68
16R-4, 17	244.61	3.50	8.80	2.65	2.56	2.71
16R-5, 57	246.51	1.70	4.47	2.76	2.71	2.76
16R-7, 86	249.63	1.15	3.13	2.82	2.79	2.82

scribed as Subunit IIA by the shipboard sedimentologists (see "Lithostratigraphy and Sedimentology" section, this chapter). Average wet-bulk, dry-bulk, and grain densities are 1.70, 1.08, and 2.66 g/cm^3, respectively, in Subunit IIA, whereas average water content and porosity are 37% and 60%, respectively. The diatom ooze horizon representing Unit I from 0 to 0.24 mbsf is not evident in the physical properties data due to the limited extent of this lithology. The presence of chert below 43.8 mbsf and the resulting poor recovery made it impossible to determine index properties for the lower sedimentary sequence of Hole 749B.

At Hole 749C the sedimentary sequence is represented by only two data points for index properties at 161.18 and 162.29 mbsf. The values determined from these two samples generally agree with those from Hole 749B for the nannofossil ooze of Subunit IIA. However, this sequence is described as Subunit IIB by the shipboard sedimentologists, primarily because of the presence of numerous chert fragments.

Basalt in Cores 120-749C-12R, -15R, and -16R provided material for the remaining determinations of index properties at this site. The range of values for index properties determined in the basalts correlates with the degree of alteration of these samples. Increased alteration is consistent with increased porosity and water content and decreased wet-bulk and dry-bulk densities in these samples. Porosity and water content in Core 120-749C-12R range from maximum values of 16.9% and 6.9% to minimum values of 8.2% and 3.0%, respectively.

In Cores 120-749C-15R and -16R porosity and water content increase in two steps from minimum values of 0.8% and 0.3% to maximum values of 17.4% and 7.4%, respectively. Wet-bulk and dry-bulk densities range from maximum values of 3.1 and 3.0 g/cm^3 to minimum values of 2.4 and 2.2 g/cm^3, respectively, over corresponding intervals.

Compressional Wave Velocity

Compressional wave velocity was determined by both continuous and discrete methods. Continuous values of *P*-wave velocity were obtained using the PWL, which consists of transducers mounted on the GRAPE unit. Discrete *P*-wave velocities were obtained using the Hamilton Frame velocimeter. The Hamilton Frame was used to measure discrete samples from the working half of the core. The methods used for obtaining these measurements are discussed in the "Explanatory Notes" chapter (this volume). The direction of propagation is generally perpendicular to the split face of the core, although some samples are tested at other orientations, using the Hamilton Frame, to investigate anisotropy in various lithologies.

The large difference between the velocities measured in the sediments and those obtained from igneous rocks (below ~203 mbsf) are graphically displayed in Figure 24. The average velocity, measured in the interval to ~40 mbsf corresponding to the nannofossil ooze of Subunit IIA, was 1542 m/s. This value increased slightly in Subunit IIB to 1573 m/s; however, this average is based on only three measurements of recovered material. The actual average velocity in Subunit IIB could be considerably greater because of the higher velocity chert fragments found throughout this unit. Compressional wave velocities measured in the basement range from 3532 to 5749 m/s (DIR = C; see Table 12). The large variability in velocity values generally correlates with changes in density and porosity (see Figs. 23 and 24). These velocity values are also related to the degree of alteration in the basalts.

Undrained Shear Strength

The undrained shear strength in the sediment cored at Site 749 is relatively low due to core disturbance and poor recovery downhole (Table 13). The maximum undrained shear strength measured is 16.5 kPa at 11.19 mbsf in Hole 749B (see Fig. 25).

Thermal Conductivity

Samples from Site 749 were measured for thermal conductivity using two techniques. For sediment, a needle probe was inserted and heated (Table 14); measurements were made over a 6-min period (Von Herzen and Maxwell, 1959). For igneous rock, a heated needle probe was sandwiched between a slab of low-conducting material and the sample, and measurements were taken for 6 min (Vacquier, 1985; Robinson, Von Herzen, et al., 1989). Only runs that displayed a temperature drift rate less than 0.04 °C/min were retained for analysis (see "Explanatory Notes" chapter, this volume). Downhole temperatures were not measured at this site.

Strong relationships exist between thermal conductivity, physical properties, and lithology. Changes in index properties, such as wet-bulk density, porosity, and water content, cause changes in thermal conductivity downhole. The minimum value of thermal conductivity is 1.20 W/m·K at 7.60 mbsf. Below this depth in Hole 749B conductivity gradually increases to a maximum of 1.54 at 37.0 mbsf. The low values at ~85 mbsf may result from increased water in these core sections.

The effects of basaltic alteration are clearly illustrated in the trends of thermal conductivity below ~207 mbsf. Porosity changes are mirrored by conductivity throughout the basement sequences. An increase in porosity to 17.4% at ~243 mbsf

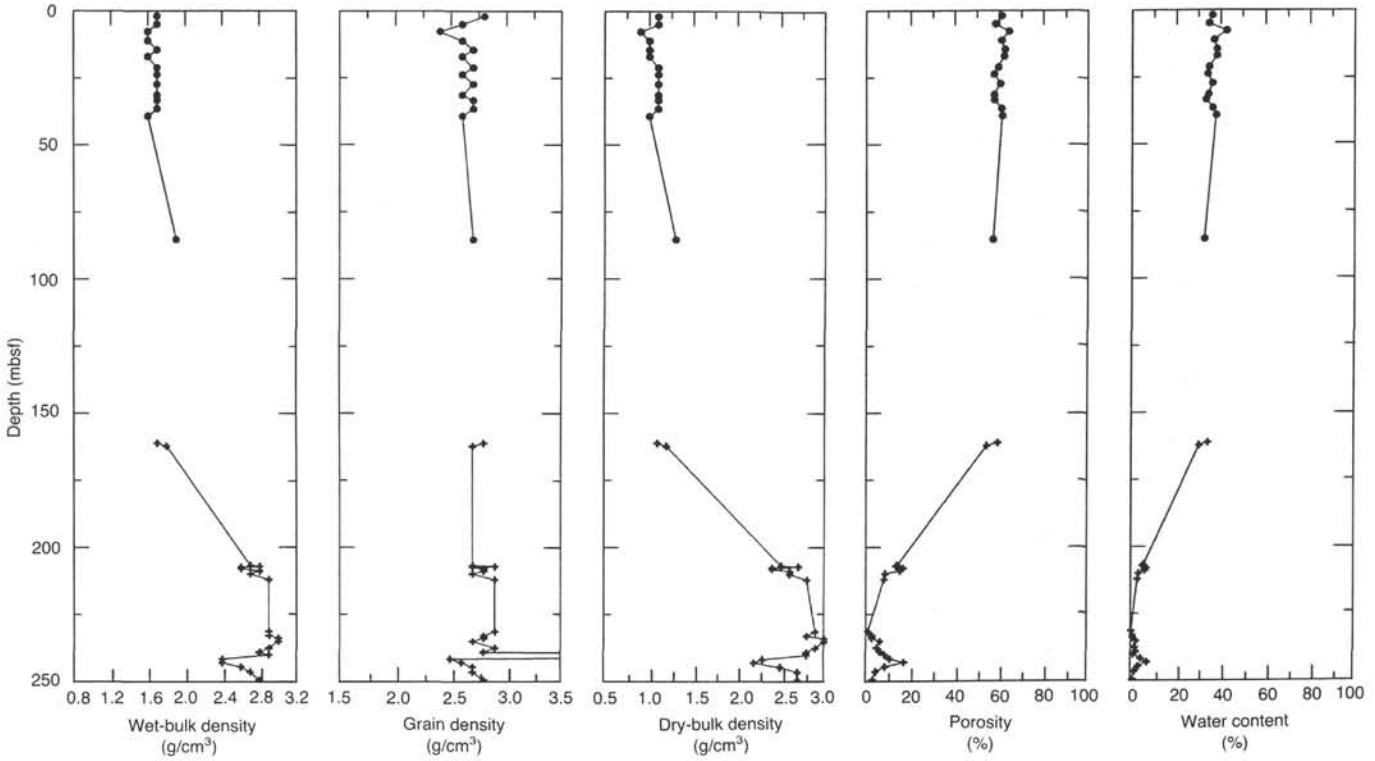

Figure 23. Downhole changes in index properties (wet- and dry-bulk density, grain density, porosity, and water content) at Site 749.

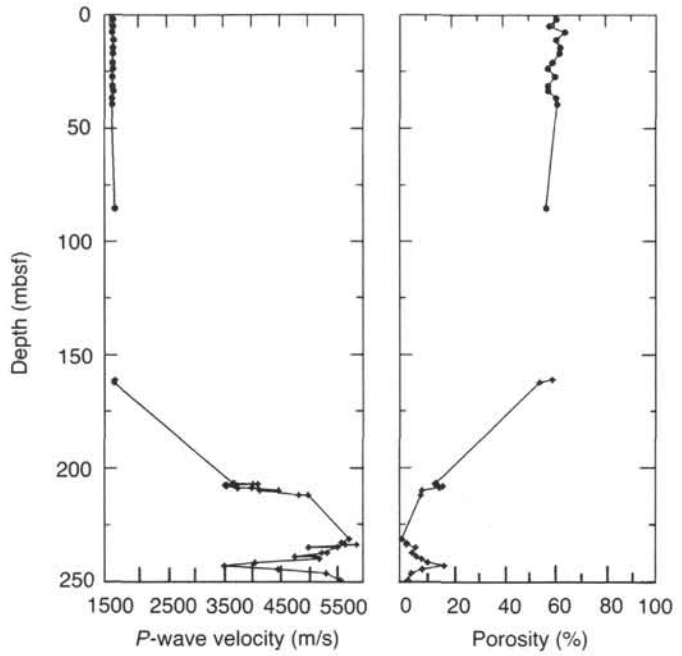

Figure 24. Comparison between compressional wave velocity measured with the Hamilton Frame and porosity values at Site 749. Increased velocities below 203 mbsf indicate basement.

causes a decrease in conductivity to 1.54 W/m·K (see Fig. 26). Thermal conductivity begins to increase below this level as both porosity and water content decrease, and wet-bulk density increases. These trends arise from basalts exhibiting less alteration downward in the flow.

GRAPE and *P*-Wave Logger

The GRAPE and the PWL provide a semicontinuous record of wet-bulk density and compressional wave velocity, respectively. These two instruments take closely spaced measurements, parallel to bedding, through the plastic core liner of the whole-round APC or XCB core sections. The data from these two techniques at Hole 749B show general trends of fairly constant GRAPE bulk density and *P*-wave velocity with depth to ~110 mbsf (see Fig. 27). These data exhibit trends that are similar to those seen in the discrete (gravimetric bulk density and compressional wave velocity) measurements discussed in previous sections of this report. Compressional wave velocities measured from discrete samples are, however, consistently higher than the continuous values from the PWL (see Fig. 27).

Conclusions

The results from Site 749 show clearly the change in physical properties between the sedimentary section and basement. The variations in index properties and velocities within the basement illustrate the effect of alteration on the physical properties of basalt at this site. The low recovery of sediment containing chert resulted in incomplete profiles of physical properties at this site.

IGNEOUS PETROLOGY

Introduction

Basement composed of fresh to highly altered basalt flows was encountered at 202 mbsf and cored to a depth of 249.5 mbsf with 49% recovery. The basement is overlain by nannofossil ooze with interlayered chert stringers of early Eocene age. The sediment-basalt contact was not recovered. However, the basement depth was inferred from a marked decrease in the penetration rate at 202 mbsf.

Table 12. Compressional wave velocity measured using the Hamilton Frame, Site 749.

Core, section, interval (cm)	Depth (mbsf)	DIR	Velocity (m/s)
120-749B-			
1H-2, 52	2.02	C	1555.6
1H-4, 52	5.02	C	1553.2
2H-2, 48	7.78	C	1535.4
2H-4, 86	11.16	C	1562.8
2H-6, 128	14.58	C	1551.5
3H-2, 27	17.07	C	1551.7
3H-4, 131	21.11	C	1543.5
3H-6, 93	23.73	C	1549.7
4H-2, 108	27.38	C	1538.8
4H-5, 62	31.42	C	1539.5
4H-6, 105	33.35	C	1555.5
5H-2, 73	36.53	C	1528.8
5H-4, 49	39.29	C	1530.1
10X-3, 50	85.30	C	1583.7
7R-2, 68	161.18	C	1583.9
7R-3, 29	162.29	C	1565.6
12R-1, 31	206.81	C	3678.5
12R-1, 31	206.81	A	3709.6
12R-1, 79	207.29	C	4115.4
12R-1, 79	207.29	A	4031.7
12R-1, 103	207.53	C	3531.9
12R-1, 103	207.53	A	3571.5
12R-2, 9	208.09	C	3568.6
12R-2, 9	208.09	A	3564.8
12R-2, 94	208.94	C	3758.5
12R-2, 94	208.94	A	4007.8
12R-3, 52	210.02	C	4490.2
12R-3, 52	210.02	A	4152.6
12R-4, 126	212.19	C	4852.6
12R-4, 126	212.19	A	5020.6
15R-1, 99	231.49	C	5749.0
15R-2, 106	233.06	C	5609.1
15R-3, 42	233.92	C	5683.9
15R-3, 42	233.92	A	5882.5
15R-4, 17	235.17	C	5027.2
15R-4, 17	235.17	A	5540.8
15R-5, 100	237.50	C	5261.7
15R-5, 100	237.50	A	5354.2
15R-6, 118	239.18	C	4782.3
15R-6, 118	239.18	A	5130.4
16R-1, 14	240.14	C	5214.2
16R-2, 24	241.74	C	4067.2
16R-3, 12	243.06	C	3524.9
16R-4, 17	244.61	C	4480.9
16R-5, 57	346.51	C	5338.8
16R-7, 86	249.63	C	5593.6

Note: DIR = direction of wave propagation; A = perpendicular to bedding; B = parallel to bedding; and C = parallel to split face of core.

Table 13. Undrained shear strength determined from Wykeham-Farrance Vane data, Site 749.

Core, section, interval (cm)	Depth (mbsf)	S_u (kPa)
120-749B-		
1H-2, 50	2.00	5.5
1H-4, 50	5.00	2.3
2H-2, 50	7.80	9.2
2H-4, 89	11.19	16.5
2H-6, 125	14.55	15.6
3H-2, 14	16.94	12.8
3H-4, 134	21.14	10.1
3H-6, 90	23.70	9.2
4H-2, 111	27.41	5.5
4H-5, 58	31.38	8.3
4H-6, 101	33.31	14.7
5H-2, 76	36.56	4.6
5H-4, 79	39.59	4.6
10X-3, 50	85.30	3.2
120-749C-		
7R-2, 63	161.13	7.3
7R-3, 32	162.32	8.7

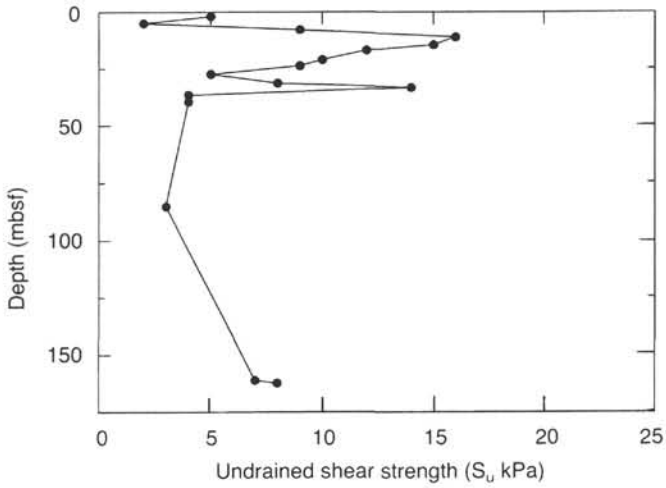

Figure 25. Undrained shear strength (S_u) in Hole 749B measured using the Wykeham-Farrance Motorized Vane device.

Basement recovery was limited to two intervals: (I) Core 120-749C-12R (53% recovery) and (II) Cores 120-749C-15R and -16R (92% recovery). These two intervals are separated by a 14.5-m zone of no recovery (i.e., Cores 120-749C-13R and -14R).

Macroscopic Core Description

All the basalt flows have altered and vesicular tops, grading into fresher, more massive basalt toward the interior.

Interval I: Basalts in this interval have been subdivided into three units (see core descriptions, this chapter): an upper and lower basalt flow (Units 1 and 3, respectively), which are crosscut by a dike (Unit 2; minimum thickness of 7.5 cm). The top flow consists of highly altered, autobrecciated sparsely phyric basalt (Fig. 28). Small phenocrysts of plagioclase (1 mm) occur in a microcrystalline matrix. The top basalt flow is truncated by a dark gray, nonvesicular, and relatively fresh, sparsely clinopyroxene and plagioclase phyric basalt. The contact is sharp and marked by a calcite-lined chilled margin 2–3 cm thick (Fig. 29). The contact between the dike and the lower flow was not recovered.

The lower flow (2.5 m recovered) consists of a sparsely plagioclase, phyric, amygdaloidal basalt. This flow is moderately altered, but it is fresher, for the most part, than the uppermost flow. The contact between the dike and this flow was not recovered. Calcite and clay-lined calcite veins crosscut the lower basalt flow (Fig. 30).

Interval II: This 18-m section of basement consists of three basalt flows that, from top to bottom, are 7.0, 2.5, and 8.5 m (minimum) thick (Units 4–6, respectively). The top flow is a phyric basalt with clinopyroxene (up to 4 mm) and plagioclase (2–4 mm) phenocrysts set in a fine-grained groundmass. Vesicles, 1–2 mm in size and infilled with calcite and zeolites, are common in the top flow. About 3 m from the top of the uppermost flow, phenocrysts decrease in size and vesicles are rare to absent.

Table 14. Thermal conductivity determinations, Site 748.

Core, section, interval (cm)	Depth (mbsf)	Thermal conductivity (W/m·K)
120-749B-		
1H-2, 30	1.80	1.3950
1H-3, 60	3.60	1.4090
1H-4, 90	5.40	1.3510
2H-2, 30	7.60	1.2030
2H-4, 60	10.90	1.2950
2H-6, 90	14.20	1.3100
3H-2, 30	17.10	1.4100
3H-4, 60	20.40	1.3960
3H-6, 90	23.70	1.4080
4H-2, 100	27.30	1.4660
4H-5, 69	31.49	1.4920
4H-6, 100	33.30	1.4490
5H-2, 120	37.00	1.5470
5H-4, 120	40.00	1.4280
10X-2, 111	84.41	1.3660
10X-3, 111	85.91	1.3230
12X-1, 116	101.96	1.5550
13X-1, 26	110.56	1.5260
120-749C-		
7R-1, 52	159.52	1.5560
7R-2, 52	161.02	1.4710
7R-3, 53	162.53	1.6600
12R-1, 100	207.50	1.9250
12R-2, 10	208.10	1.6210
12R-3, 54	210.04	1.7080
15R-1, 98	231.48	2.1060
15R-2, 107	233.07	2.1370
16R-1, 17	240.17	2.0980
16R-2, 26	241.76	2.2620
16R-2, 12	243.06	1.5410
16R-4, 18	244.62	1.6920
16R-5, 61	246.55	1.8630
16R-7, 88	249.65	1.9310

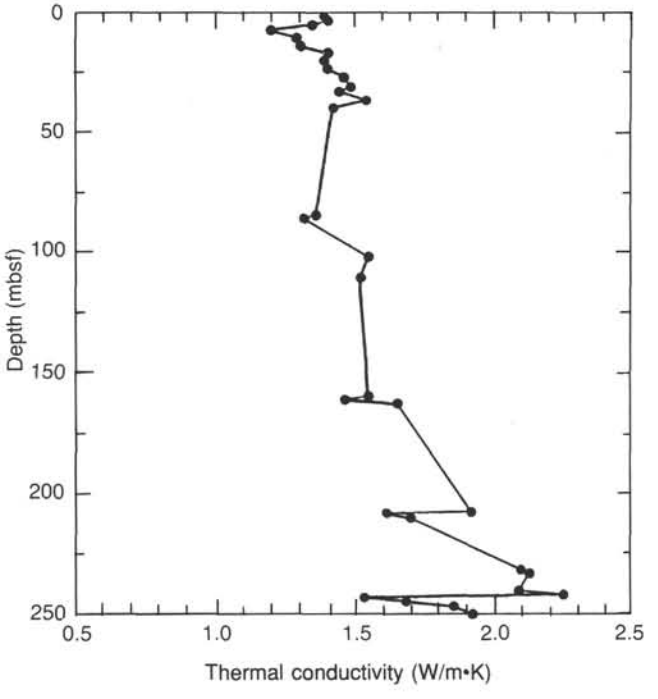

Figure 26. Thermal conductivity measured at Site 749.

The bottom 1 m of this flow is vesicle free and contains only occasional (1 mm) clinopyroxene phenocrysts. The basalt is slightly altered at the top and grades into fresh basalt toward the bottom of the flow.

The contact between the top flow and the middle flow is marked by a microcrystalline chilled margin. Between the flows, there is a 1-cm interval of breccia. The middle basalt flow is amygdaloidal and aphyric. The amygdules are round and are aligned horizontally to subhorizontally (Fig. 31); they consist of smectites and zeolites. The largest amygdules are 3 cm across and occur in the middle of the flow. The bottom of this flow is microcrystalline and finer grained than the interior.

The bottom flow is a massive plagioclase glomeroporphyritic basalt. The top 2 m are moderately to highly altered (clays, zeolites, and calcite); the remainder of the flow consists of fresh basalt. Amygdules and cavities up to 2 cm are found in the top 4 m of the flow and are commonly filled with prismatic zeolites. Plagioclase phenocrysts (up to 7 mm) constitute approximately 30% of the rock and occur as glomeroporphyritic aggregates up to 1.5 cm in size within a leucocratic fine-grained groundmass (Fig. 32).

The absence of hyaloclastites, glassy rims, and pillow structures and the presence of vesicles indicate that the lavas were erupted in a subaerial environment.

Petrography

Interval I: The uppermost flow is a microcrystalline, highly amygdaloidal and altered, brecciated plagioclase-phyric basalt. Small plagioclase phenocrysts up to 1 mm constitute approximately 3% of the rock. The microcrystalline groundmass contains abundant, skeletal, and cubic Fe-Ti oxides, together with clinopyroxenes and plagioclase laths. The breccia fragments appear to be more porphyritic than the enclosing basalt matrix. The contact between the breccia fragments and the matrix is diffuse, suggesting fragmentation just before solidification.

The lower flow consists of a fine-grained, slightly altered, sparsely plagioclase-phyric basalt. Plagioclase phenocrysts form subhedral to euhedral laths and range in size from 1 to 2 mm. They are sometimes zoned and their rims may exhibit slight resorption textures. The fine-grained groundmass consists of a network of euhedral plagioclase laths with intergranular anhedral clinopyroxenes and euhedral Fe-Ti oxides.

The dike that crosscuts the two flows is a nonvesicular, microcrystalline, sparsely plagioclase-clinopyroxene phyric basalt. The plagioclase phenocrysts range in size from 0.5 to 1.5 mm and are often associated with subhedral clinopyroxene laths (up to 0.5 mm). The groundmass is composed of thin plagioclase laths (0.05–0.1 mm), small clinopyroxenes, and disseminated opaques in a microcrystalline, devitrified clay matrix.

Interval II: The uppermost basalt flow contains plagioclase and clinopyroxene phenocrysts set in a fine-grained groundmass with an intergranular texture. Plagioclase (An_{60-87}) forms elongated euhedral laths and ranges in size from 2 to 4 mm. They are often associated with elongated, euhedral clinopyroxene laths (2–4 mm). The groundmass consists of a network of plagioclase (An_{55-60}) with intergranular clinopyroxene and Fe-Ti oxides. The size of crystals within the groundmass ranges from 0.5 to 1 mm.

The middle basalt flow is a microcrystalline, locally amygdaloidal, aphyric basalt. The groundmass consists of small euhedral plagioclase laths (0.05 mm), clinopyroxenes (0.02–0.05 mm), and interstitial Fe-Ti oxides, within a microcrystalline matrix composed essentially of smectites (devitrified glass?).

The lower flow consists of a very distinctive plagioclase glomeroporphyritic basalt. Glomerocrysts consist of three to five zoned, euhedral plagioclase phenocrysts (An_{60-88}) ranging in

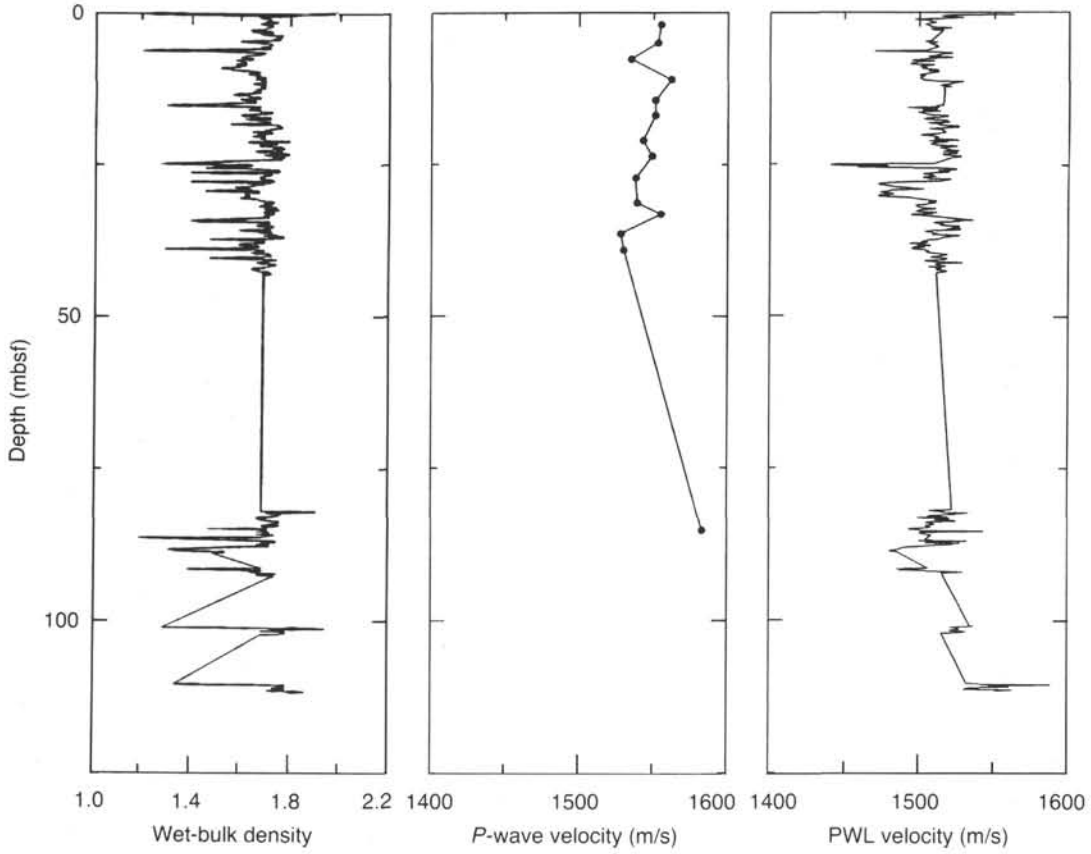

Figure 27. Downhole profiles of GRAPE bulk density and discrete and continuous compressional wave velocity measurements, Hole 749B.

size from 2 to 7 mm. Occasional subhedral aggregates of green clays (2 mm) probably represent pseudomorphs of olivine phenocrysts. The groundmass is fine grained and composed of euhedral plagioclase laths (0.1–0.3 mm), intergranular clinopyroxenes (0.1–0.2 mm), and elongated thin Fe-Ti oxides. The top meter of the flow is highly amygdaloidal and altered. Here, the plagioclase phenocrysts have been transformed to zeolites, and the microcrystalline matrix is partly composed of smectites.

The lavas drilled at Hole 749C are plagioclase phyric basalts with rare clinopyroxene phenocrysts. Olivine is absent apart from the possible pseudomorphs observed in the lower flow. Mineralogically, they differ from the transitional basalts of Hole 747C, which contain both plagioclase and olivine phenocrysts. This may suggest a higher water pressure during crystallization but could also result from magma mixing.

Alteration

The basalts are slightly to highly altered; the secondary mineral assemblage consists of zeolites, smectites, calcite, and minor quartz. They occur in the groundmass, vesicles, and veins and as replacements for plagioclase phenocrysts (Fig. 33). Identification of the secondary minerals was made by optical microscopy and X-ray diffraction (XRD).

Plagioclase phenocrysts in the most altered basalts have been replaced by an undetermined fibrous zeolite. Green to brown smectites together with occasional calcite are observed in the groundmass. The amygdules and some veins may be filled exclusively by green smectite whereas others show a strong mineralogical zonation. In the latter case, the following crystallization sequence can be inferred: green smectite, as a lining of the vesicle or fracture walls, is successively overgrown by zeolite (Fig. 33), calcite, and, in some cases, quartz. This sequence may be repeated more than once in the larger amygdules. The green smectite exhibits a complex XRD pattern, which may suggest the presence of two or more interlayered smectites. The zeolites consist of prismatic laumontite and radial stilbite.

The alteration mineral assemblage developed in basalts from Hole 749C, like that from Hole 747C, has a different character from that commonly observed in Mid-Ocean Ridge basalts (MORB). The main difference is the absence of phillipsite. The absence of sulfide minerals and the presence of goethite indicates that some of the alteration occurred in an oxidizing environment.

The observed secondary mineralogy of Hole 749C bears some resemblance to that of high heat flow in the extensive subaerial tholeiitic flood basalts of Iceland (Kristmannsdòttir and Tòmasson, 1978; Pàlmason et al., 1979). The presence of laumontite and interlayered smectites corresponds to the high-temperature (100°–200°C) zone of the zeolite facies.

Geochemistry

Whole-rock major and trace element analyses are presented in Tables 15 and 16. All samples selected for geochemical analyses are relatively fresh, as evidenced by low loss on ignition (LOI) values (−0.08% to 2.14%). Based on their major element composition, basalts from Hole 749C are olivine or quartz normative tholeiitic basalts.

Since the basalts are variably altered, only elements that are largely immobile during secondary processes are considered in the following discussion of the geochemistry.

The variable Mg# numbers (47–58), chromium (134–280 ppm), and nickel contents (32–92 ppm) indicate that the basalts have

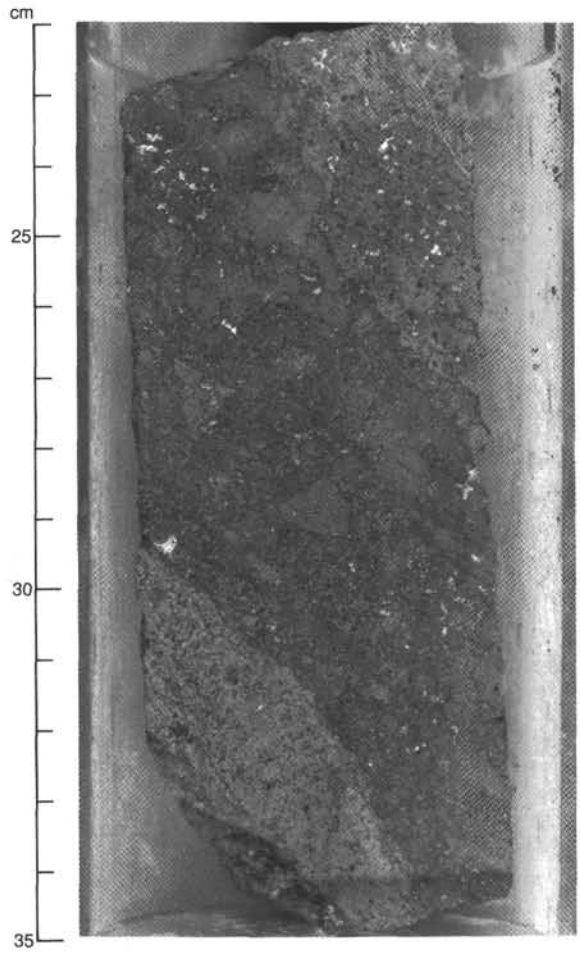

Figure 28. Altered basalt breccia at a flow top (Core 120-749C-12R-2, 22–35 cm).

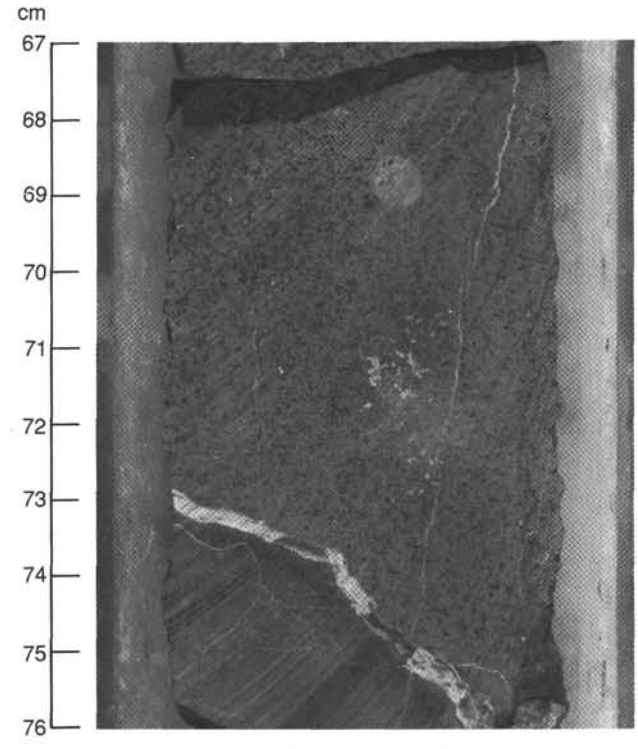

Figure 29. Contact between upper vesiculated basalt flow and darker, aphanitic basalt dike (Core 120-749C-12R-3, 67–76 cm).

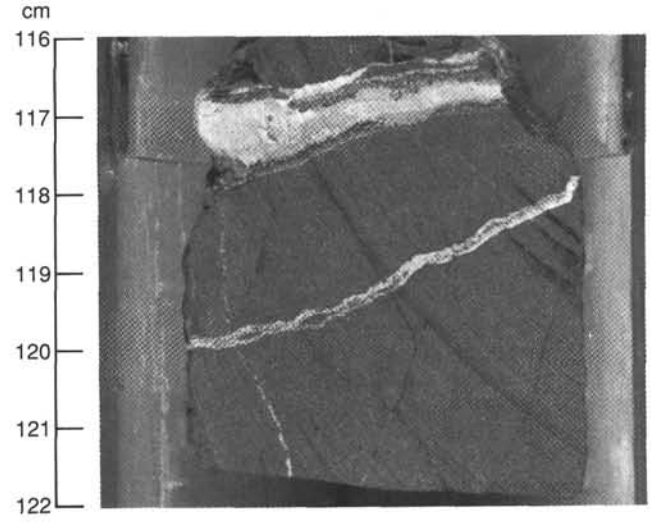

Figure 30. Vertical and subhorizontal calcite and clay-lined calcite veins crosscutting basalt (Core 120-749C-12R-4, 116–122 cm).

undergone different degrees of olivine and clinopyroxene fractionation or accumulation. However, the absence of systematic variations among the Mg# and Ni, Cr, Sr, and the CaO/Al_2O_3 ratios indicates that the individual flows are not necessarily related to each other by fractional crystallization.

Incompatible elements (e.g., Zr, Nb, Y, Ti, and P) show well-correlated trends with positive slopes on correlation diagrams. Hole 749C basalts have lower abundances of incompatible elements than Hole 747C basalts, but similar Zr/Nb ratios (see Fig. 34). Hole 749C and 747C basalts have trace element characteristics that are intermediate between Indian Ocean MORB and ocean-island basalts (OIB) from Site 748 and Kerguelen and Heard islands (Fig. 35). They are similar, however, to some plateau basalts from Kerguelen Island (Storey et al., 1988), basalts from the Nauru Basin (Saunders, 1985) and transitional MORB from the Southwest Indian Ridge, within close proximity of the Bouvet Triple junction (le Roex et al., 1983).

Summary

Five flows and a dike were recovered during basement drilling at Site 749. The flows, which were probably erupted in a subaerial environment, consist of moderately fractionated, plagioclase, and plagioclase-clinopyroxene phyric tholeiitic basalts. Apart from the lowermost flow recovered, olivine is absent from the phenocryst assemblage. In this respect, basalts from Hole 749C differ from those of Hole 747C in that the main ferromagnesian phenocryst phase is clinopyroxene rather than olivine.

The basalts are fresh to highly altered containing zeolites, pure and possibly interlayered smectites, calcite, and minor quartz in amygdules and veins. The possible occurrence of coexisting laumontite and interlayered smectites is diagnostic of the high-temperature zone of the zeolite facies (100°–200°C), indicative of a relatively high paleoheat flow.

Basalts from Hole 749C are more depleted in incompatible elements than those from Hole 747C (for comparable Mg#), although both have similar incompatible element ratios. In this respect, basalts from both sites have compositional characteristics that are transitional between normal MORB and OIB. They are similar to some plateau basalts from Kerguelen Island, transitional basalts from the Southwest Indian Ridge, and basalts from the Nauru Basin.

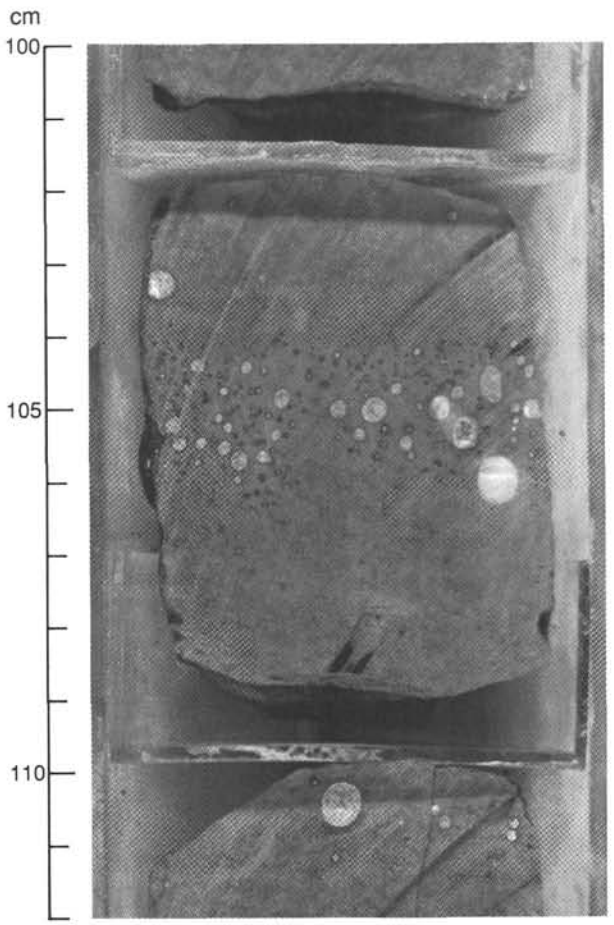

Figure 31. Round amygdules filled with laumontite and smectite (Core 120-749C-15R-6, 100–112 cm).

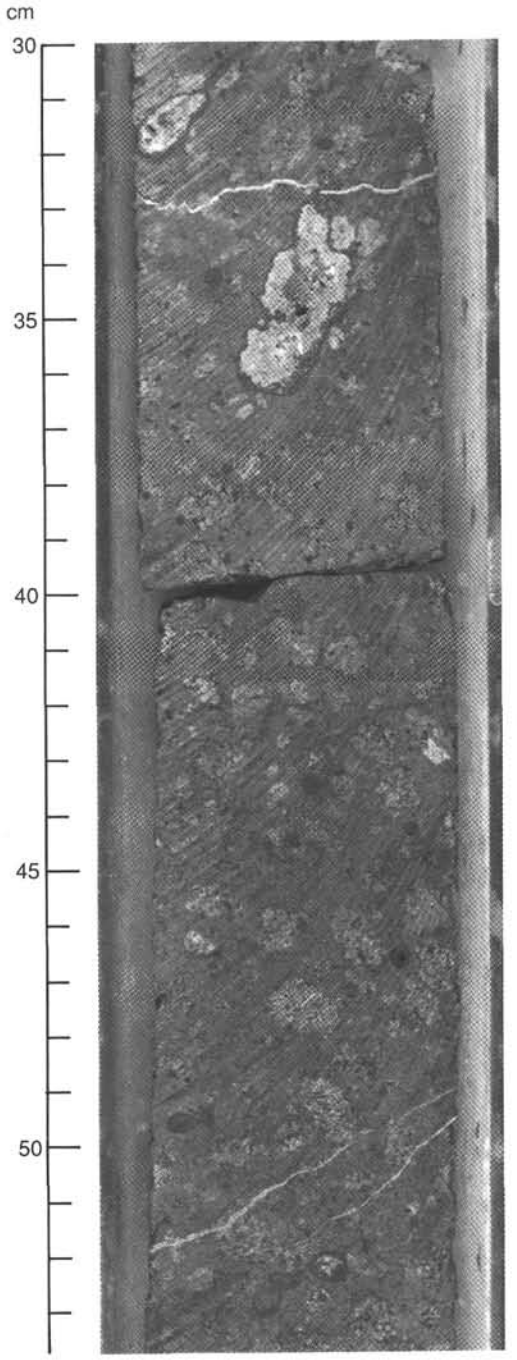

Figure 32. Plagioclase glomeroporphyritic basalt (Core 120-749C-16R-5, 30–54 cm).

SEISMIC STRATIGRAPHY

The seismic sections at Site 749 (Figs. 2, 6, and 7) show a very strong basement reflector overlain by a homogeneous sedimentary sequence (see "Site Geophysics" section, this chapter). This simple subdivision is also observed in the lithologic column (see "Lithostratigraphy and Sedimentology" section, this chapter) and the physical properties measurements (see "Physical Properties" section, this chapter).

The sedimentary section at Site 749 shows only small lithologic changes, which apparently are unable to generate any significant seismic reflector. The sedimentary section is divided into two main lithologic units. Unit I consists of 0.24 m of Pleistocene to mid-Pliocene diatom oozes with foraminifers and ice-rafted debris. Unit II is divided into two subunits and consists of 201.76 m of upper Oligocene to lower Eocene nannofossil ooze with foraminifers, chert, chalk, and porcellanite.

The boundary between Subunit IIA and Subunit IIB lies at 43.6 mbsf and is related to the first occurrence of cherts. The top of Unit III, at 202 mbsf, obviously corresponds to the basement reflector at 0.22–0.24 s TWT. The physical properties (index properties, compressional wave velocities, thermal conductivity) measured on board at Site 749 also indicate a clear change at a depth of about 200 mbsf, which corresponds to the top of Unit III.

The mean compressional wave velocity for Unit I and Subunit IIA is well defined by the shipboard measurements and is 1.55 km/s (Fig. 24). The low recovery of sediment containing chert, mainly in the lower part of Subunit IIB, precluded any significant velocity measurements. Compressional wave velocity measurements on basalt samples yielded values ranging between 3.53 and 5.75 km/s. These large variations in velocity values correlate with changes in density and porosity and appear to be related to the degree of alteration in the basalt.

The basement reflector at Site 749 lies on the *Marion Dufresne* seismic line MD47-13 (shot point 5670) at a depth of 0.22 s TWT below seafloor and on the *JOIDES Resolution* seismic profile (Line 3), at a depth of 0.24 s TWT below seafloor. As previously discussed (see "Site Geophysics" section, this chapter), a basement depth of 0.23 s TWT is adopted at the location of the site. The corresponding mean compressional wave veloc-

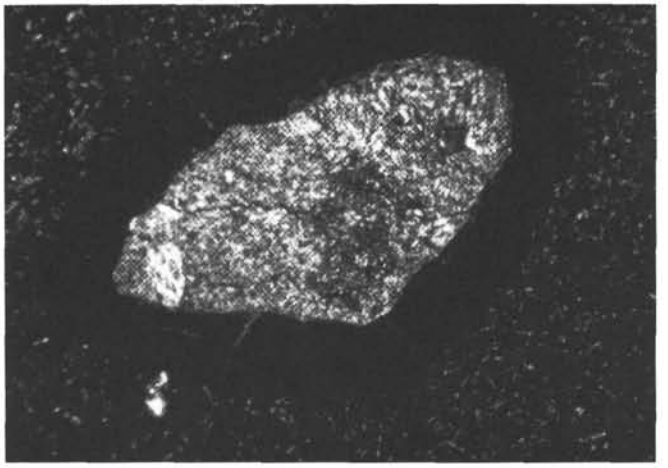

Figure 33. Photomicrograph of a clay-lined, zeolite-filled amygdule. Width of field of view = 2.5 mm. Sample 120-749C-16R-1, 99–101 cm, cross-polarized light.

Table 15. Major element analyses and normative composition of basalts from Hole 748C.

Core, section, interval (cm)	12R-3 106–108	12R-5 49–51	15R-2 35–37	15R-5 73–75	15R-6 124–126	16R-6 111–113	16R-7 107–109
SiO_2	55.18	52.24	52.77	52.20	50.27	49.05	49.03
TiO_2	1.60	1.49	1.46	1.45	1.73	0.91	0.89
Al_2O_3	15.81	14.77	14.32	14.31	14.43	19.68	19.18
Fe_2O_3	11.09	11.12	11.88	11.67	13.47	8.73	9.42
MnO	0.14	0.14	0.18	0.16	0.15	0.10	0.12
MgO	6.31	5.78	6.42	6.61	6.75	6.45	7.24
CaO	8.24	9.51	9.72	9.25	9.68	12.50	12.20
Na_2O	4.11	3.55	3.40	3.42	3.68	3.06	3.03
K_2O	0.71	0.65	0.48	0.51	0.25	0.10	0.09
P_2O_5	0.17	0.16	0.15	0.15	0.19	0.08	0.08
Total	99.35	99.40	100.77	99.74	100.60	100.65	101.28
LOI	1.70	0.71	−0.08	0.29	0.59	2.14	1.77
Mg#	46.65	47.75	48.64	49.86	46.88	56.54	57.46
Qz	0	0.01	0.37	0	0	0	0
Ne	0	0	0	0	0	0.54	0.55
Lc	0	0	0	0	0	0	0
Or	4.21	3.90	2.85	3.06	1.49	0.59	0.53
Ab	34.85	30.47	28.80	29.28	31.27	24.89	24.48
An	22.64	22.77	22.42	22.44	22.21	39.66	38.24
Di	14.34	19.92	20.60	19.01	20.58	17.90	17.55
Hy	4.61	17.44	19.49	20.65	7.09	0	0
Ol	13.71	0	0	0.09	10.95	12.78	14.94
Ap	0.37	0.35	0.33	0.33	0.42	0.17	0.17
Il	3.05	2.88	2.78	2.74	3.31	1.73	1.68
Mt	2.21	2.25	2.37	2.35	2.69	1.74	1.86

Note: LOI = loss on ignition.

Table 16. Trace element analyses of basalts from Hole 749C.

Core, section, interval (cm)	Rb	Ba	Nb	Sr	Zr	Y	Zn	Cu	Cr	Ni
120-749C-										
12R-3, 106–108	9	108	7	215	99	27	137	64	241	32
12R-5, 49–51	10	101	8	219	99	28	109	64	219	28
15R-2, 35–37	7	95	7	214	91	28	106	57	216	25
15R-5, 73–75	8	97	8	210	93	28	111	55	213	24
15R-6, 124–126	4	91	9	210	101	29	101	107	134	35
16R-6, 111–113	<1	48	4	226	48	16	63	82	257	59
16R-7, 107–109	1	45	5	215	46	16	64	67	280	92

ity for the entire sedimentary column, as derived from drilling and seismic data, is 1.76 km/s.

Based upon the measured compressional wave velocity of 1.55 km/s for Unit I and Subunit IIA (43.8 m), it is possible, taking into account the remaining traveltime (0.17 s TWT), to

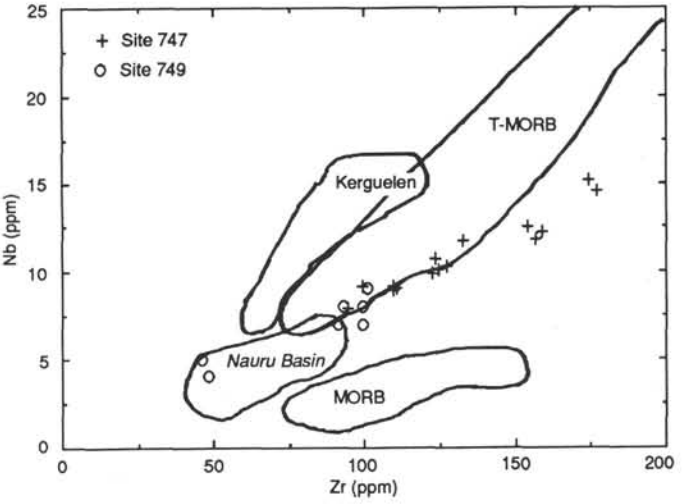

Figure 34. Zr vs. Nb plot showing the well-correlated linear array of data from Sites 747 and 749. Field of oceanic basalts from the Indian Ocean from Nauru Basin (Saunders, 1985), MORB (Price et al., 1986), Kerguelen Island (Storey et al., 1988), and T-MORB (le Roex et al., 1983). T-MORB = transitional basalts from the Southwest Indian Ridge.

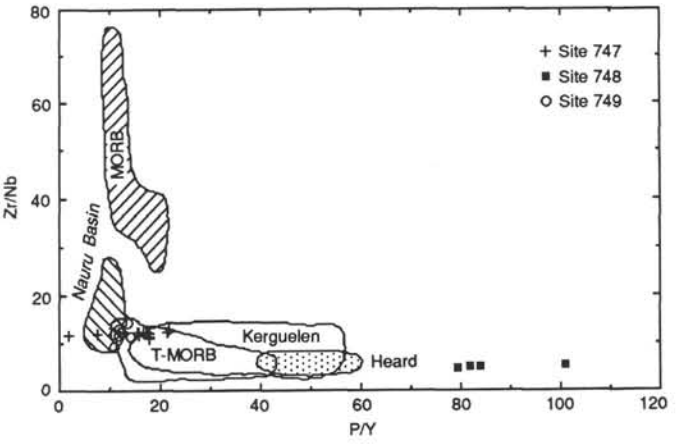

Figure 35. Zr/Nb vs. P/Y plot showing data from Sites 747, 748, and 749 with respect to MORB, Nauru, Kerguelen Island, T-MORB, and Heard Island fields. Heard Island data from Storey et al. (1988). See Figure 34 caption for references to Indian Ocean fields.

calculate a mean compressional wave velocity of about 1.85 km/s for Subunit IIB. This value is compatible with the presence of chert stringers in the nannofossil ooze and chalk of Subunit IIB. Subunits IIA and IIB are characterized by low-amplitude reflectors with high continuity. The corresponding seismic sequence thins by toplap and onlap on approach to the site. The interpreted seismic section (*Marion Dufresne*, MD47-13) at Site 749 is given in Figure 36.

The basement recovered at Site 749 consists of five basalt flows that are crosscut by a 7.5-cm dike. The basalts are fresh to highly altered and were probably erupted in a subaerial environment. Their compositional characteristics are transitional between normal MORB and OIB; moreover, they are similar to some Kerguelen Island plateau basalts (see "Igneous Petrology" section, this chapter).

The sedimentary section recovered at Site 749 spans the lower Eocene and the upper Oligocene and reflects only a lim-

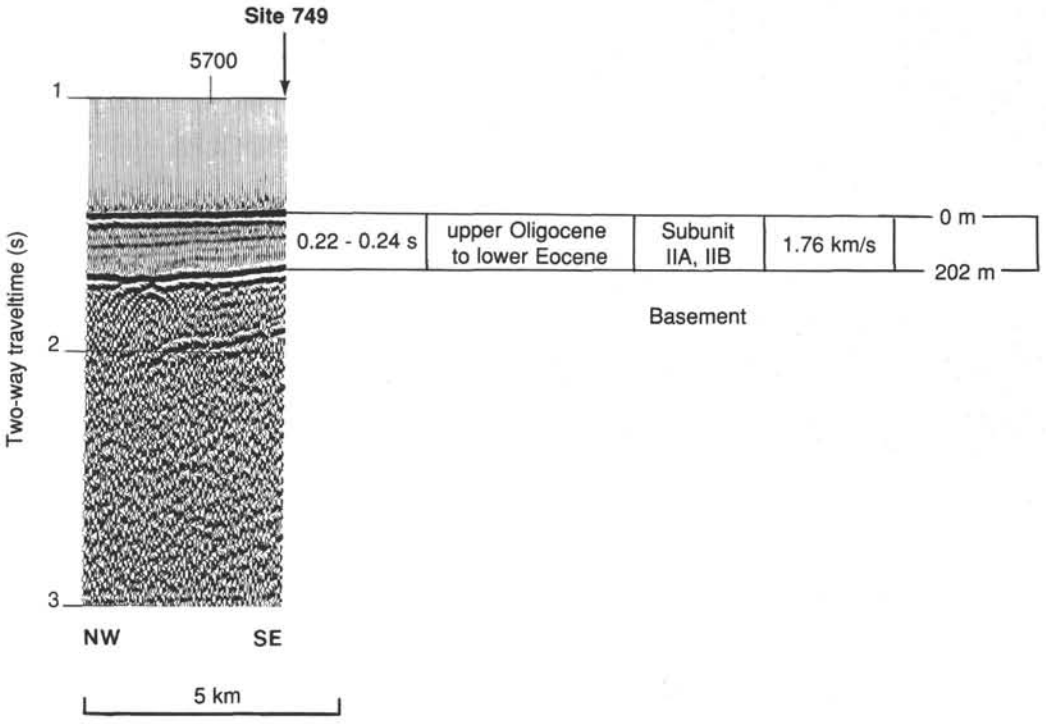

Figure 36. Interpretation of the *Marion Dufresne* (MD47-13) seismic reflection profiles at Site 749 with corresponding lithostratigraphic units. The uninterpreted seismic section is shown in Figure 7.

ited part of the evolution of the Southern Kerguelen Plateau (Banzare Bank). It is clear that most of the reflectors observed on the seismic section (MD47-13) disappear by onlap at the contact with the basement; thus, the sediments resting upon the basalt flows at Site 749 are significantly younger than the basalt itself. Basement was formed close to sea level, whereas the paleodepth of the lower Eocene sediments ranged between 1000 and 1500 m; the corresponding subsidence rate will be evaluated later after shore-based age determination of the basalt flows.

Sedimentation rates are highly variable. During the early Eocene, the rate is extremely high and reaches 70 m/m.y.; between the middle Eocene and the late Oligocene, the rate varies from 8 to 3.6 m/m.y. The sedimentary section is characterized by two hiatuses. The first hiatus, which lasts at least 2 m.y., occurred in the middle Eocene. If confirmed by complementary shore-based studies, this event could be related to the separation by seafloor spreading of the Northern Kerguelen Plateau and Broken Ridge dated at 43–42 Ma (Munschy and Schlich, 1987). The second hiatus, observed between the late Oligocene and mid-Pliocene (26 m.y.), may be related to major erosional events.

SUMMARY AND CONCLUSIONS

Site 749 (proposed Site SKP-4A; 58°43.03′S, 76°24.45′E; water depth = 1069.5 m) is a short-term reentry site located on the western flank of the Banzare Bank, on the Southern Kerguelen Plateau. The Banzare Bank corresponds to a smooth basement rise that crests east of the site at a water depth of about 700 m. The sediments gradually thin toward the top of the bank where several faults cut the basement structure. The site is intended to recover extensive basement rocks from the Southern Kerguelen Plateau with penetration of at least 200 m.

Operations

The upper 43.8 m of section was cored with 100% recovery using the APC, whereupon middle Eocene cherts were encountered, which reduced recovery via the APC and XCB to only 26% over the next 80 m. A change to the RCB yielded only 7% recovery through cherts, chalks, and oozes to the basement contact at 202 m. After obtaining 5 m of basalt in the next core, the succeeding two cores were essentially empty, and a model LH minicone was deployed to allow the hole to be reentered after a bit change. This was the first use of a free-fall Hayes minicone for a dedicated basement site.

Inspection of the BHA on deck showed that severe pounding of the bit against hard bottom in high seas at this shallow site had resulted in a badly worn bit and a broken flapper valve. The latter had precluded any recovery in the last two cores. A novel decision was made by the ODP Cruise Operations Manager, Mr. Lamar Hayes, to core without a flapper valve, and to institute instead a weighted mud program to prevent backflow of cuttings into the BHA. After a 16-min reentry, this procedure worked beyond expectations because the next two cores produced 17.83 m of basalt at a recovery rate of 94%. As the last core was being cut, a medical emergency involving Mr. Hayes ended operations at this site, and the *JOIDES Resolution* was put on course for Fremantle, Australia. Mr. Hayes died on 28 March 1988; the ship arrived at Fremantle on 5 April 1988.

Geophysics

Site 749 is located on French MCS line MD47-13 (shot point 5670) trending northwest across the Banzare Bank. The seismic section shows a very strong basement reflector overlain near the site by a thin sedimentary sequence that thickens downslope in all directions, essentially by toplap and without obvious unconformity. As stated previously, the Banzare Bank, west of the Raggatt Basin, corresponds to a clear topographic high that crests at about 700 m below sea level. The central portion of this domal feature is about 40 km across and has been eroded to expose basement outcrops. To the north the Banzare Bank extends to the southern end of the 77°E Graben; normal faults to the

north (north trending) and to the south and southeast (northwest trending) affect the basement structure.

At Site 749 the basement reflector lies at about 0.22 s TWT below seafloor on the *Marion Dufresne* seismic line and 0.24 TWT on the *JOIDES Resolution* seismic record. The difference may be explained by a slight discrepancy in navigation, but it can also be related to the characteristics of the seismic equipment used on both ships. Taking into account the mean velocity derived from a previous sonobuoy experiment and the calculated seismic reflection stack velocities, basement was expected at about 200 m below seafloor.

Lithobiostratigraphy and Igneous Petrology

Lithologic units (Table 2) recognized at Site 749 are presented as a composite section from the seafloor down as follows:

Unit I: depth, 0–0.24 mbsf; age, Pleistocene to mid-Pliocene; diatom ooze with foraminifers. A lag of volcanic and ice-rafted debris forms the base of the unit above a major disconformity; a minor disconformity separates the Pliocene and Pleistocene.

Unit II: depth, 0.24–202 mbsf; age, late Oligocene to early Eocene; nannofossil ooze with chert, chalk, and porcellanite, divisible into two subunits based on the first occurrence of chert.

Subunit IIA: depth, 0.24–43.6 mbsf; age, late Oligocene to middle Eocene; nannofossil ooze with foraminifers plus some siliceous microfossils and minor volcanic ash in the upper 25 m.

Subunit IIB: depth, 43.6–202 mbsf; age, middle Eocene to early Eocene; nannofossil ooze, with chalk, chert, and porcellanite; 3% sponge spicules and radiolarians between 53 and 82 mbsf only.

Unit III: depth, 202–249.5 mbsf; clinopyroxene-plagioclase phyric basalts. The 23.1 m of basalt recovered consists of five flows and one dike. Most flows have altered and vesicular tops but grade to fresh and more massive basalt toward the interior of the flow. The basalts are either quartz or olivine normative tholeiites and range in Mg# from 46.5 to 57.5. The high Mg# basalt contains olivine and plagioclase phenocrysts. All other basalts have plagioclase (An_{60-87}) as the main phenocryst phase, together with occasional clinopyroxene. The groundmass phases consist of plagioclase (An_{55-60}), clinopyroxene, and Fe-Ti oxides.

Paleomagnetism of Basaltic Basement

Basement samples were taken at Site 749 from five basalt flows and from one dike for paleolatitude determinations. All samples except one possess single-component magnetizations; the directions of magnetization are very stable and tightly clustered on the stereographic projection. The six remaining samples have absolute inclination values ranging from 52° to 69° (Table 5). A preliminary arithmetic average of one thermally demagnetized and six AF demagnetized samples gave a mean inclination of −63°, which is equivalent to a mean magnetic paleolatitude of 45° under the assumption of an axial geocentric dipole field.

Physical Properties

Index properties were measured for the nannofossil ooze downhole to 43.8 mbsf, but the presence of chert and the consequent poor recovery made it impossible to determine those properties for the lower sedimentary sequence. The mean compressional wave velocity for the pelagic sediments of Subunit IIA is 1542 m/s. The range of values for index properties determined in the basalts correlates with the degree of alteration, that is, increased alteration correlates with increased porosity and water content and decreased wet-bulk and dry-bulk densities. Compressional wave velocites also varied with alteration and corresponding changes in density and porosity; they ranged between 3532 and 5749 m/s. Because of chert in the section, it was not possible to take heat flow measurements.

Seismic Stratigraphy, Nature of Basement, and Sedimentary History

As stated previously, the seismic section at Site 749 is characterized by a very strong reflector at 0.22–0.24 s TWT, which obviously corresponds to the top of Unit III (basement). The sedimentary section shows only small lithologic changes, which apparently are unable to generate any significant seismic reflectors. The mean compressional wave velocity for the entire sedimentary column, as derived from drilling and seismic data, is 1.76 km/s. Based upon the measured compressional wave velocity of 1.55 km/s for Unit I and Subunit IIA, the calculated mean velocity for Subunit IIB is 1.85 km/s. This value is compatible with the presence of chert stringers in the nannofossil ooze and chalk of Subunit IIB.

The basement basalts at Site 749 are more depleted in incompatible trace elements than those from Site 747, although basalts from both sites do have similar Zr/Nb and P/Y ratios (Figs. 34 and 35). Both Site 747 and 749 basalts are slightly more enriched in incompatible elements than normal MORB. They are compositionally similar to transitional MORB and oceanic flood basalts such as those from the Nauru Basin (DSDP Leg 89). In contrast to basalts from Site 747, the basalts from Site 749 do not form a coherent group or trend on key variation diagrams. This indicates that the basalts from Site 749 cannot be related to each other by simple fractional crystallization or partial melting alone.

Alteration in these basalts occurs in the groundmass, amygdules, and veins and as a replacement for plagioclase phenocrysts. The alteration assemblage consists of laumontite, stilbite, interlayered smectite, calcite, and occasional quartz, which is diagnostic of the high-temperature zeolite facies (100°–200°C). This alteration assemblage at Site 749 is not observed at normal mid-ocean ridge segments, but it does occur in places associated with a high heat flow such as Iceland. The shallow depth of this alteration zone combined with its relative high temperature indicates a high paleoheat flow.

The oldest sediments above basement are dated from 54 to 55 Ma (nannofossil Zone NP12). Most of the reflectors observed on the seismic section (MD47-13) disappear by onlap at the contact with the basement; thus, the sediments resting on the basalt flows at Site 749 are significantly younger than the basalt itself. Benthic foraminifers indicate that the paleodepth at this site has been virtually constant (between 1000 and 1500 m or lower bathyal water depths) since the early Eocene. Sedimentation rates, however, vary considerably, being inferred to be as high as 70 m/m.y. for the lower and lower middle Eocene, then dropping to 6.5 to 8 m/m.y. for the middle middle to upper middle Eocene and a very low 3.6 m/m.y. for the upper Eocene and Oligocene.

The abnormally high sedimentation rate for the early and early middle Eocene may be attributable to constant synsedimentary scouring and redeposition of pelagic oozes, particularly from nearby exposed basement surfaces, thereby contributing to a type of sediment "drift" deposit at this site. The onlap of Eocene strata onto basement only 10 km southeast of Site 749 (Fig. 2) indicates that the basement high could indeed have been exposed and continually scoured in this region during the deposition of the lower Eocene strata at Site 749.

The range in sedimentation rates given for the middle Eocene (6.5 or 8 m/m.y.) is a function of the control points used. The presence of a disconformity of at least 2 m.y. related to the separation by seafloor spreading of the Kerguelen Plateau and Broken Ridge (Munschy and Schlich, 1987) might explain the ambiguity. A more obvious disconformity separates the mid-Pliocene

from the lower upper Oligocene. The corresponding hiatus represents a minimum of 25 m.y. (from 4 to 29 Ma).

Large burrows within the uppermost Oligocene strata just below the disconformity contain a mixture of mid-Pliocene, upper Miocene, and Oligocene diatoms. No trace, however, remains of an upper Miocene unit above the disconformity, and presumably any such unit has been eroded away after the burrows were formed and filled. Instead, a mid-Pliocene diatom-bearing sand-gravel (IRD) lag deposit lies above the disconformity. This lag, apparently deposited under the influence of a strong current regime, is disconformably overlain in turn by 15–20 cm of lower Pleistocene diatom ooze, which caps the sequence at this site.

REFERENCES

Aubry, M. P., 1983. Corrélations biostratigraphiques entre les formations paléogènes épicontinentales de l'Europe du Nord-Quest, basées sur le nannoplancton calcaire: essai d'intégration dans l'echelle magnétostratigraphique standard et d'interprétation en fonction des variations eustatiques globales. *Doc. Lab. Geol. Fac. Sci. Lyon*, No. 89.

Berggren, W. A., Kent, D. V., and Flynn, J., 1985a. Jurassic to Paleogene: Part 2, Paleogene geochronology and chronostratigraphy. *In* Snelling, N. J. (Ed.), *The Chronology of the Geological Record.* Geol. Soc. Mem. (London), 10:141–195.

Berggren, W. A., Kent, D. V., Flynn, J. J., and Van Couvering, J. A., 1985b. Cenozoic geochronology. *Geol. Soc. Am. Bull.*, 96:1407–1418.

Berggren, W. A., and Miller, K. G., in press. Cenozoic deep-water benthic foraminiferal stratigraphy. *Micropaleontology.*

Boyce, R. E., 1976. Definitions and laboratory techniques of compressional sound velocity parameters and wet-water content, wet-bulk density, and porosity parameters by gravimetric and gamma ray attenuation techniques. *In* Schlanger, S. O., Jackson, E. D., et al., *Init. Repts. DSDP*, 33: Washington (U.S. Govt. Printing Office), 931–955.

_____, 1977. Deep Sea Drilling Project procedures for shear strength measurements of clayey sediment using modified Wykeham Farrance laboratory vane apparatus. *In* Barker, P. F., Dalziel, I.W.D., et al., *Init. Repts. DSDP*, 36: Washington (U.S. Govt. Printing Office), 1059–1068.

Chen, P.-H., 1975. Antarctic radiolaria. *In* Hayes, D. E., Frakes, L. A., et al., *Init. Rept. DSDP*, 28: Washington (U.S. Govt. Printing Office), 437–513.

Drever, J. I., 1982. *The Geochemistry of Natural Waters:* London (Prentice-Hall).

Furuta, T., and Levi, S., 1983. Basement paleomagnetism of Hole 504B. *In* Cann, J. R., Langseth, M. G., Honnorez, J., Von Herzen, R. P., White, S. M., et al., *Init. Repts. DSDP*, 69: Washington (U.S. Govt. Printing Office), 697–703.

Gieskes, J. M., and Peretsman, G., 1986. Water chemistry procedures on SEDCO 471—some comments. *ODP Tech. Note*, No. 5.

Hays, J. D., 1965. Radiolaria and late Tertiary and Quaternary history of Antarctic Seas. *Biology of Antarctic Seas II.* Antarc. Res. Ser. 5: 124–184.

Hays, J. D., and Opdyke, N. D., 1967. Antarctic radiolaria, magnetic reversals and climate change. *Science*, 158:1001–1011.

Houtz, R. E., Hayes, D. E., and Markl, R. G., 1977. Kerguelen Plateau bathymetry, sediment distribution and crustal structure. *Mar. Geol.*, 25:95– 130.

Kaminski, M. A., Gradstein, F. M., and Berggren, W. A., 1989. Paleogene benthic foraminiferal biostratigraphy and paleoecology at Site 647, Southern Labrador Sea. *In* Arthur, M., Srivastava, S., et al., *Proc. ODP, Sci. Results,* 105: College Station, TX (Ocean Drilling Program): 705–730.

Kono, M., 1980. Statistics of paleomagnetic inclination data. *J. Geophys. Res.*, 85:3878–3882.

Kristmannsdòttir, H., and Tòmasson, J., 1978. Zeolite zones in geothermal areas in Iceland. *In* Sand, L. B., and Mumpton, F. A. (Eds.), *Natural Zeolites: Occurrence, Properties, and Use:* Oxford (Pergamon), 277–284.

Lambe, T. W., and Whitman, R. V., 1969. *Soil Mechanics:* New York (John Wiley).

le Roex, A. P., Dick, H.J.B., Erlank, A. J., Reid, A. M., Frey, F. A., and Hart, S. R., 1983. Geochemistry, mineralogy and petrogenesis of lavas erupted along the Southwest Indian Ridge between the Bouvet triple junction and 11 degrees east. *J. Petrol.*, 24:267–318.

McElhinny, M. W., 1973. *Paleomagnetism and Plate Tectonics:* Cambridge (Cambridge Univ. Press).

Mackensen, A., 1987. Benthische foraminiferen auf dem Island-Schottland Rücken: umwelt-anzeiger an der grenze zweier ozeanischer räume. *Palaeontol. Z.*, 61:149–179.

Mackensen, A., and Douglas, R. G., in press. Down-core distribution of live deep-water benthic foraminifera in box cores from the eastern Weddell Sea and northern Pacific Ocean. *Deep-Sea Res.*

Mackensen, A., Sejrup, H. P., and Jansen, E., 1985. The distribution of living benthic foraminifera on the continental slope and rise off southwest Norway. *Mar. Micropaleontol.*, 9:275–306.

Munschy, M., and Schlich, R., 1987. Structure and evolution of the Kerguelen-Heard Plateau (Indian Ocean) deduced from seismic stratigraphy studies. *Mar. Geol.* 76:131–152.

Pàlmason, G., Arnòrsson, S., Fridleifsson, I. B., Kristmannsdòttir, H., Saemundsson, K., Stefànsson, V., Steingrimsson, B., Tòmasson, J., and Kristjànsson, L., 1979. The Iceland crust: evidence from drillhole data on structures and processes. *In* Talwani, M., Harrison, C. G., and Hayes, D. E. (Eds.), *Deep Drilling Results in the Atlantic Ocean: Ocean Crust:* Washington (American Geophysical Union). Maurice Ewing Series, 3:43–65.

Pechersky, D. M., Tikhonov, L. V., and Pertsev, N. N., 1983. Magnetic properties of basalts, Deep Sea Drilling Project Legs 69 and 70. *In* Cann, J. R., Langseth, M. G., Honnorez, J., Von Herzen, R. P., White, S. M., et al., *Init. Repts. DSDP*, 69: Washington (U.S. Govt. Printing Office), 705–710.

Petrushevskaya, M. G., 1975. Cenozoic radiolarians of the Antarctic, Leg 29. *In* Kennett, J. P., Houtz, R. E., et al., *Init. Repts. DSDP,* 29: Washington (U.S. Govt. Printing Office), 541–675.

Price, R. C., Kennedy, A. K., Riggs-Sneeringer, M., and Frey, F. A., 1986. Geochemistry of basalts from the Indian Ocean triple junction: implications for the generation and evolution of Indian Ocean Ridge basalts. *Earth Planet. Sci. Lett.*, 78:379–396.

Robinson, P. T., Von Herzen, R. P., et al., 1989. *Proc. ODP, Init. Repts.*, 118: College Station, TX (Ocean Drilling Program).

Saunders, A. D., 1985. Geochemistry of basalts from the Nauru Basin, Deep Sea Drilling Project Legs 61 and 89: implications for the origin of oceanic flood basalts. *In* Moberly, R., Schlanger, S. O., et al., *Init. Repts. DSDP*, 89: Washington (U.S. Govt. Printing Office), 499–517.

Schlich, R., 1975. Structure et âge de l'océan Indien occidental. *Mem. Hors Ser., Soc. Geol. Fr.*, 6:1–103.

Schlich, R., Coffin, M. F., Munschy, M., Stagg, H.M.J., Li, Z. G., and Revill, K., 1987. *Bathymetric Chart of the Kerguelen Plateau.* [Jointly edited by Bureau of Mineral Resources, Geology and Geophysics, Canberra, Australia; Institut de Physique du Globe, Strasbourg, France; and Territoires des Terres Australes et Antarctiques Françaises, Paris, France.]

Storey, M., Saunders, A. D., Tarney, J., Leat, P., Thirlwall, M. F., Thompson, R. N., Menzies, M. A., and Marriner, G. F., 1988. Geochemical evidence for plume-mantle interactions beneath Kerguelen and Heard Islands, Indian Ocean. *Nature*, 336:371–374.

Toumarkine, M., and Luterbacher, H., 1985. Paleocene and Eocene planktic foraminifera. *In* Bolli, H. M., Saunders, J. B., and Perch-Nielsen, K. (Eds.), *Plankton Stratigraphy:* Cambridge (Cambridge Univ. Press), 87–154.

Vacquier, V., 1985. The measurement of thermal conductivity of solids with a transient linear heat source on the plane surface of a poorly conducting body. *Earth Planet. Sci. Lett.*, 74:275–279.

Van Morkhoven, F.P.C.M., Berggren, W. A., and Edwards, A. S., 1986. Cenozoic cosmopolitan deep-water benthic foraminifera. *Bull. Centr. Rech. Explor.-Prod. Elf-Aquitaine, Mem.* 11.

Von Herzen, R. P., and Maxwell, A. E., 1959. The measurement of thermal conductivity of deep-sea sediments by a needle probe method. *J. Geophys. Res.*, 65:1557–1563.

Welton, J. E., 1984. *SEM Petrology Atlas:* Tulsa, OK (Am. Assoc. Pet. Geol.).

Ms 120A-111